Thesis for the Degree of Doctor of Philosophy

Compact RF Integration and Packaging Solutions Based on Metasurfaces for Millimeter-Wave Applications

Abbas Vosoogh

CHALMERS

Department of Electrical Engineering
Division of Communication and Antenna Systems, Antenna Group
Chalmers University of Technology

Göteborg, Sweden 2018

Compact RF Integration and Packaging Solutions Based on Metasurfaces for Millimeter-Wave Applications

Abbas Vosoogh

ISBN: 978-91-7597-802-4

Doktorsavhandlingar vid Chalmers tekniska högskola
Ny serie nr 4483
ISSN 0346-718X

Department of Electrical Engineering
Division of Communication and Antenna Systems, Antenna Group
Chalmers University of Technology
SE–412 96 Göteborg
Sweden
Telephone: +46 (0)31 – 772 1000
Email: abbas.vosoogh@chalmers.se

Front Cover: The figure on the front cover is a compact integrated full duplex radio front-end module for multi-Gbit/s point-to-point links at *E*-band.

Typeset by the author using LaTeX.

Chalmers Reproservice
Göteborg, Sweden 2018

To my family

Abstract

The millimeter-wave frequency range has got a lot of attention over the past few years because it contains unused frequency spectrum resources that are suitable for delivering $Gbit/s$ end-user access in areas with high user density. Due to the limited output power that the current RF active components can deliver in millimeter-wave frequencies, antennas with the features of low profile, high gain, high efficiency and low cost are needed to compensate free space path loss and increase the communication distance for the emerging high data rate wireless systems. Moreover, it is desired to have a compact system by integrating the antenna with passive and active components at high frequencies.

In order to move towards millimeter-wave frequencies we need to face significant hardware challenges, such as active and passive components integration, packaging problems, and cost-effective manufacturing techniques. The gap waveguide technology shows interesting characteristics as a new type of waveguide structure. The main goal of this thesis is to demonstrate the advantages of gap waveguide technology as an alternative to the traditional guiding structures to overcome the problem of good electrical contact due to mechanical assembly with low loss. This thesis mainly focuses on high-gain planar array antenna design, integration with passive and active components, and packaging based on gap waveguide technology. We introduce several low-profile multilayer corporate-fed slot array antennas with high gain, high efficiency and wide impedance bandwidth operating at the millimeter-wave frequency band. A system demonstration consisting of two compact integrated antenna-diplexer and Tx/Rx MMICs for Frequency-division duplex (FDD) low latency wireless backhaul links working at E-band is presented, to show the advantages of gap waveguide technology in building a complete radio front-end. Moreover, the use of several new manufacturing methods, such as die-sink Electric Discharge Machining (EDM), direct metal 3-D printing, and micro-molding are evaluated to fabricate gap waveguide components in a more effective way.

Furthermore, a novel air-filled transmission line, so-called multi-layer waveguide (MLW), that exhibits great advantages such as low-cost, simple fabrication, and low loss, even for frequencies beyond 100 GHz, is presented for the first time. To constitute an MLW structure, a rectangular waveguide transmission line is formed by stacking several thin metal layers without any electrical and galvanic contact requirement among the layers. The proposed concept could become a suitable approach to design millimeter-wave high-performance passive waveguide components, and to be used in active and passive components integration ensuring mass production at the same time.

Keywords: aperture efficiency, bandpass filter (BPF), electromagnetic band gap (EBG), electric discharge machining (EDM), low sidelobe, gap waveguide, grating lobe, high efficiency, millimeter-wave, multi-layer waveguide (MLW), slot array antenna.

Preface

This thesis is in partial fulfillment for the degree of Doctor of Philosophy at Chalmers University of Technology, Gothenburg, Sweden.

The work resulting in this thesis was carried out between July 2014 and October 2018 at the Antenna Systems Group, Division of Communication and Antenna Systems, Department of Electrical Engineering, Chalmers. The late Professor Per-Simon Kildal (till April 2016) and Professor Herbert Zirath are the main supervisors, and Professor Jian Yang is the examiner. In addition, Associate Professor Vessen Vassilev and Assistant Professor Ashraf Uz Zaman are the co-supervisors.

This work is partially supported by the Swedish Governmental Agency for Innovation Systems VINNOVA via a project within the VINN Excellence center Chase, and the European Research Council (ERC) under the 7^{th} Framework Program ERC grant number 321125.

Acknowledgment

Finishing this thesis would not have been possible without the continuous support and help of many individuals. I have had the luxury to work with wonderful experts during the course of my PhD; and I would like to extend my sincere appreciation to all of them.

First and foremost, I want to express my deepest gratitude to my mentor, role model, source of inspiration and beloved supervisor, the late Professor Per-Simon Kildal. I am extremely grateful for the great opportunity he gave me to start this PhD journey, and for his continuous support, enthusiasm, kindness and encouragement in many aspects of my research and life in general. I indeed consider myself fortunate for the opportunity I had to work with him. He taught me to never give up in what you truly believe, and that it is very important to follow your dreams. The first two years of my PhD really constituted the best period of my career as a PhD student. I will never forget all the wonderful moments we could spend together, from deeply interesting technical discussions to fantastic ski trips that he kindly arranged for the whole Antenna Group.

My sincere gratitude goes to Professor Herbert Zirath and Professor Jian Yang for accepting to become my main supervisor and examiner, respectively, in a very critical moment of my PhD studies. I am very grateful for the so many fruitful technical discussions, and your guidance, attention and precious time you have put in the follow-up of my work. Furthermore, I wish to especially thank my co-supervisors Assistant Professor Ashraf Uz Zaman and Associate Professor Vessen Vassilev for the expert advices, valuable help and constructive feedbacks. I would also like to acknowledge my co-authors Professor Ahmed Kishk, Assistant Professor Simon He, Dr. Milad Sharifi Sorkherizi, and Dr. Abolfazl Haddadi for the enjoyable discussions and great collaboration that we have had during all my PhD years. Special thanks go to all the industrial partners involved within the Gap Waveguide project, especially Lars-Inge Sjöqvist and Stefan Carlsson from Gapwaves AB, and Trajan Badju from Gotmic AB.

I am highly indebted to my Spanish sister, Dr. Astrid María Rosa de Lima Algaba Brazález. There are not enough words to express how grateful I am for your extremely kind and loyal friendship, invaluable and constant support, for being always there for both the good and hard moments no matter what, and moreover, for spending so much time proofreading almost all my papers, and especially this thesis. Thank you so much for being part of my life during these years, for the interesting discussions about research and nonsense topics, and for arranging lot of fun events and unforgettable trips all around the world.

A special acknowledgment goes to all former and current colleagues in the Antenna Systems Group, for creating a nice and enjoyable work environment. It has been a great pleasure to work with all of you in such a friendly and multi-cultural place. I would like to particularly thank my dear friends Sadegh, Aidin, Madeleine, Carlo, Jinlin, Navid, Oleg, Wan-Chun, and Artem. We have spent together so many fun and enjoyable moments both at work and afterwork time. I also wish to thank Natasha Adler Gønbech, Christine Johansson, Rebecka Andersson, and Rebecca Alfredsson for their administrative help and for preparing the letters for renewing my visa every year.

I have had great time being surrounded by so many fantastic friends in the large Iranian community in, and around Chalmers. Samar, Parastoo, Maryam, Pegah, Ramin, Fatemeh, Taha, Kamran, Sina, Alireza, Mohammad Ali, Ebrahim, Morteza, Masoud, Bita, Mehrzad, Yasi, Mohammad Hossein, Fazeleh, and Ahad, thank you all for reminding me home, when I am so far from it.

Last but not least, I would like to express my deepest gratitude to my parents for always being there for me, supporting no matter what and encouraging me at every step I take.

Abbas
Göteborg, September 2018

List of Publications

This thesis is based on the work contained in the following appended papers:

Paper A
A. Vosoogh and P.-S. Kildal, "Simple Formula for Aperture Efficiency Reduction Due to Grating Lobes in Planar Phased Arrays," in *IEEE Transactions on Antennas and Propagation*, vol. 64, no. 4, pp. 2263–2269, 2016.

Paper B
P.-S. Kildal, **A. Vosoogh**, and S. Maci, "Fundamental Directivity Limitations of Dense Array Antennas: A Numerical Study Using Hannan's Embedded Element Efficiency," in *IEEE Antennas and Wireless Propagation Letters*, vol. 15, pp. 766–769, 2016.

Paper C
A. Vosoogh, A. A. Brazález, and P.-S. Kildal, "A V-band Inverted Microstrip Gap Waveguide End-coupled Bandpass Filter," in *IEEE Microwave and Wireless Components Letters*, vol. 26, no. 4, pp. 261-263, 2016.

Paper D
A. Vosoogh and P.-S. Kildal, "Corporate-Fed Planar 60 GHz Slot Array Made of Three Unconnected Metal Layers Using AMC pin surface for the Gap Waveguide," in *IEEE Antennas and Wireless Propagation Letters*, vol. 15, pp. 1935-1938, 2016.

Paper E
A. Vosoogh, P.-S. Kildal, and V. Vassilev, "Wideband and High-Gain Corporate-Fed Gap Waveguide Slot Array Antenna with ETSI Class II Radiation Pattern in V-band," in *IEEE Transactions on Antennas and Propagation*, vol. 65, no. 4, pp. 1823-1831, 2017.

Paper F
A. Vosoogh, M. Sharifi Sorkherizi, A. Uz Zaman, J. Yang, and A. A. Kishk, "An Integrated Ka-band Diplexer-Antenna Array Module Based on Gap Waveguide Technology With Simple Mechanical Assembly and No Electrical Contact Requirements," in *IEEE Transactions on Microwave Theory and Techniques*, vol. 66, no. 2, pp. 962-972, 2018.

Paper G
A. Vosoogh, A. Uz Zaman, V. Vassilev, and J. Yang, "Zero-gap Waveguide: A Parallel Plate Waveguide With Flexible Mechanical Assembly for mm-Wave Antenna Applications," submitted to *IEEE Transactions on Components, Packaging and Manufacturing Technology*, 2018.

Paper H
A. Vosoogh, A. Haddadi, A. Uz Zaman, J. Yang, H. Zirath, and A. A. Kishk, "W-Band Low-Profile Monopulse Slot Array Antenna Based on Gap Waveguide Corporate-Feed Network," accepted for publication in *IEEE Transactions on Antennas and Propagation*, 2018.

Paper I
A. Vosoogh, A. Uz Zaman, and J. Yang, "Simple and Broadband Transition Between Rectangular Waveguide and Groove Gap Waveguide for mm-Wave Applications," in *Proceedings of the 2018 IEEE International Symposium on Antennas and Propagation (APS/URSI)*, Boston, Massachusetts, USA, July 2018.

Paper J
A. Vosoogh, A. Haddadi, A. Uz Zaman, and J. Yang, "Wideband Horn Array Antenna With Gap Waveguide Corporate-Feed Network at E-Band," to be submitted to *IEEE Transactions on Antennas and Propagation*, 2018.

Paper K
A. Vosoogh, M. Sharifi Sorkherizi, V. Vassilev, A. Uz Zaman, J. Yang, Z. S. He, A. A. Kishk, and H. Zirath, "Compact Integrated Full Duplex Gap Waveguide Based Radio Front-end For Multi-Gbit/s Point-to-Point Backhaul Links at E-band," submitted to *IEEE Transactions on Microwave Theory and Techniques*, 2018.

Paper L
A. Vosoogh, H. Zirath, and Z. S. He, "Novel Air-Filled Waveguide Transmission Line Based on Multi-Layer Stacked Thin Metal Plates," submitted to *IEEE Transactions on Microwave Theory and Techniques*, 2018.

Other Publications

Additional related publications by the Author, not included in this thesis. The content partially overlaps with the appended papers or is out of the scope of the thesis.

Journal Papers

[i] A. A. Brazález, E. Rajo-Iglesias, J. L. Vázquez-Roy, **A. Vosoogh**, and P.-S. Kildal, "Design and validation of microstrip gap waveguides and their transitions to rectangular waveguide, for millimeter-wave applications," in *IEEE Transactions on Microwave Theory and Techniques*, vol. 63, no. 12, pp. 4035–4050, 2015.

[ii] U. Nandi, A. Uz Zaman, **A. Vosoogh**, and J. Yang, "Novel millimeter wave transition from microstrip line to groove gap waveguide for MMIC packaging and antenna integration," in *IEEE Microwave and Wireless Components Letters*, vol. 27, no. 8, pp. 691–693, 2017.

[iii] J. Liu, **A. Vosoogh**, A. Uz Zaman, and J. Yang, "Design and fabrication of a high-gain 60-GHz cavity-backed slot antenna array fed by inverted microstrip gap waveguide," in *IEEE Transactions on Antennas and Propagation*, vol. 65, no. 4, pp. 2117–2122, 2017.

[iv] J. Yang, F. Fan, P. Taghikhani, and **A. Vosoogh**, "Half-height-pin gap waveguide technology and its applications in high gain planar array antennas at millimeter wave frequency," in *IEICE Transactions on Communications*, vol. 101, no. 2, pp. 285–292, 2018.

[v] J. Liu, **A. Vosoogh**, A. Uz Zaman, and J. Yang , "A slot array antenna with single-layered corporate-feed based on ridge gap waveguide in the 60-GHz band," accepted for publication in *IEEE Transactions on Antennas and Propagation*, 2018.

Conference Papers

[1] **A. Vosoogh**, P.-S. Kildal, "Study of grating efficiency of planar arrays," in *Proceedings of the 9th European Conference on Antennas and Propagation (EuCAP 2015)* , Lisbon, Portugal, April 2015.

[2] J. Liu, **A. Vosoogh**, A. Uz Zaman, and P.-S. Kildal, "Design of a cavity-backed slot array unit cell on inverted microstrip gap waveguide," in *Proceedings of the 2015 International Symposium on Antennas and Propagation (ISAP)*, Tasmania, Australia, November 2015.

[3] **A. Vosoogh** and P.-S. Kildal, "High efficiency 2×2 cavity-backed slot sub-array for 60 GHz planar array antenna based on gap technology," in *Proceedings of the*

2015 International Symposium on Antennas and Propagation (ISAP), Tasmania, Australia, November 2015.

[4] **A. Vosoogh**, P.-S. Kildal, and V. Vassilev, "A multi-layer gap waveguide array antenna suitable for manufactured by die-sink EDM," in *Proceedings of the 10th European Conference on Antennas and Propagation (EuCAP 2016)*, Davos, Switzerland, April 2016.

[5] M. Sharifi Sorkherizi, **A. Vosoogh**, A. A. Kishk, and P.-S. Kildal, "Design of integrated diplexer-power divider," in *Proceedings of the 2016 IEEE MTT-S International Microwave Symposium (IMS)*, San Francisco, California, USA, May 2016.

[6] **A. Vosoogh**, and P.-S. Kildal, "V-band high efficiency corporate-fed 8× 8 slot array antenna with ETSI class II radiation pattern based on gap technology," in *Proceedings of the 2016 IEEE International Symposium on Antennas and Propagation (APS/URSI)*, Fajardo, Puerto Rico, USA, June 2016.

[7] **A. Vosoogh**, P.-S Kildal, V. Vassilev, A. Uz Zaman, and S. Carlsson, "E-band 3-D metal printed wideband planar horn array antenna," in *Proceedings of the 2016 International Symposium on Antennas and Propagation (ISAP)*, Okinawa, Japan, October 2016.

[8] J. Liu, **A. Vosoogh**, A. Uz Zaman, and P.-S Kildal, "Design of 8× 8 slot array antenna based on inverted microstrip gap waveguide," in *Proceedings of the 2016 International Symposium on Antennas and Propagation (ISAP)*, Okinawa, Japan, October 2016.

[9] **A. Vosoogh**, A. Uz Zaman, and V. Vassilev, "Wideband cavity-backed slot subarray with gap waveguide feed-network for D-band applications," in *Proceedings of the 11th European Conference on Antennas and Propagation (EuCAP 2017)*, Paris, France, April 2017.

[10] P. Taghikhani, J. Yang, and **A. Vosoogh**, "High gain V-band planar array antenna using half-height pin gap waveguide," in *Proceedings of the 11th European Conference on Antennas and Propagation (EuCAP 2017)*, Paris, France, April 2017.

[11] U. Nandi, A. Uz Zaman, **A. Vosoogh**, and J. Yang, "Millimeter wave contactless microstrip-gap waveguide transition suitable for integration of RF MMIC with gap waveguide array antenna," in *Proceedings of the 11th European Conference on Antennas and Propagation (EuCAP 2017)*, Paris, France, April 2017.

[12] **A. Vosoogh**, M. Sharifi Sorkherizi, A. Uz Zaman, J. Yang, and A. A. Kishk, "Diplexer integration into a Ka-band high-gain gap waveguide corporate-fed slot array antenna," in *Proceedings of the 2017 IEEE International Symposium on Antennas and Propagation (APS/URSI)*, San Diego, California, USA, June 2017.

[13] J. Liu, **A. Vosoogh**, A. Uz Zaman, and J. Yang, "A high-gain high-efficiency corporate-fed slot array antenna directly fed by ridge gap waveguide at 60-GHz," in *Proceedings of the 2017 International Symposium on Antennas and Propagation (ISAP)*, Phuket, Thailand, October 2017.

[14] **A. Vosoogh**, M. Sharifi Sorkherizi, A. Uz Zaman, J. Yang, and A. A. Kishk, "An E-band antenna-diplexer compact integrated solution based on gap waveguide technology," in *Proceedings of the 2017 International Symposium on Antennas and Propagation (ISAP)*, Phuket, Thailand, October 2017.

[15] J. Liu, **A. Vosoogh**, A. Uz Zaman, and J. Yang, "Slot antenna array unit cell directly fed by inverted microstrip gap waveguide," in *Proceedings of the 2017 International Symposium on Antennas and Propagation (ISAP)*, Phuket, Thailand, October 2017.

[16] **A. Vosoogh**, Z. S. He, and H. Zirath, "A Cost-effective D-band Multi-layer Rectangular Waveguide Transmission Line Based on Glide-Symmetric EBG Structure," in *Proceedings of the 12th European Conference on Antennas and Propagation (EuCAP 2018)*.

Thesis

Some of the work presented in this thesis, such as text, figures and tables may partly or fully reused from [∗], which is part of author's doctoral studies.

[∗] A. Vosoogh, "Towards Gap Waveguide Array Antenna for Millimeter Wave Applications," Tekn. Lic Thesis, Department of Signals and Systems, Antenna Systems Division, Chalmers University of Technology, 2016.

Patents

- P.-S. Kildal, A. Vosoogh, F. Hadavy, S. Carlsson, and L. Sjöqvist, "Waveguides and transmission lines in gaps between parallel conducting surfaces," US Patent App. US20170084971A1, 2017.
- A. Vosoogh, Z. S. He, "Multi-layer waveguide, arrangement, and method for production thereof," SE Patent App. 1751333-4, 2017.

List of Awards

- Best Student Paper Award of the 2015 International Symposium on Antennas and Propagation, Tasmania, Australia, 2015, [Paper 3].
- Honorable mention, Student Paper Competition of the 2016 IEEE AP-S international Symposium on Antennas and Propagation and USNC-URSI Radio Science Meeting, Fajardo, Puerto Rico, 2015, [Paper 6].
- Best Student Paper Award of the 2016 International Symposium on Antennas and Propagation, Okinawa, Japan, 2016, [Paper 7].
- Best Paper Award of the 2016 International Symposium on Antennas and Propagation, Okinawa, Japan, 2016, [Paper 7].
- CST University Publication Awards 2016, [Paper D].
- First Prize Student Award of the 2017 IEEE AP-S International Symposium on Antennas and Propagation and USNC-URSI Radio Science Meeting, San Diego, USA, [Paper 12].
- 3rd Best Student Paper Award of the 2017 International Symposium on Antennas and Propagation, Phuket, Thailand, 2017, [Paper 14].

Acronyms

4G/5G	Fourth/Fifth Generation
AMC	Artificial Magnetic Conductor
AWG	Arbitrary Waveform Generator
BER	Bit Error Rater
BPF	Bandpass Filter
CNC	Computer Numerical Control
CPW	Coplanar Waveguide
DRIE	Deep Reactive Ion Etching
EBG	Electromagnetic Bandgap
EDM	Electric Discharge Machining
ETSI	European Telecommunications Standards Institute
EVM	Error Vector Magnitude
FCC	Federal Communications Commission
FDD	Frequency Division Duplexing
GaAs	Gallium Arsenide
GGW	Groove Gap Waveguide
HetNet	Heterogeneous Network
IF	Intermediate Frequency
IIR	Image Rejection Ratio
ITU	International Telecommunication Union
LCP	Liquid Crystal Polymer
LO	Local Oscillator
LSB	Lower Sideband
LTCC	Low Temperature Co-fired Ceramic
MEMS	Micro-Electro-Mechanical Systems
MLW	Multi-Layer Waveguide
MMIC	Monolithic Microwave Integrated Circuit
MSE	Mean Squared Error

NF	Noise Figure
NRE	Non-Return Engineering
PA	Power Amplifier
PEC	Perfect Electric Conductor
PMC	Perfect Magnetic Conductor
PNA	Performance Network Analyzer
PRBS	Pseudo-Random Binary Sequence
PVD	Physical Vapor Deposition
QAM	Quadrature Amplitude Modulation
Q-TEM	Quasi Transverse Electromagnetic
RF	Radio Frequency
RGW	Ridge Gap Waveguide
RX	Receiver
SAR	Synthetic Aperture Radar
SIW	Substrate Integrated Waveguide
SLA	Stereolithography Apparatus
SLM	Selective Laser Melting
SNR	Signal to Noise Ratio
SOI	Silicon On Insulator
TE	Transverse Electric
TEM	Transverse Electromagnetic
TM	Transverse Magnetic
TX	Transmitter
USB	Upper Sideband
UV	Ultraviolet
VGA	Variable Gain Amplifier
VNA	Vector Network Analyzer
VSA	Vector Signal Analysis

Contents

Part I

Introductory Chapters

Chapter 1

Introduction

The continuously growing demand for higher data traffic and speed in cellular mobile networks leads to the use of higher frequency bands. There are requirements that will be challenging to address within the traditionally used frequency spectrum resources for mobile communication. One of these challenges is how to deliver multi-Gbit/s end-user access in areas with high user densities. It is expected that there will be a need for extremely high peak data rates, in the order of 10 to 50 Gbit/s at backhaul to the core network in the near future [1]. Nowadays, smart phones are not only used for voice call, but also employed for applications that involve an extensive data consumption. For example, for a typical fourth-generation (4G) cellular network the required backhaul data exceeds 250 Mbit/s [2]. Moreover, the number of mobile devices and demand for higher data connectivity are rapidly growing, which requires cost-effective novel high capacity wireless systems.

Fig.1.1 shows a system overview of mobile networks in dense and scattered urban

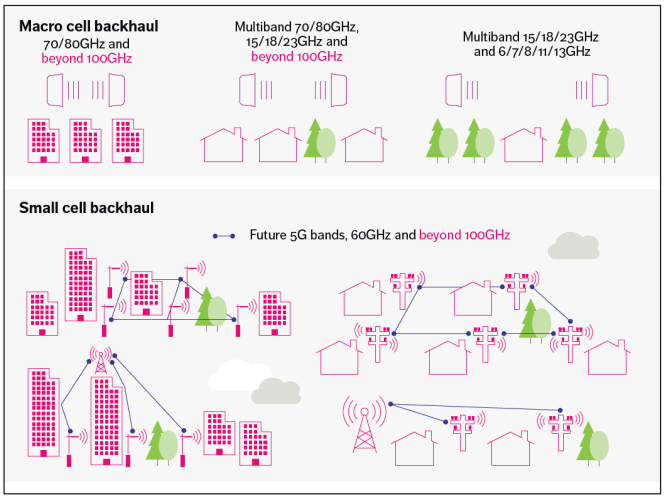

Figure 1.1: System overview of the next generation cellular network backhauling [3].

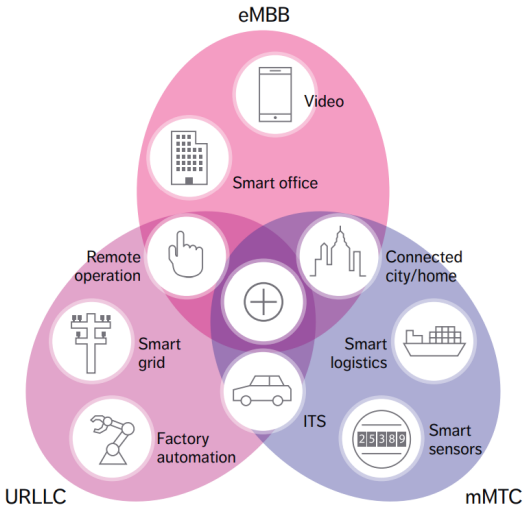

Figure 1.2: Three main 5G use cases [5].

areas. Heterogeneous network (HetNet) is one alternative to have a cost-effective and energy efficient backhaul solution in order to deliver the demanding capacity growth for the densely deployed mobile terminals in the fifth-generation (5G) mobile networks. In HetNet, small cell base stations incorporated with macro cells will be deployed in a conventional cellular network to extend coverage in crowded environments and improve the capacity [4]. However, this dense deployment creates the problem of an extensive data traffic in the backhaul side of the network.

To achieve multigigabit data rates, it would be beneficial to use wider frequency bands in the order of several GHz. Finding these continuous frequency bandwidths below 20 GHz is unlikely. Instead, the research effort for these ultra-high speed radio access interfaces has been targeting the millimeter-wave frequency range (30-300 GHz), where it is easier to get access to wider bandwidths [1]. There is a demand for ultra-high data rate backhaul point-to-point wireless links as a flexible and cost-effective alternative to fiber optic networks to provide multi-Gbit/s speed for the 5G wireless cellular networks, as shown in Fig.1.1. The wireless backhaul solution has the advantage of fast and easy installation compared to fiber optic networks. However, due to the lower capacity of microwave backhaul links, the usage of fiber optic is currently unavoidable. By using the millimeter-wave range of spectrum, we can achieve high capacity backhaul wireless links able to provide high speed and low latency as fiber optic networks.

1.1 Millimeter-Wave and 5G Applications

The use of millimeter-wave frequencies is growing in many applications such as automotive anti-collision radar at 77 GHz [6] , vehicle-to-vehicle communication [7], high resolution

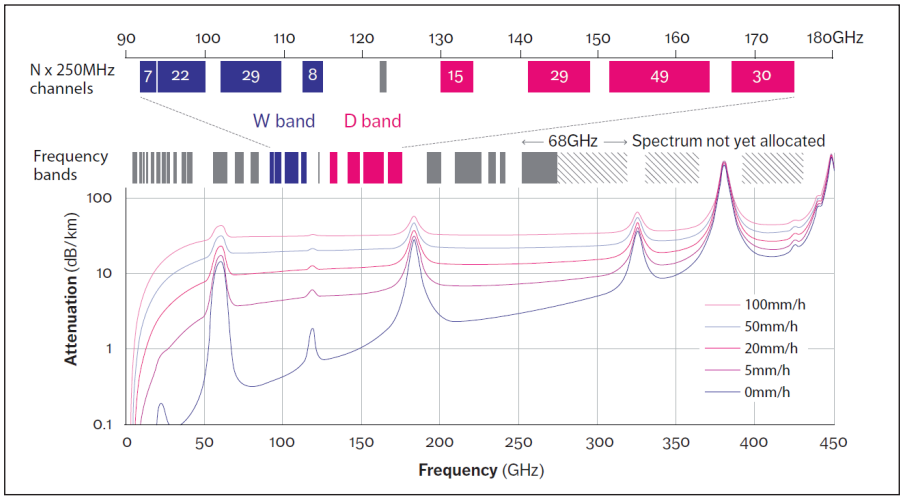

Figure 1.3: Average atmospheric attenuation for different rain rate and spectrum allocation for backhaul links at W- and D-band [3].

millimeter-wave imaging [8], satellites cross-link communication in space [9], indoor wireless data transmission at 60 GHz [10], and outdoor E-band (70/80 GHz) point-to-point backhaul terminals [11]. Fig.1.2 shows some use cases that 5G systems will offer in the future.

Millimeter-wave wireless communication systems suffer from high path loss, atmospheric absorption and they are vulnerable to weather conditions and precipitation [2]. All these factors limit the hop length to a couple of kilometers at millimeter-wave frequencies. The atmospheric absorption is higher at certain frequencies due to the oxygen molecule resonance frequency and water vapor [12]. Fig.1.3 shows the average atmospheric absorption in dB/km for different precipitation rates. The attenuation level mainly depends on temperature, pressure, and humidity. At 60 GHz, due to high atmospheric absorption, relatively secure communications can be implemented. On the other hand, the negligible atmospheric absorption at 28 and 38 GHz makes these frequencies good candidates for long-range radio links and emerging 5G cellular systems.

The high attenuation in the atmosphere and large absorption in urban scattering obstacles at millimeter-wave frequencies could be advantageous for some applications. This enables frequency reuse over small distances and higher security. There are several license free bands in the millimeter-wave frequency band. For example 9 GHz from 57 to 66 GHz (V-band) are allocated in United States and Europe for unlicensed use. The V-band is suitable for short-range high data rate communication systems with a low probability of intercept. The frequency band 59 to 64 GHz is attractive in particular due to a high atmospheric absorption (i.e. over 10 dB/km) which provides an opportunity for short range point-to-point links. Moreover, atmospheric absorption drops down significantly in the frequency range 64-66 GHz, which is attractive for similar applications where longer communication distances are required. For these purposes, highly-directive antennas with

high aperture efficiency are needed. Directive antennas for radio links are generally realized by using reflector antennas [13]. However, planar array antennas are more attractive for these new applications, due to their lower volume and weight. Furthermore, array antennas can provide rapid electronic beam steering.

An atmospheric window exists at E-band (71-76 GHz and 81-86 GHz) with low atmospheric attenuation of around 0.4 dB/km [2]. This makes the E-band a potential candidate to provide multi-Gbit/s data transfer and complements the conventional wireless links that operate in the microwave frequency band. In [14] path loss measurements during ten months versus weather conditions for a 1 km link at 71-76 GHz is presented. The measured attenuations for the rain rate of 20 mm/h and 40 mm/h in one kilometer are estimated to be 10 dB and 16.4 dB at 86 GHz, respectively, which are with good agreement with the ITU-R attenuation model in [15]. In the 71-76/81-86 GHz bands longer communication distance can be obtained due to relatively smaller gas absorption compared with the V-band band. Therefore, this band is suitable for long range high-capacity communication with negligible atmospheric attenuation. Most applications are foreseen for fixed and mobile infrastructure in this band [1]. The official license and spectrum allocation are other restricting challenges that the development of the millimeter-wave applications are facing. Since the frequency spectrum in millimeter-waves has not yet been unified in different countries, the potential frequency interference could cause legal disputes [1].

1.2 Millimeter-Wave Hardware Challenges

At microwave frequencies, passive components such as high-Q bandpass filters and slot array antennas are commonly realized in hollow waveguide structures, due to low insertion loss and high power handling. However, the manufacturing cost of the hollow waveguide structures becomes too high at millimeter-wave frequencies due to the strict tolerance requirements in the split-block construction technique. Planar technologies such as microstrip, coplanar waveguide (CPW) and substrate integrated waveguide (SIW), are more suitable for integration with active and passive components and easier to fabricate than standard hollow waveguide structures. However, these transmission lines suffer from high dielectric and ohmic losses as well as radiation leakage, especially when increasing the operating frequency.

To move towards millimeter-wave frequencies we need to face significant hardware challenges such as active and passive components integration, packaging problems and the need of cost-effective manufacturing techniques. The previously mentioned traditional technologies do not fulfill the strict requirements of the emerging millimeter-wave applications.

According to the Friis transmission formula, the power transmitted from one antenna and received by another antenna, under idealized conditions in a certain distance, is given

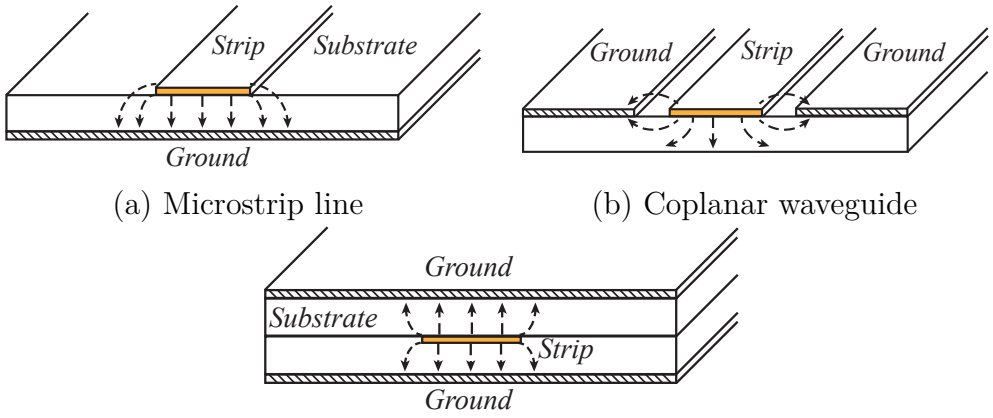

(a) Microstrip line

(b) Coplanar waveguide

(c) Stripline

Figure 1.4: Planar transmission lines and fundamental E-field mode distribution. (a) Microstrip line. (b) Coplanar waveguide. (c) Stripline.

by:

$$P_{\mathrm{r}} = P_{\mathrm{t}} + G_{\mathrm{t}} + G_{\mathrm{r}} + 20\log_{10}(\frac{\lambda}{4\pi R}) \tag{1.1}$$

where P_r is the receiving signal output power, P_t is the transmitting signal output power, G_r and G_t are the receiving and transmitting antenna gains, λ is the wavelength, and R is the distance between the antennas. Free-space path loss is more critical in millimeter-wave spectrum than lower frequencies due to a limitation related to their wavelength.

For a given transmitted power and antenna gains, the shorter the wavelength, the shorter the transmission range. In order to improve signal to noise ratio (SNR) at the receiver and, thereby increase the transmission range, we need to increase the power of the transmitting signal, or use more directive antennas. Due to the limited output power that the current active components can deliver in millimeter-waves, we can only increase the antenna gains in order to increase the communication distance and compensate free-space path loss. Therefore, high gain and low loss antenna is one of the most necessary components of millimeter-wave short- and long-range wireless communication systems. Moreover, millimeter-wave hardware modules need to have a compact size, to be highly-integrated, and all this has to be achieved at the lowest possible cost.

1.2.1 Traditional transmission line issues at high frequencies

Planar transmission line structures such as microstrip, CPW and stripline, are printed circuit technologies that constitute a compact and low cost solution. They are more suitable for integration with active and passive components and easier to fabricate compared to the standard waveguide structures. However, these transmission lines suffer from high dielectric and ohmic losses and radiation leakage, especially when increasing the operating

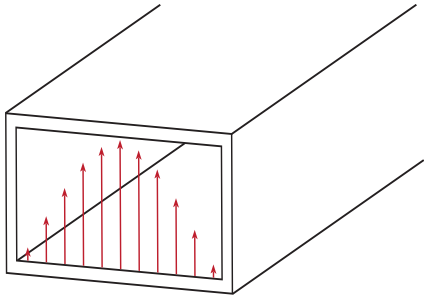

Figure 1.5: Rectangular waveguide structure and TE_{10} fundamental mode distribution.

frequency. Fig.1.4 shows the planar transmission lines configuration and their fundamental mode distribution.

Thin film substrate layers can be used to decrease the dielectric loss [16–18]. However, in order to have a 50 Ω line impedance, a narrower strip must be used for a thin substrate, which increases the conductive loss due to higher resistance. Surface waves and higher order modes can also be generated especially in the presence of discontinuities, bends, open-ends and steps, for example in bandpass filters and the feed-network of array antennas.

As already mentioned, standard hollow waveguides have some benefits compared to planar technologies such as low loss and high power handling capability (Fig.1.5). The non-planar structure of hollow waveguides makes difficult to use them in integration of passive and active components in the same module. Manufacturing and assembly tolerances, especially at millimeter-waves, are the other disadvantages of this technology. However, if we want to design a high-Q filter or a low loss and high-efficiency array antenna, we have to use hollow waveguides instead of dielectric based transmission lines.

The fabrication of complex waveguide structures at millimeter-waves presents a challenging task. There are several ways to fabricate waveguide structures, such as CNC machining and Electronic Discharge Machining (EDM). Waveguide structures are typically manufactured in split-blocks that can be connected by screwing, diffusion bonding or deep-brazing techniques. Accurate machining techniques are needed at millimeter-wave frequencies, which constitute difficult, expensive, and time-consuming processes.

The substrate integrated waveguide (SIW) or post-wall waveguide is introduced in [19, 20] as an attractive technology with the advantages of both planar transmission lines and hollow waveguides (Fig.1.6). The structure of SIW is similar to a rectangular dielectric-filled waveguide structure, where two rows of metalized via holes replace the narrow walls of waveguide. The upper and lower metal plates and via holes form a current loop in the cross-section, similar to the metal waveguide. All these via holes should be placed closely to avoid possible leakage. Because there are vias at the sidewalls, transverse magnetic (TM) modes do not exist and thereby this transmission line only supports propagation of TE_{m0} modes of the traditional rectangular waveguide.

SIW has a planar profile which makes them interesting for integration with active

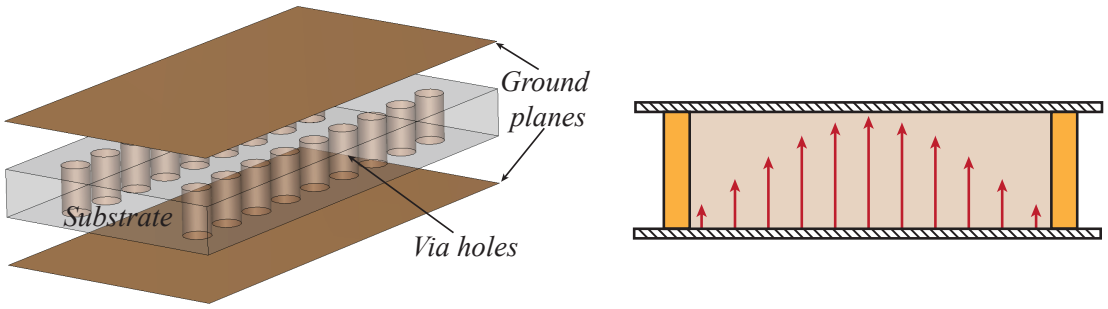

(a) (b)

Figure 1.6: (a) Substrate Integrated Waveguide. (b) Fundamental TE_{10} mode distribution.

components. However, due to the presence of dielectric, SIW faces the same problem as microstrip transmission lines and shows higher loss than hollow waveguides. Moreover, radiation losses and leakage can occur in a bad design, because the via holes do not provide a perfect shielding [21, 22].

1.2.2 Array antenna challenges

The design of high gain, high efficiency and low profile antennas is one of the main challenges of millimeter-wave wireless systems. Planar array antennas are very popular and widely used because of their advantages such as flat structure, low volume and weight. Furthermore, in array antennas the main beam direction can be rapidly changed by electronic steering. These facts make them attractive for many applications.

In the design of a broadside-radiating antenna array, the element spacing is required to be within one wavelength to avoid high grating lobes. However, the element spacing may become larger than one wavelength in order to accommodate a fully feeding branched also called corporate distribution network, especially at high frequencies. Therefore, it is important to know the grating lobe behavior and its effect on the aperture efficiency. [Paper A] makes such a study and validates a simple formula for the efficiency reduction due to grating lobes. Several methods have been developed to suppress grating lobes, such as aperiodic array configurations including rotated sub arrays [23], ring-grid array with trapezoid sub-arrays [24], arrays of random subarrays [25], random element and subarray positioning [26], and processing techniques in synthetic aperture radar (SAR) systems [27, 28].

A high gain array antenna with a large number of elements requires long transmission lines in the distribution network, and these lines must have very low losses. Although microstrip and SIW arrays have low profile, they suffer from dielectric and ohmic losses, which is a disadvantage for high gain millimeter-wave applications [29–31]. The losses can be partly reduced by using low loss dielectrics, but these materials are expensive, and also

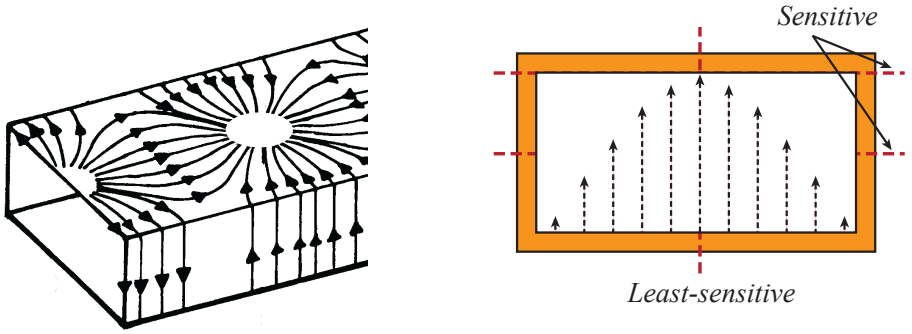

(a) (b)

Figure 1.7: (a) Surface Currents distribution for TE_{10} mode in rectangular waveguide walls [35]. (b) Sensitive and least-sensitive places for joining walls.

quite soft which can affect in the performance due to mechanical tolerances. Moreover, it becomes difficult to machine and make via holes through those types of planar structures. Leakage and surface waves may become a major problem in microstrip array antennas, especially in a big distribution network [32]. They can have a large effect on the radiation patterns, and thus, lead to a reduction in the antenna efficiency and thereby affecting the gain. Hybrid corporate-fed array antennas are proposed in [33] and [34] to reduce the dielectric loss of the distribution network, by using a microstrip ridge gap waveguide feed network and Substrate Integrated Cavity (SIC) radiating layer.

Slotted waveguide array antennas have been known for years and still are the best choice for high efficiency and high power applications. The basic principle of the slot antenna is disturbing the surface current on the waveguide walls by introducing slots. Hollow waveguide distribution networks show low loss and high efficiency, which make them suitable for such applications that require high gain antennas [36–38]. However, the tiny gaps between the antenna blocks can also cause leakage and radiation, if they disturb the surface current (Fig.1.7). Therefore, the fabrication of a complex waveguide structure is a challenging task, especially at millimeter-wave frequencies. The requirement of having good electrical contact between the building blocks to avoid leakage increases the fabrication cost and manufacturing complexity. This is especially critical when building up multilayer waveguide slot array antennas where precise assembly is needed.

Series-fed slotted waveguide arrays are simple but provide a narrow bandwidth due to the long line effect [39]. In a single layer structure, it is normally not possible to feed each radiating element in parallel (full corporate-feed) because of the space limitations associated with keeping the element spacing smaller than one wavelength (λ_0) to avoid grating lobe [40]. Multi-layer corporate distribution networks [41] show a wider bandwidth than series-fed arrays [42]. In these antennas, radiating elements are fed in parallel by using a corporate-feed network, formed by waveguide power dividers. However, it is very difficult to achieve good electrical contact between the vertical walls and the upper layer

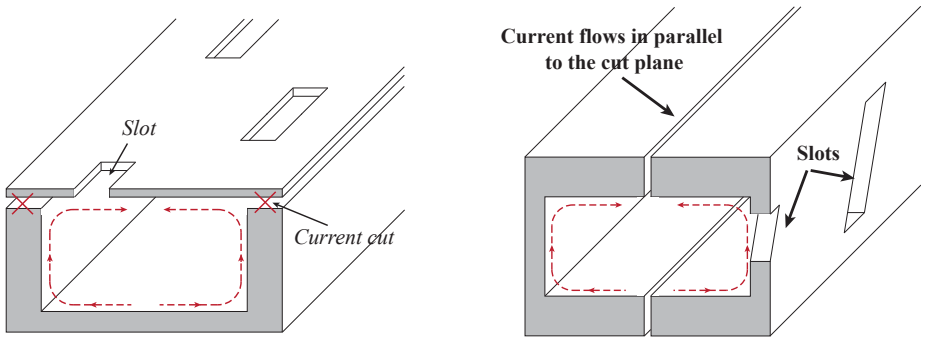

(a) (b)

Figure 1.8: Surface current distortion in slotted waveguide antennas. (a) Current cut in broad-wall slot antenna. (b) Narrow-wall slot antenna without problem of disturbing current.

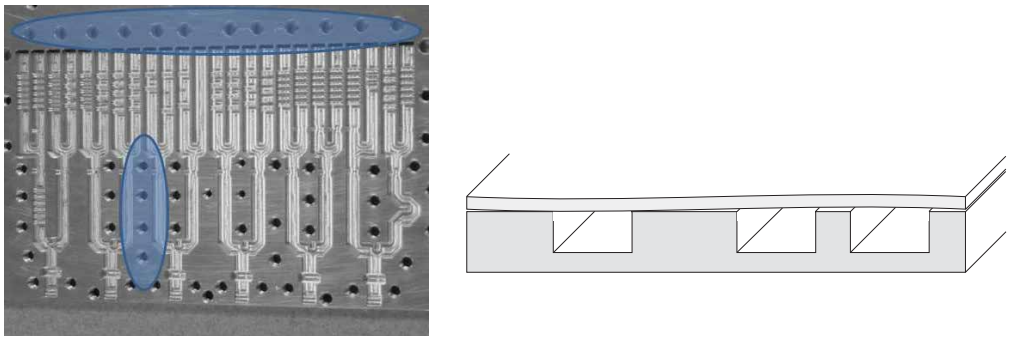

(a) (b)

Figure 1.9: (a) Array antenna feed-network with many screws. (b) Flatness problem.

in a distribution network, where a narrow vertical wall is separating each closely spaced waveguide branch [42, 43].

To overcome the problem of leakage due to the assembly in the broad-wall slotted waveguide antenna, a narrow-wall slotted waveguide can be used (Fig.1.8). This antenna can be manufactured in E-plane split-block without disturbing and cutting the surface current on the waveguide walls.

The flatness of the metal layers is another key aspect to assure good electrical contact between plates. Guaranteeing good plate flatness, especially in a large surface, is not an easy task. A high-quality surface finishing over the whole metal contacts, as well as good alignment of the two blocks, must be achieved in order to remove the gaps between the two split-blocks and achieve a good electrical contact. Moreover, lots of screws are needed to ensure good contact, and this is not always successful (Fig.1.9).

In [Paper G] we have further studied the mentioned problems at V-band. We have manufactured a rectangular waveguide line in H-plane split-block and used several screws

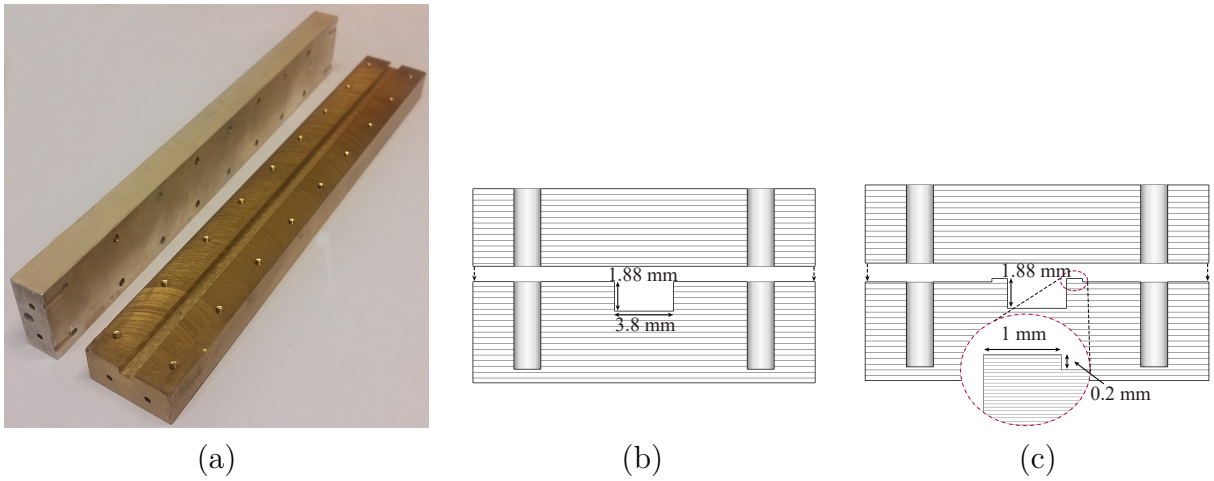

(a) (b) (c)

Figure 1.10: (a) Photograph of the fabricated H-plane split-block rectangular waveguide. (b) Cross-section of the original line. (c) Cross-section of the modified line.

on the side walls to assemble the two pieces. Fig. 1.10 (a) shows the manufactured prototype. Fig. 1.11(a) shows measured S-parameters of the rectangular waveguide line with flat top walls, as illustrated in Fig. 1.10 (b). The measurement shows significant leakage due to the existing tiny gap between the two blocks. To improve the electrical contact between the blocks, and thereby reduce the leakage, the bottom block of the prototype is modified by making small steps at the sides of the waveguide walls. The cross-section of the modified waveguide is shown in Fig. 1.10 (c). The measured S-parameters of the modified waveguide are presented in Fig. 1.11(b). In this measurements we can observe that by adding a small step the performance drastically improves. It is worthy mentioning that the fabricated rectangular waveguide is a straight line and in presence of discontinuity the performance will degrade as well.

The previously mentioned strict mechanical requirements lead to use complex and high-precision manufacturing techniques and innovative ideas. A corporate-fed multilayer rectangular waveguide cavity-backed slot array antenna is reported in [44]. This is based on normal rectangular waveguide technology realized by diffusion bonding of many thin copper plates in order to achieve good electrical contact between all the plates. It shows high efficiency and wideband performance, but the diffusion bonding technique is expensive in mass production. Diffusion bonding is a solid-state welding technique capable of joining metals. Diffusion bonding is typically implemented by applying both high pressure and high temperature to the materials to be welded. Another attempted solution, a novel over-sized post-wall waveguide fed by a $quasi-TEM$ mode array antenna in a parallel-plate waveguide configuration is introduced in [45]. In this design, a compact design is achieved by using densely placed posts on the same layer as the parallel plate. This solution has a narrow bandwidth and also $quasi-TEM$ mode is difficult to obtain by combining TE_{n0} modes. Several attempts have been made for solving the junction

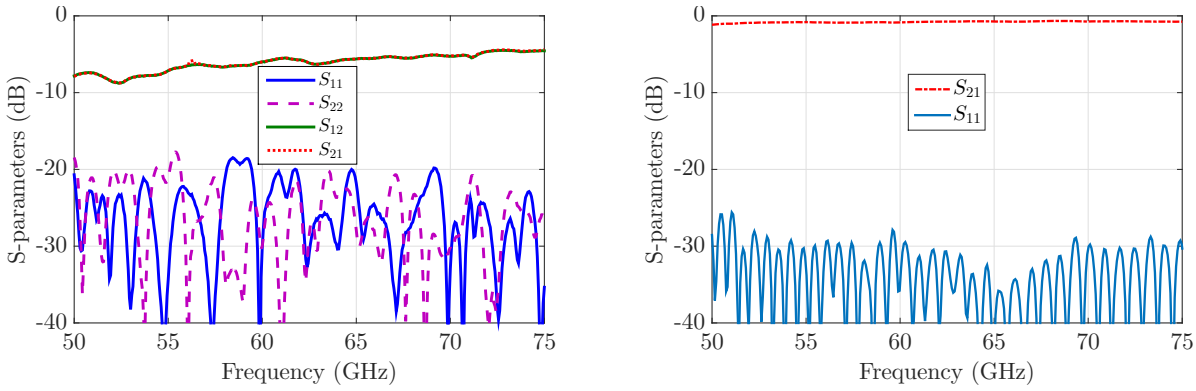

Figure 1.11: (a) Measured S-parameters of the rectangular waveguide with flat top walls. (b) Measured S-parameters of the modified line by adding small steps [Paper G].

problem at the radiating layer where screws cannot be inserted, such as alternating-phase fed single-layer slotted waveguide array which removes the need of the electrical contact between plates [46].

1.3 Thesis Motivation and Contribution

There exists a big gap between planar transmission lines such as microstrip, CPW and SIW, and the non-planar hollow waveguides in terms of performance such as loss and fabrication flexibility. Fig.1.12 compares the performance of some reported planar high gain array antennas based on different technologies in terms of loss, fabrication complexity and cost. Microstrip and SIW array antennas have lower profile and cost than hollow waveguide arrays, but they suffer from higher loss which is a disadvantage for high gain antennas. Therefore, we instead realize slot array antennas in separated metal layers that are assembled without requiring any metal contact between them. This is possible by using the new metamaterial-based gap waveguide technology. Our research goal is to introduce a solution to overcome and reduce the mentioned gap between planar transmission lines and hollow waveguides.

The aim of this thesis is to design efficient array antennas and integration with passive components, as well as RF circuitry for next generation millimeter-wave wireless communication systems. One of the main current research challenges is to find a new type of transmission line which can be fabricated in a cost-effective and flexible way, and that also shows low-loss at millimeter-wave frequencies. We explore and demonstrate the advantages of gap waveguide technology as an alternative to the traditional guiding structures to overcome the problem of good electrical contact due to mechanical assembly providing a low loss solution, especially at high frequencies. The gap waveguide technology is suitable for millimeter and sub-millimeter-wave frequencies, since high integration capability

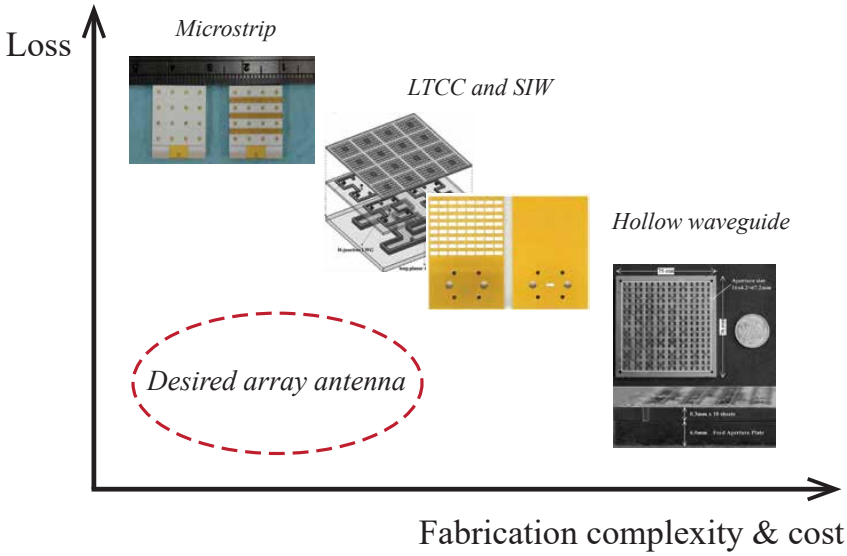

Figure 1.12: Comparison of different array antenna technologies performance. (Microstrip array antennas [47], LTCC and SIW array antennas [48, 49], Hollow waveguide slot arrays [44])

of active and passive components are required for these new emerging systems, although a lot of challenges still need to be solved. Some of the major issues found at these frequencies are the strict manufacturing and assembly tolerances. Moreover, we introduce a novel air-filled multilayer waveguide (MLW) transmission line for the first time with advantages of low form factor, low loss, mass-producible, and cost-effective at the millimeter frequency band, especially for frequencies above 100 GHz.

Wireless communication systems are traditionally built up by designing separately the main building blocks of the system, i.e. antenna, diplexer, and RF circuitry, whereas the realization of the whole system package comes afterwards. Fig.1.13 shows an overview of the appended papers of this thesis classified in different categories. The main goal of this thesis is to design a complete gap waveguide radio front-end by integrating a high gain array antenna, a diplexer, and Tx/Rx monolithic microwave integrated circuits (MMICs) circuitry in one package, in order to show the advantages of gap waveguide technology in terms of system integration and packaging.

This thesis contains the design, implementation, and performance characterization of several hardware prototypes to reach our goal as follows:

1. **Low-loss and high performance passive components design**

   - High gain antennas are essential components to compensate for the losses in point-to-point wireless links, due to the high path loss at millimeter-wave frequencies. The gap waveguide technology presents some benefits for high frequency antenna

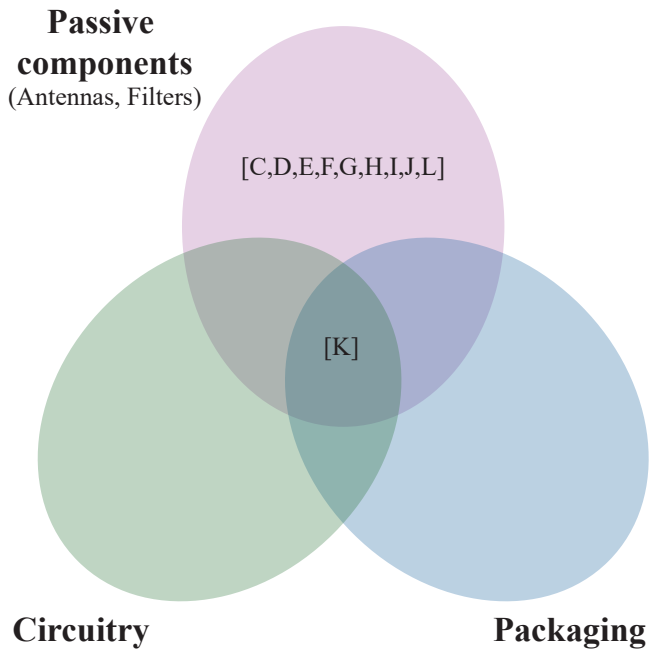

Figure 1.13: Trend towards more integrated and interconnected system in future.

applications. It has a planar profile, and it can be used as a low loss distribution network for an antenna array. This thesis is partially focused on the design of passive components, particularly array antennas and bandpass filters based on gap waveguide technology for millimeter-wave applications. Several low profile multilayer corporate-fed slot array antennas with high gain, high efficiency and wide impedance bandwidth for V- and E-band have been designed and are thoroughly explained in this thesis.

2. **Realization and manufacturing techniques**

- In gap waveguide, periodic textured structures, in the form of pins or mushrooms, are used to realize an Artificial Magnetic Conductor (AMC). The fabrication of the textured structure presents a challenging task, especially at millimeter-wave frequencies, due to the relatively complex pattern and physical dimensions. The conventional Computer Numerical Control (CNC) machining technique is very time-consuming and not effective to manufacture gap waveguide structures. The realization of gap waveguide structures with faster and cheaper approaches is another part of this thesis. A fast modern planar 3-D manufacturing method called die-sink Electric Discharge Machining (EDM) is used for the first time to manufacture a large planar high gain antenna at millimeter-wave. Direct Metal Laser Sintering (DMLS) 3-D printing technique and Reaction Injection Micro-Molding (RIM) are examples of alternative manufacturing methods that we have explored to manufacture gap

waveguide array antennas at E- and D-band, respectively. Moreover, MLW waveguide structures are fabricated with cost-effective and mass-producible technologies, i.e. metal chemical etching and laser-cutting.

3. **Integration with active and passive components**

- The integration of active and passive components, such as bandpass filters (BPFs), diplexers, amplifiers and monolithic microwave integrated circuits (MMICs) with the feed-network of an array antenna based on gap waveguide technology is the main goal of this thesis. A more compact system can be realized with higher level integration. To go towards this goal, a co-design of different parts is required in order to obtain a high performance module.

1.4 Thesis Outline

The thesis is divided in two main parts. The purpose of the first part, organized in seven chapters, is to introduce the subject and the background needed in order to have a better understanding of the appended papers, presented in the second part.

The first part of the thesis is organized as follows: in **Chapter 2** a brief description of the theoretical background of array antennas is introduced. The results of a generic study on grating lobe in a directive fixed beam array antenna is presented. In this chapter, the fundamental directivity limitations in dense array antennas due to mutual coupling, and sparse arrays caused by grating lobes are discussed as well. The content of this chapter is related to papers [A],[B] appended in the second part of this thesis. **Chapter 3** outlines an overview of gap waveguide where the fundamental operating principle of this technology is briefly described. Furthermore, previous investigations performed on the design and experimental evaluation of passive components, array antennas and packaging on all possible variants of gap waveguide technology at different frequency bands are summarized in this chapter. In **Chapter 4** the designs of several passive components such as high gain array antennas performed by the author of this thesis are presented. The integration of a diplexer and a monopulse comparator network, together with the feed-network of an array antenna based on gap waveguide, is also another topic of this chapter. Papers [C-J] annexed in the second part of the thesis are related to Chapter 4. A brief description of the design and the performance evaluation of a compact integrated antenna-diplexer-circuit module is given in **Chapter 5**. This is more thoroughly explained in [Paper K] attached at the second part of this thesis, where a multi-Gbit/s real-time data transmission at E-band is also successfully demonstrated. In **Chapter 6** a novel air-filled multilayer waveguide (MLW) transmission line is introduced together with a manufactured demonstrator at D-band as a proof-of-concept. [Paper L] deals in detail about the content of chapter 6. Finally, **Chapter 7** summarizes and concludes the first

part of the thesis with a brief summary of the listed contributions together with potential future research opportunities.

The most relevant contributions of the author are included in the form of 12 appended papers [A-L], which are presented in the second part of the thesis . Additionally, other related publications of the author can be found as references in the section List of Publications.

Chapter 2

Theoretical Background

An antenna with a large directivity requires to have an aperture with a large dimension. Conventionally, reflector antennas with a large aperture size have been used to obtain a high directivity. Another approach is to use array antennas, which contain several interfering antenna elements that are located in different places, and possibly with different spacing between elements to form a larger aperture. This type of antennas is very popular and widely used because of their advantages such as flat structure, low volume and weight. Furthermore, in array antennas the main beam direction can be rapidly changed by electronic steering. This makes them attractive for many applications. Array antennas can be constituted of different grid and lattice, have a linear or planar profile or also be regular, aperiodic or conformal. In regular arrays, the elements have a uniform spacing. In contrast, in aperiodic array antennas, the element spacing between the consisting elements of the array is not equal in different locations.

Usually, in the design of regular array antennas, the element spacing is required to be within one wavelength in order to avoid high grating lobes. However, the element spacing may become larger than one wavelength, especially at high frequencies, due to limited space to accommodate the feeding or beam forming network. Several methods have been developed to suppress grating lobes, such as aperiodic arrays configurations including rotated sub arrays [23], ring-grid array with trapezoid subarrays [24], arrays of random subarrays [25], random element and subarray positioning [26], and processing techniques in synthetic aperture radar (SAR) systems [27, 28]. Although it is required to have small element spacing to avoid grating lobes, having very small element spacing also rises another issue related to the mutual coupling between the elements. Mutual coupling becomes a critical problem in dense arrays where the array's elements are placed very close to each other ($< 0.5\lambda$), since it affects the impedance matching of the elements.

This chapter presents a brief theoretical basis of array antennas and fundamental directivity limitations in sparse and dense regular arrays. The effect of element spacing in directivity, aperture efficiency, and radiation pattern has been studied for two extreme cases, i.e. when the element spacing becomes larger than 1λ in [Paper A], and for an

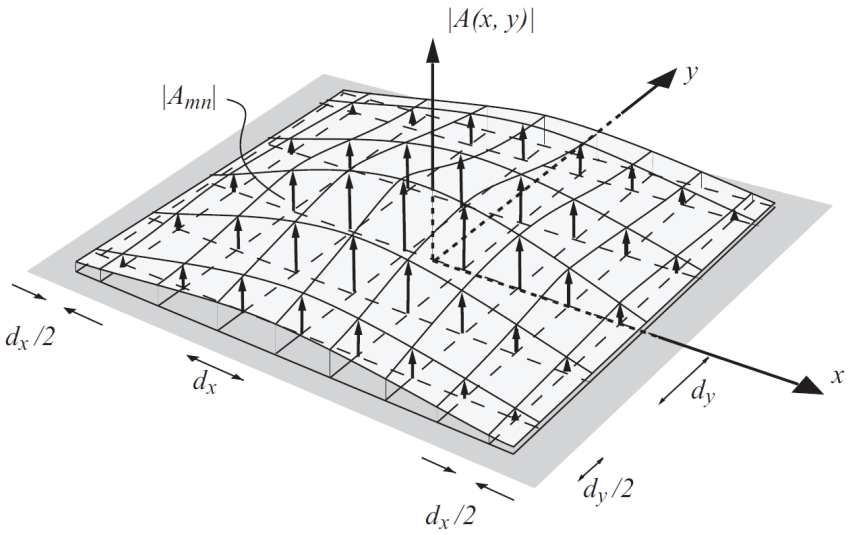

Figure 2.1: Array antenna with rectangular lattice [50].

element spacing smaller than 0.5λ in [Paper B].

2.1 Planar Regular Array

Fig. 2.1 shows a planar array with a rectangular lattice in xy-plane. The far-field function of the array can be calculated by multiplying the far-field function of the element ($\boldsymbol{G(\hat{r})}$), and the array factor ($\boldsymbol{AF(\hat{r})}$) as shown in (2.1) [50].

$$\boldsymbol{G_A(\hat{r})} = \boldsymbol{G(\hat{r})}\boldsymbol{AF(\hat{r})} \tag{2.1}$$

the array factor ($\boldsymbol{AF(\hat{r})}$) can be calculated by summation of element-by-element with different excitation weight ($A_{mn}e^{j\Phi_{mn}}$), as shown in (2.2) [50].

$$\boldsymbol{AF(\hat{r})} = \sum_{n=1}^{N}\sum_{m=1}^{M} A_{mn}e^{j\Phi_{mn}}e^{jkr_{mn}\cdot\hat{r}} \tag{2.2}$$

Calculating the array factor with (2.1) becomes time consuming for large arrays. Another approach is to calculate the array factors as grating lobes sum, as shown in (2.3) [50].

$$\boldsymbol{AF(\hat{r})} = e^{j\Phi_c}\frac{1}{d_x d_y}\sum_{p=-\infty}^{\infty}\sum_{q=\infty}^{\infty}\tilde{A}(k_x - k_{\Phi_x} - p\frac{2\pi}{d_x}, k_y - k_{\Phi_y} - p\frac{2\pi}{d_y}) \tag{2.3}$$

where k_{Φ_x} and k_{Φ_y} are the propagation constants of the phase excitations in x and y directions, and $\tilde{A}(x, y)$ is the two-dimensional Fourier transform of the excitation distribution $A(x, y)$ as follows [50]:

$$\tilde{A}(k_x, k_y) = \int_{-\infty}^{\infty}\int_{-\infty}^{\infty} A(x, y)e^{jk_x x}e^{jk_y y}dxdy \tag{2.4}$$

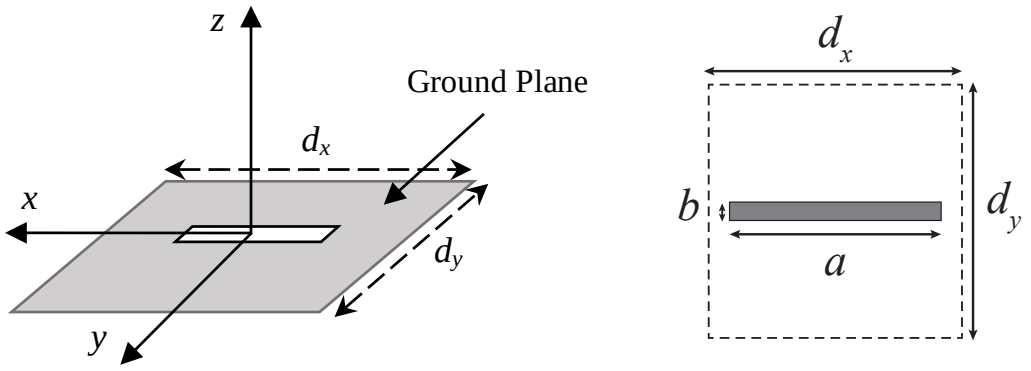

(a) (b)

Figure 2.2: Slot unit cell geometry that is used as the element of a regular array.

2.2 Grating Efficiency

In a regular array antenna, when the element spacing becomes greater than one wavelength, the first grating lobes appear in the visible region for a broadside scan. The main negative effect of these grating lobes is a reduction in the antenna directivity. The grating lobes can appear even for an element spacing smaller but, close to one wavelength when the main beam steers. The level of the grating lobes, and consequently the directivity reduction, depends on the element far-field function and the element or subarray spacing. A simple formula called "grating efficiency" is presented in [50] (Sec.10.3.5). The grating efficiency is the reduction in directivity and therefore the aperture efficiency due to the power lost in the grating lobes. It is given by the following formula:

$$e_{\text{grt}} = \frac{|\boldsymbol{G}(\theta_0, \varphi_0)|^2}{\sum\limits_{pq} |\boldsymbol{G}(\theta_{pq}, \varphi_{pq})|^2 \frac{\cos\theta_0}{\cos\theta_{pq}}} \tag{2.5}$$

The sum is taken over all visible grating and main lobes. In (2.5) $\boldsymbol{G(\theta, \varphi)}$ is the vector far-field function of the single embedded element, (θ_0, φ_0) is the direction of main beam and $(\theta_{pq}, \varphi_{pq})$ are the directions of the grating lobes. The embedded element far-field function is the far-field function of the whole array when only one element is excited and all the other elements are terminated in the port impedance. This formula is derived under the following assumptions:

1. All grating lobes are in the visible region and no grating lobe are located at grazing angle.
2. The array is large and provides a pencil beam.
3. The edge effects are approximated by assuming that all elements have the same embedded radiation pattern.

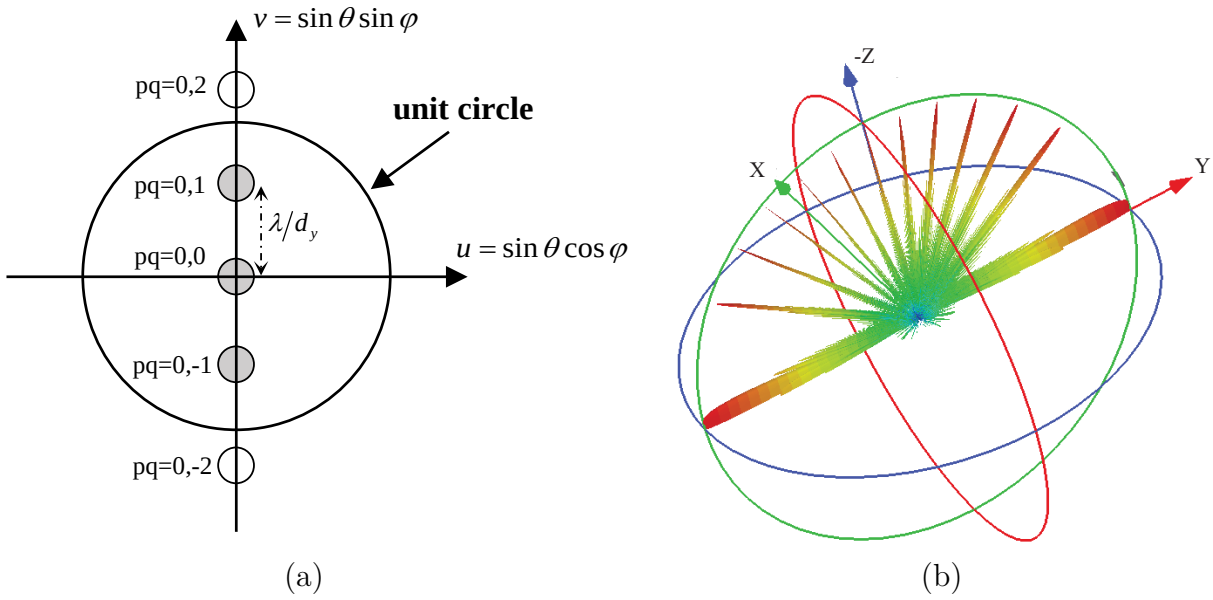

(a) (b)

Figure 2.3: (a) Grating lobes and main beam spectrum for element spacing greater than one wavelength in E-plane. (b) Radiation far-field pattern of 32×32-element array with element spacing equal to 6λ in E-plane, and smaller than λ in H-plane.

With the simple formula (2.5) and the knowledge of the radiation pattern of the element, we can analytically estimate the aperture efficiency and, thereby, the directivity of the array in the presence of grating lobes. In the following sections the accuracy evaluation of the grating efficiency formula for two cases, i.e. grating lobes in E- and H-planes, is presented by a comparison with numerical and analytical solutions. More elaborate explanation and details can be found in [Paper A].

2.2.1 Grating lobes in E-plane

Fig. 2.2 shows a half-wavelength slot antenna in an infinite ground plane as the array unit cell. The slot has a length of $a = 0.505\lambda$ and a width of $b = 0.067\lambda$ ($\ll \lambda$). The far-field function of narrow slots is well-known, and that is the main motivation to use this antenna for analytical evaluation purpose. The spectrum of grating lobes of a case with grating lobes only in E-plane for an in-phase rectangular grid is shown in Fig. 2.3(a). To satisfy this assumption, the element spacing in H-plane is smaller than one wavelength. Fig. 2.3(b) shows the radiation pattern of a 32×32 slot array when the element spacing in E-plane is equal to 6λ. As can be seen, grating lobes appear with the same level of the main beam, since the slot antenna has an omnidirectional radiation pattern in the E-plane. In order to verify the accuracy of formula (2.5), the numerical and analytical results of the grating efficiency have been compared with the aperture efficiency obtained from full-wave numerical simulations.

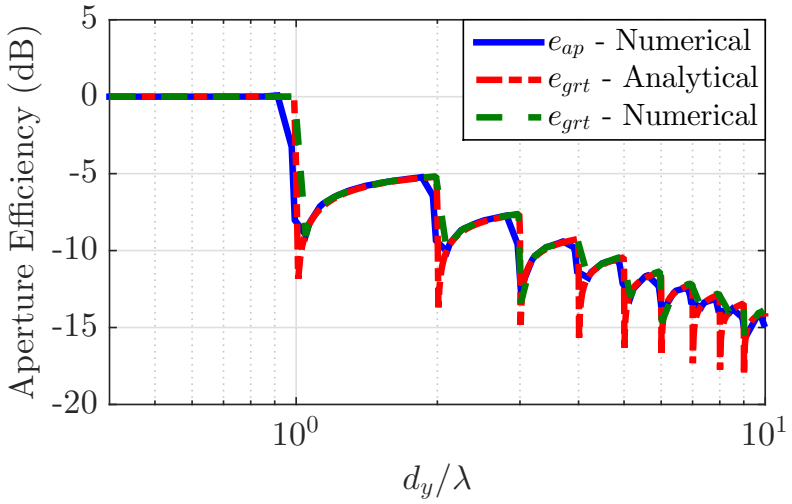

Figure 2.4: Aperture efficiency of 32×32-element slot array with different element spacing in E-plane.

Fig. 2.4 shows the aperture efficiency of an array with different element spacing in E-plane. The element spacing in E-plane varies from 0.4λ to 10λ while the element spacing is fixed to $d_x = 0.67\lambda$ in H-plane. For the numerical approach, the single element has been simulated in an infinite array environment by applying the Master/Slave boundary condition in HFSS. By using this, and combined with a truncation to 32×32 elements (done by HFSS), the directivity and the far-field function of the 32×32 array for different element spacings is obtained. Then the aperture efficiency is calculated by using $e_{ap} = D/D_{max}$, where D_{max} is the maximum achievable directivity from an aperture ($D_{max} = 4\pi A/\lambda^2$). These results are in Fig. 2.4 marked with "e_{ap} - Numerical". Furthermore, the grating efficiency is calculated by substituting the level of the main beam and grating lobes obtained from the simulated radiation patterns into the grating efficiency formula. These results are marked with "e_{grt} - Numerical".

The analytical and simulated grating lobe levels show good agreement with each other except when there are grating lobe directions near the end-fire directions (along the ground plane). The reason for this difference is that the isolated element pattern is here used instead of the embedded element pattern.. According to Fig. 2.4, the isolated element pattern is quite accurate for calculating the grating lobe level except when there are grating lobes radiating along the ground plane.

2.2.2 Grating lobes in H-plane

The spectrum of grating lobes for the case where the grating lobes only appear in H-plane is shown in Fig. 2.5(a). The radiation pattern of a 32×32 slot array with a H-plane element spacing of 6λ is shown in Fig. 2.5(b). Compared to Fig. 2.3(b), there is no grating

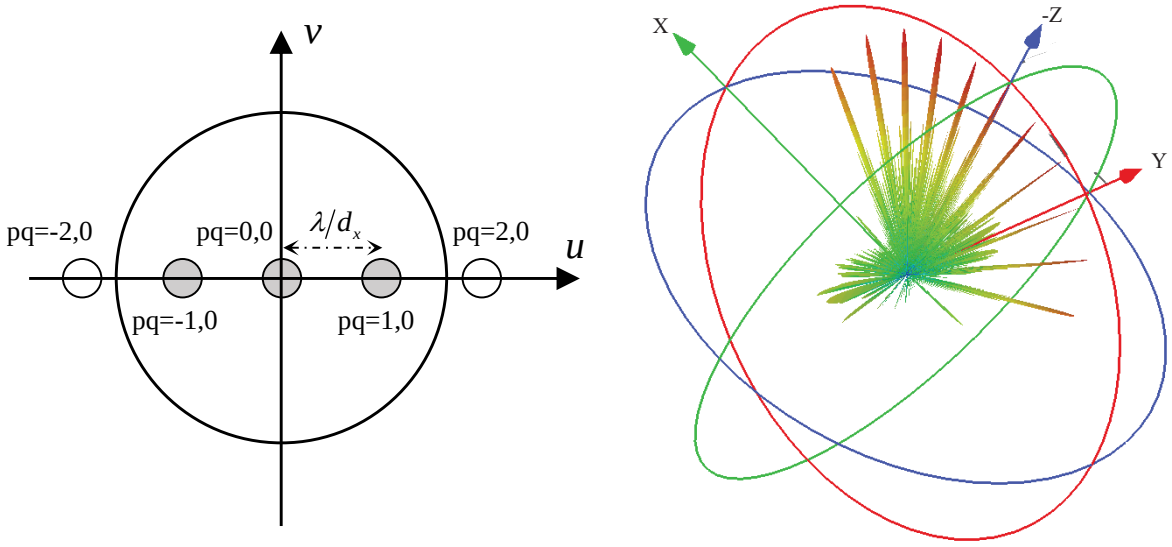

(a) (b)

Figure 2.5: (a) Grating lobes and main beam spectrum for element spacing greater than one wavelength in H-plane. (b) Radiation far-field pattern of 32×32-element array with element spacing equal to 6λ in H-plane, and smaller than λ in E-plane.

lobe at the grazing angle since the slot element has a cosine shape pattern in H-plane, which tapers the total array's far-field radiation pattern. The aperture efficiency of a 32×32-elements array with different element spacing in H-plane is shown in Fig. 2.6. The element spacing in H-plane varies from 0.6λ to 10λ, and the element spacing is fixed to $d_y = 0.67\lambda$ in E-plane, contrary to our assumptions in the previous section. The accuracy of the grating efficiency formula on the presence of grating lobes in different planes, and even when scanning the beam, is evaluated in [Paper A] in more detail. It is expected that this formula would also be quite accurate for other types of array elements that radiate from or above metal ground planes.

2.3 Embedded Element Efficiency

In 1964, Hannan addressed the so-called element-gain paradox in antenna arrays by introducing an embedded element efficiency concept [51]. In the element-gain paradox, the array gain is always smaller than the sum of the element gains. In [Paper B] the usefulness of his approach has been shown by evaluating directivities and aperture efficiencies of an array of slots by using commercial full-wave EM solvers. The results show that by using embedded element analysis, the realized gain of regular arrays actually becomes equal to the sum of the realized gains of the embedded elements. Therefore, the embedded element efficiency is more practical to use in design and numerical analysis, than the more commonly used active element pattern approach. The more popular approach to analyze

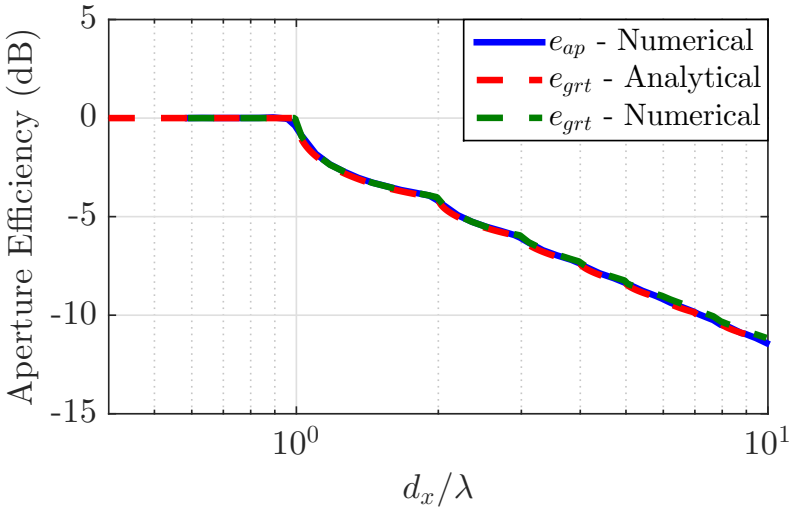

Figure 2.6: Aperture efficiency of 32×32-element slot array with different element spacing in H-plane.

array antennas is to use the active element pattern [52, 53]. The active element pattern is the far-field function when all elements are excited. However, the active element pattern is a theoretical construction that cannot be directly measured, whereas the embedded element is very practical and directly measurable on its ports.

Dense arrays suffer from strong mutual coupling among the ports of the neighboring elements. The overall effect of the mutual coupling is characterized by the radiation efficiencies of the embedded elements of the array, and this is the essential degrading performance parameter of multi-port antennas for MIMO systems [54].

Consider again an array of 32×32 open-ended waveguides, each of them with aperture dimensions $a = 0.505\lambda$ and $b = 0.067\lambda$ along y-and x-directions as shown in Fig. 2.2. Fig. 2.7 shows the realized gain of the array as a function of the element spacing in E-plane. The element spacing is fixed to $d_x = 0.67\lambda$ in x-direction (H-plane) and it varies from 0.1λ to 10λ in y-direction (E-plane). Therefore, when the element spacing is 0.1λ, parallel slots are extremely close to each other, and when the element spacing is 10λ they are very far apart. The maximum available directivity ($D_{max} = 4\pi A/\lambda^2$) of the array is plotted as the straight solid diagonal line in Fig. 2.7 marked as "maximum available". The realized gains of the whole array and of its elements have been calculated by three different full-wave numerical approaches:

(a) **Infinite array approach**: This consists of simulating a unit cell of the array with periodic boundary conditions, and corresponds to exciting all waveguide elements with the same amplitude and phase.

(b) **Embedded element approach**: An element in the center of the array is simulated when all the other elements are present and terminated. The realized gain of the

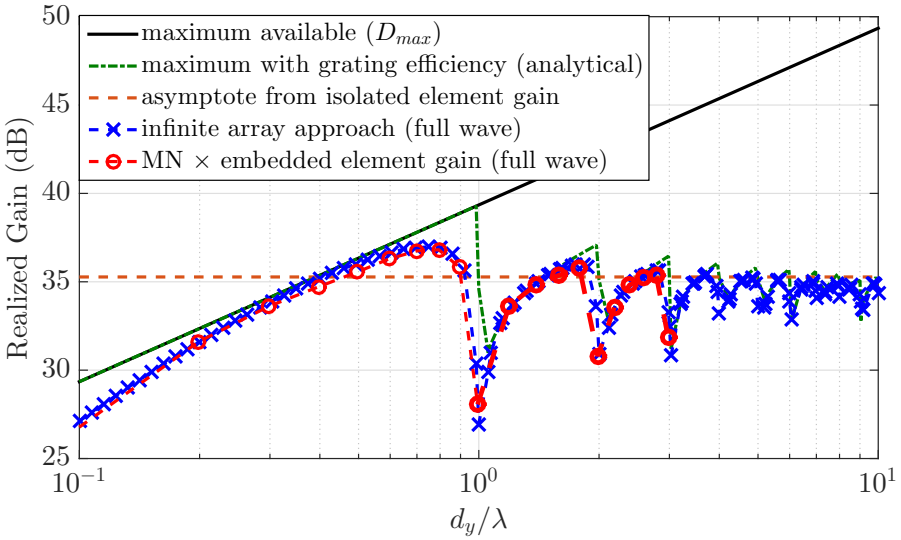

Figure 2.7: Realized gain of 32×32 element regular array of open-ended waveguides in infinite ground plane when the element spacing in H-plane is $d_x = 0.67\lambda$ for different element spacings in E-plane, by using different methods.

total array is $G_{arr} = MNG_{emb}$.

(c) **Isolated element approach**: This is one open-ended waveguide in an infinite ground plane. An approximate array gain can be obtained from $G_{arr} = MNG_{iso}$. This result is shown as the curve called "asymptote from isolated element gain" in Fig. 2.7. The directivity of the isolated element can in our case also be found analytically to be 5.2 dBi from the analytical far-field function of a single slot [50].

Fig. 2.7 shows that the gain simulated with the infinite array method approaches the isolated element asymptote in a slowly oscillating manner for large d_y. The slow convergence is due to all the grating-lobes that appear with periodic intervals of 1λ. They have a large effect in E-plane because the isolated element pattern of a slot is omnidirectional in E-plane.

Fig. 2.8 represents the embedded element efficiencies evaluated in different ways for small element spacing d_y/λ. The continuous straight red line shows Hannan's asymptotic formula as follows:

$$e_{\text{emb}} = \pi \frac{d_x}{\lambda} \frac{d_y}{\lambda} \tag{2.6}$$

The continuous blue line with squares is obtained by using the definition of the embedded element efficiency for a lossless multi-port antenna following the next equation:

$$(e_{emb})_j = 1 - \sum_{i=1}^{MN} |S_{ij}|^2 \tag{2.7}$$

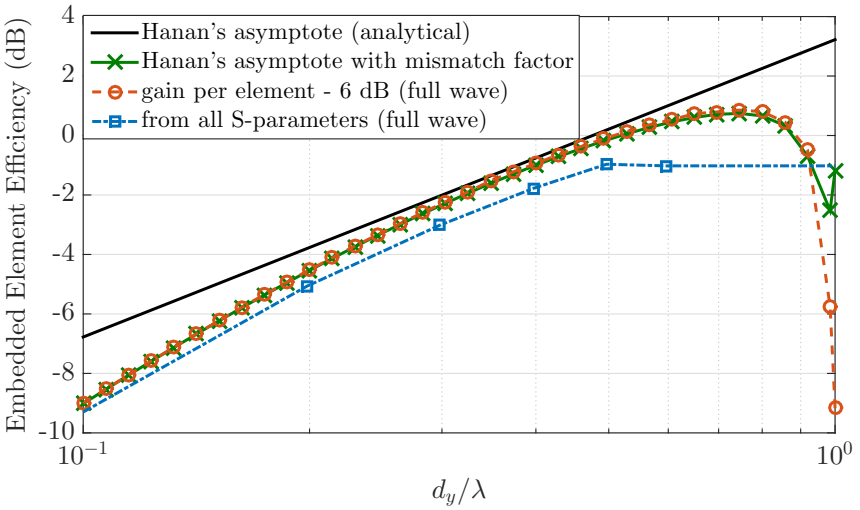

Figure 2.8: Embedded element efficiency of the same 32×32 array as in Fig. 2.7, evaluated by different accurate and approximate methods.

where S_{ij} is the S-parameter between ports i and j. It is evaluated numerically from all S-parameters obtained from the embedded element simulations described in (b) and marked as "from all S-parameters". Therefore, the embedded element efficiency is seen to represent the sum of the power lost in the matched source impedance on the excited port, as well as in the matched loads on all unexcited ports.

The dashed green line shows the embedded element efficiency when correcting Hannan's asymptote by the mismatch factor of the fully-excited array, i.e., the mismatch factor when all elements are equally excited. The final curve of circles is marked "gain per element minus 6 dB". This is obtained by taking the result from the infinite array approach, dividing it with MN to get the realized gain per element, and finally removing the 6 dB directivity of a single embedded element in a dense array.

The results show that Hannan's asymptote represents the highest efficiency for all d_y/λ. Thus, it is the fundamental limiting factor describing the fact that the embedded element will have low radiation efficiency in dense arrays. By correcting this with the mismatch factor, the same result has been obtained from the full wave simulation ("gain per element minus 6 dB"). This demonstrates that it is very easy to correct from Hannan's asymptote to get the actual realized gain in dense regular arrays, but then we need to know the S-parameters of the array elements when all the elements are excited. Finally, we can see that the actual embedded element efficiency evaluated from all S-parameters using (2.7) is lower than the four other results, and approaches them for small element spacing.

Eq. (2.7) can never be larger than unity (0 dB) by definition. However, the three other curves can be larger than unity when the assumptions $d_x \ll \lambda$ and $d_y \ll \lambda$ for which they are evaluated, are not satisfied. This assumption is implicit also in the full wave

efficiencies when assuming that the directivity of the embedded element is 6 dBi. If the directivity is larger, the computed value of the embedded element efficiency will be lower and, thereby, satisfy the physical requirement of $e_{emb} \leqslant 1$.

2.4 Summary and Conclusions

In this chapter, a brief theoretical background of array antennas is presented. Two extreme cases where the element spacing becomes larger than one wavelength and smaller than half a wavelength have been carefully investigated. We have presented and verified a simple formula called "grating efficiency" for calculating the aperture efficiency of regular array antennas in the presence of grating lobes. This formula is verified by considering a large uniformly excited planar slot array antenna and using EM simulations and analytical approach. The agreement is good for both the broadside radiation and steered main beam, as shown in [Paper A]. Moreover, we have numerically shown that the embedded element efficiency fully explains the so-called element-gain paradox as theoretically predicted by Hannan [51] and Kahn [55].

Chapter 3

Gap Waveguide Technology Principle and Overview

The gap waveguide technology was recently introduced in [56] as an extension of previous studies on *hard* and *soft* surfaces presented in [57]. In brief, gap waveguide technology can be explained as a new metamaterial-based wave-guiding structure that uses a periodic electromagnetic band gap (EBG) geometry around a certain type of guiding path, such as strip, ridge or groove to control the power flow direction. The foundation of gap waveguide is originated from *soft/hard* boundary conditions and the cutoff of electromagnetic waves on a parallel *PEC/PMC* waveguide configuration. The *soft* surface has the ability to stop the propagation of any polarization wave along the surface. For example, corrugations act as a *soft* surface along the direction of the corrugation. On the other hand, the *hard* surface supports the propagation of waves along its surface.

3.1 Gap Waveguide Concept

As briefly mentioned, the fundamental operating principle of gap waveguide technology is based on the cutoff of any propagating wave on a PEC/PMC parallel-plate waveguide configuration. When the air gap between the two plates is smaller than $\lambda/4$, no wave can propagate between the plates, due to the existing PEC/PMC boundary conditions. This idea is shown in Fig.3.1. By introducing a metal strip in the PMC surface, a *TEM* mode will be able to propagate along the strip. Therefore, in the latter situation we can control the propagation of waves in desired directions between the two plates.

In practice, the PMC condition is artificially realized by using Artificial Magnetic Conductors (AMCs) to emulate the high impedance boundary condition of a PMC surface [58]. In gap waveguides, the AMC is realized in the form of periodic textured structures (e.g. metal pins or mushroom structures) in combination with a smooth metal plate, with an air gap between them. When the air gap is smaller than quarter wavelength there is a cutoff of all propagating modes within the gap due to the high surface impedance created

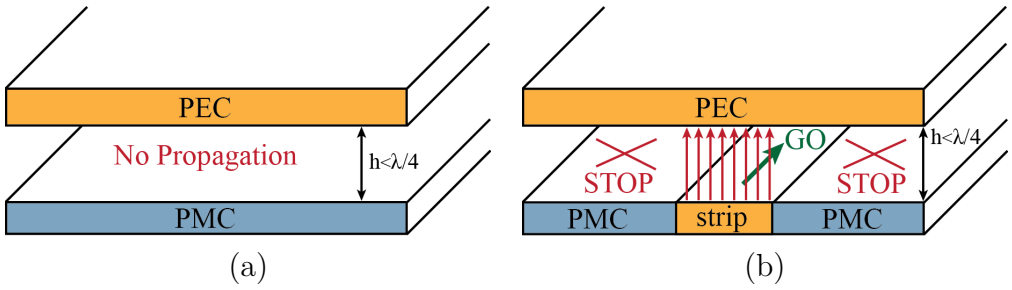

Figure 3.1: Basic operating principle of gap waveguide. (a) $PEC - PMC$ Parallel-plate electromagnetic wave cutoff. (b) TEM local waves propagation.

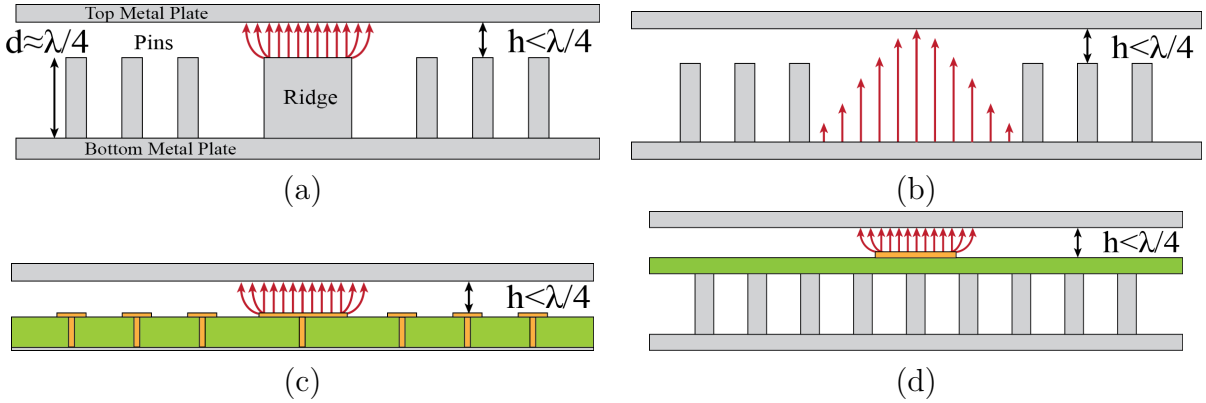

Figure 3.2: Different gap waveguide geometries and desired modes of propagation. (a) Ridge gap waveguide. (b) Groove gap waveguide. (c) Microstrip gap waveguide. (d) Inverted-microstrip gap waveguide. [60]

by the periodic texture [59]. This can be used to control the direction of propagation of the wave without leaking away in other directions.

Based on the type of guiding line, propagation characteristics and band gap structure, the gap waveguide can be realized in different versions. Ridge gap waveguide [61], groove gap waveguide [62], microstrip gap waveguide [63], and inverted microstrip-ridge gap waveguide [64] are the four basic varieties of gap waveguide technology. Fig.3.2 shows the different gap waveguide configurations and the fundamental modes. The ridge gap and groove gap waveguides can be seen as equivalent versions of ridge waveguide and rectangular waveguide transmission lines, respectively [65].

The printed versions, i.e. microstrip and inverted-microstrip gap waveguides, use the advantages of printed circuit board (PCB) technology to fabricate the guiding line with a simple and cost-effective method. The inverted-microstrip gap waveguide consists of a strip line placed on a substrate layer. In this configuration, a quasi-TEM mode propagates in the gap between the strip and the top plate. The substrate is packaged with a bed of nails from the backside, which eliminates any possible leakage and surface waves within the substrate. In microstrip gap waveguide, the periodic EBG structure is embedded

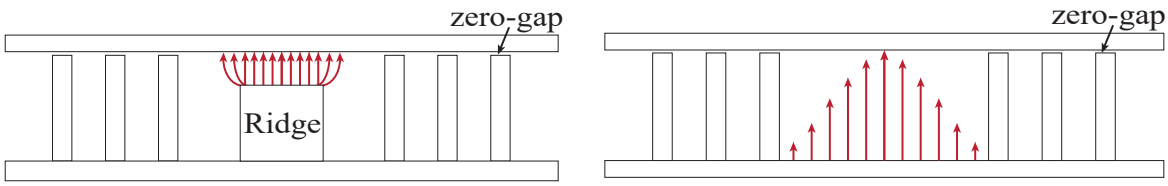

(a) (b)

Figure 3.3: Cross-sections of zero-gap concept. (a) Ridge zero-gap waveguide, and (b) Groove zero-gap waveguide.

within the substrate by using mushrooms, which offers a compact design. In the printed gap waveguide, the field is mainly propagating within the air gap between the strip line and the upper lid. However, it has been shown in [64,64] that the fringing field goes inside the substrate and increases the insertion loss.

Gap waveguides have interesting characteristics such as low loss, flexible planar manufacturing, and cost-effectiveness [66]. The most remarkable advantage compared to traditional planar transmission lines like microstrip , CPW and SIW, is that the gap waveguide provides a planar profile with low loss, since the wave propagates in the air. This new technology has almost no dielectric loss (especially in ridge and groove gap waveguide configurations), and it is mechanically more flexible to fabricate and assemble than hollow waveguide structures. This mechanical flexibility is due to the fact that good electrical contact between the different building blocks of a gap waveguide prototype is not needed because any possible leakage of fields is eliminated by the inherent cutoff principle provided by the PEC/PMC configuration.

Previous works on gap waveguide in [64, 67] show that at high frequencies the assembly tolerances, specially related to the gap stability, can affect the overall component performance. A new gap waveguide concept, so-called zero-gap, is presented in [Paper G], where the air gap between the upper lid and the pin texture of the conventional gap waveguide structures has been reduced to almost zero. Fig.3.3 shows a sketch of ridge zero-gap waveguide and groove zero-gap waveguide structures. When the air gap is reduced, the periodic metal pin layer (which emulates the AMC characteristics) may come in contact with the top metal lid. A statistical analysis of a random contact of the pin texture and the top metal plate is performed in [Paper G] in order to investigate the effect of uncertain capacitances between the pins and upper plate. In this new gap waveguide variety, the periodic pin texture creates a stopband for parallel plate modes, and it is also used as a mechanical support while assembling the waveguide structure. This represents a significant manufacturing advantage especially for corporate feed-network of array antennas at millimeter-wave frequencies. All the designed antennas, diplexers, and integrated modules presented in this thesis are based on ridge and groove zero-gap waveguides as shown in Fig.3.3.

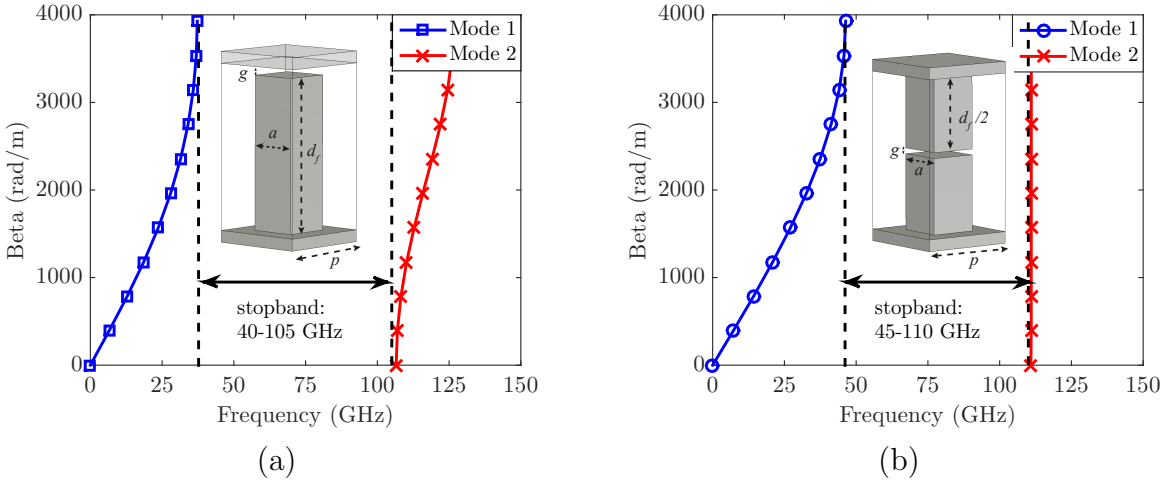

Figure 3.4: Dispersion diagram for the infinite periodic pin unit cell (a=0.4 mm, d_f=1.3 mm, p=0.8 mm, and g=0.05 mm).

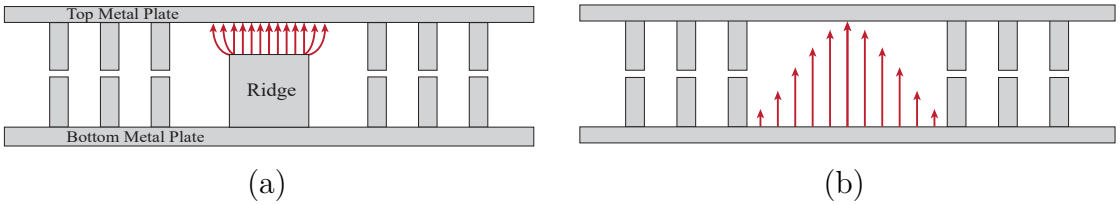

Figure 3.5: Geometry of (a) ridge gap waveguide, and (b) groove gap waveguide with half-height pin unit cell.

3.1.1 Dispersion diagram of periodic EBG

As mentioned before, the periodic texture (e.g. pins or mushrooms) creates a stopband for the parallel-plate modes and suppresses undesired modes and any potential field leakage. It acts as a high impedance surface when the air gap is smaller than $\lambda/4$. The dispersion diagram of the unit cell of the periodic structure is the most important parameter when designing the stopband, which is a function of the geometrical parameters of the structure. In [59] a generic study and performance evaluation of different periodic EBG structures, such as pins, corrugations, and mushrooms to use in gap waveguide technology is thoroughly evaluated.

Fig. 3.4 shows the dispersion diagrams of two pin unit cells that create the stopband for the parallel plate modes presenting more than one octave bandwidth. The dispersion diagrams of these unit cells are calculated using the Eigenmode solver of CST Microwave Studio by considering periodic boundary conditions. The pin dimensions have been suitably chosen to provide a stopband that covers sufficiently the whole V-band. Fig. 3.4(a) shows a conventional pin unit cell that is typically used to form ridge and groove gap

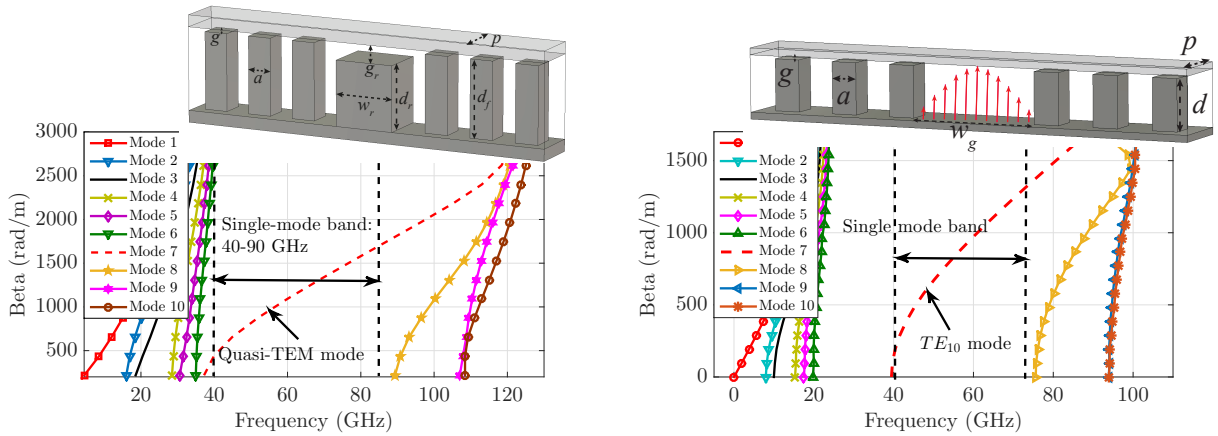

Figure 3.6: Dispersion diagram for the infinite periodic unit cell including, (a) A ridge embedded within a pin texture (a=0.4 mm, d_f=1.3 mm, p=0.8 mm, g=0.05 mm, g$_r$=0.25 mm, w_r=1 mm, and d_r=1.1 mm), and (b) A groove within pins texture (w_g=3.78 mm, d=1.5 mm, a=0.75 mm, g=0.05 mm, and p=1.8 mm).

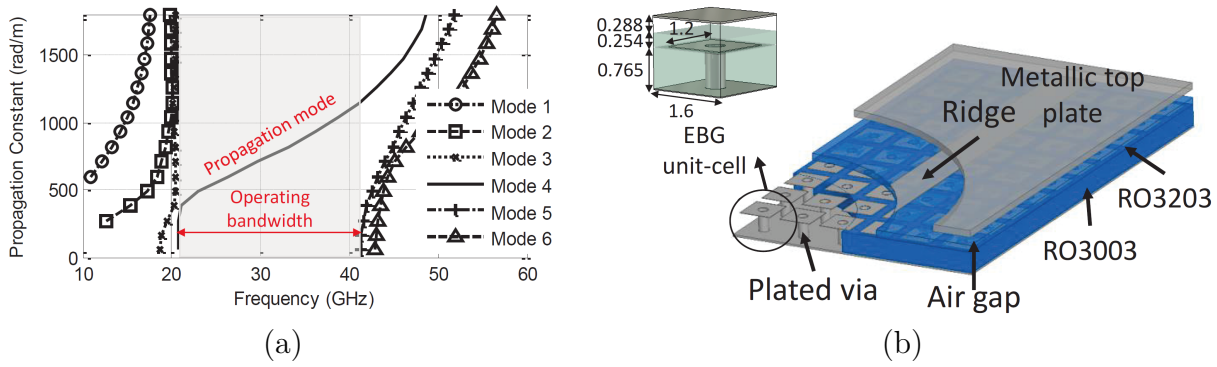

Figure 3.7: (a) Geometry of printed inverted-microstrip gap waveguide, and (b) Dispersion diagram of the EBG unit cell [68].

waveguide transmission lines of Fig. 3.2(a) and (b). As can be seen, the aspect ratio of the pin (the ratio of the height to the width) is very high (3.25:1), which makes it difficult to manufacture especially with some fabrication techniques such as injection molding. In [69, 70] a new form of pin unit cell, so-called half-height, is presented to facilitate the fabrication. Fig. 3.4(b) shows a half-height pin and its corresponding dispersion diagram. In this unit cell both the upper and lower plates have pins with half of the height of the original ones as shown in Fig. 3.4(a). Fig. 3.5 illustrates the geometry of rigde gap waveguide and groove gap waveguide with half-height pin texture in contrast with the conventional gap waveguide technology types of Fig. 3.2.

By introducing a ridge between the pin texture, a quasi-TEM mode propagates in

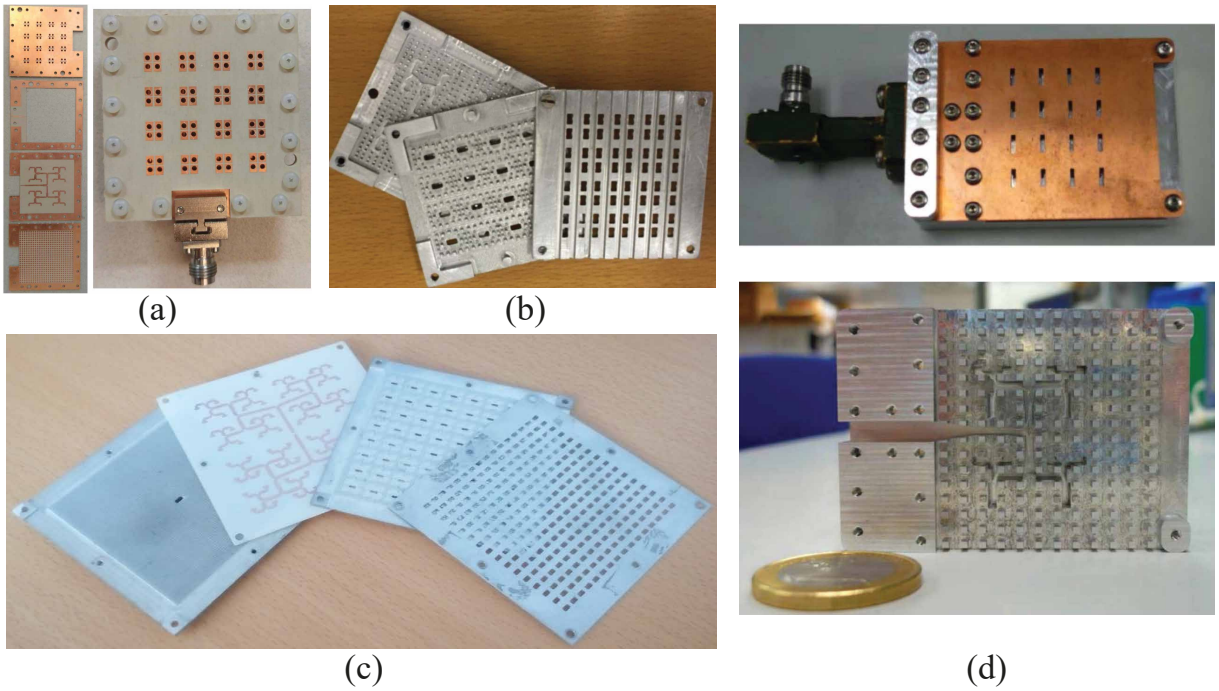

Figure 3.8: Gap waveguide array antennas. (a) Magneto-electric dipole antenna with microstrip gap waveguide feed network [71], (b) Cavity-backed slot array antenna with ridge gap waveguide feed network [72], (c) Slot array antenna with inverted gap waveguide feed network [73], and (d) Single-layer slot array antenna with groove gap waveguide feed network [74].

the air gap between the ridge and the upper plate. Fig. 3.6(a) shows that there is a single propagating mode over the frequency band 40-90 GHz, which covers the whole unlicensed 60 GHz frequency band. The pin texture can also be used to constitute a groove that supports the propagation of the fundamental TE_{10} mode, as shown in Fig. 3.6(b). Moreover, the bed of nails of the inverted-microstrip waveguide can also be replaced by a mushroom-type EBG structure as illustrated in Fig. 3.7. It is important to remark that in all these gap waveguide variants there is no need for good electrical contact between the textured surface and the upper metal plate. This is due to the electromagnetic bandgap properties provided by the pin or mushroom-type EBG surfaces.

3.2 Gap Waveguide Benefits and Early Studies

The usefulness of gap waveguide technology has been evaluated and demonstrated in many different applications. A summary and an overview of some pioneer works that have been explored and shown the advantages of gap waveguide are presented in this section.

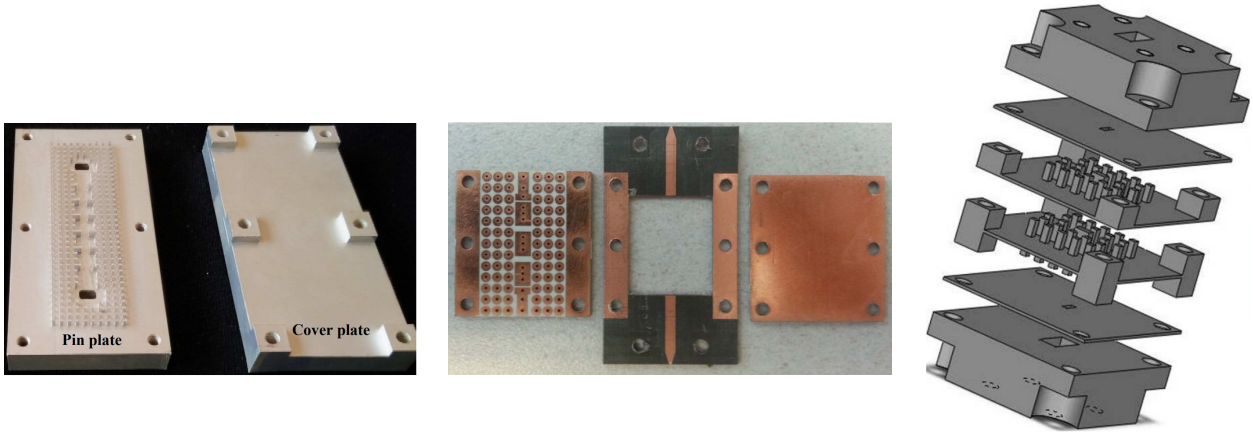

(a) (b) (c)

Figure 3.9: Gap waveguide bandpass filters based on, (a) groove gap waveguide [91], (b) microstrip gap waveguide [92], and (c) ridge gap waveguide stacked resonators [93].

3.2.1 Transitions

Since the gap waveguide is a new type of transmission line, there is a critical need for transitions between different gap waveguide variants and conventional transmission lines. Several transitions working at different frequency bands and showing diverse arrangements, such as ridge gap waveguide to coaxial [75], inverted-microstrip gap waveguide to rectangular waveguide [64], ridge gap waveguide to CPW [76], ridge gap waveguide to microstrip line [67, 77, 78], groove gap waveguide to microstrip line [79, 80], and groove gap waveguide to rectangular waveguide [81], have been introduced and experimentally validated.

3.2.2 Planar array antennas

Hollow waveguide array antennas have a rather complex structure that makes the fabrication and assembly a challenging task at high frequencies. Due to the low loss performance and no strict requirement for good electrical and galvanic contact between the building blocks, gap waveguide technology offers a huge potential to design high gain and high efficiency array antenna. Several array antennas with gap waveguide corporate feed network showing features of low loss in groove and ridge gap waveguide [72, 74, 82–87] , and compactness in PCB versions of gap waveguide technology [33, 71, 73, 88–90] have been demonstrated.

3.2.3 Resonators and filters

Bandpass filters require low loss cavities and resonators to achieve high Q-factor. Several bandpass filters have been realized based on different varieties of gap waveguide

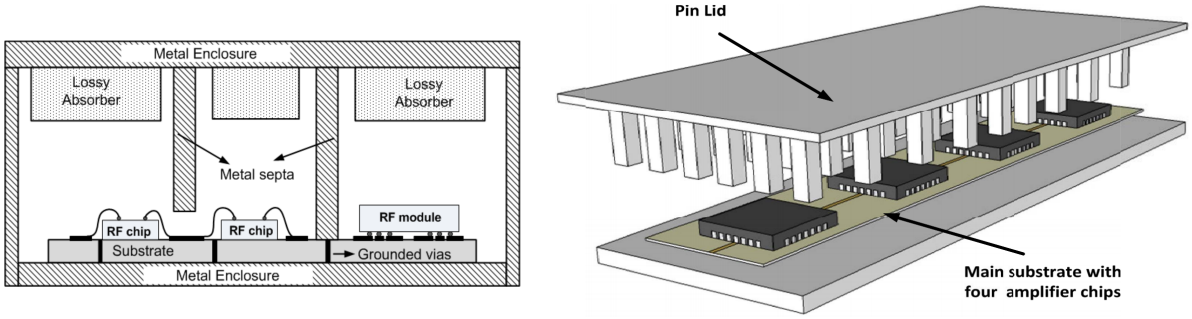

(a) (b)

Figure 3.10: RF circuit module packaging. (a) Sketch of conventional packaging approach by using shielding box and absorber. (b) PMC gap waveguide packaging solution [106].

technology. The Q-factors of the ridge and groove gap waveguide resonators have been investigated in [94] and compared with the Q value of a conventional rectangular waveguide. If high Q-factor and low loss performance are required, groove gap waveguide is the best choice. Different types of bandpass filters based on groove gap waveguide have been reported in [91, 95–101]. Moreover, compact bandpass filters using ridge gap waveguide [93, 102, 103], microstrip gap waveguide [92], inverted-microstrip gap waveguide [104], and printed inverted-microstrip gap waveguide [105], have also been numerically and experimentally evaluated.

3.2.4 Packaging

Microstrip and CPW transmission lines are open structures and the final product needs to be protected from interferences and physical damages. The traditional packaging method is based on using metal shielding boxes, where the main drawback is the appearance of cavity resonance modes when two of the dimensions of the box are larger than half wavelength. It is possible to suppress these resonances by applying absorber materials. The use of absorbers placed in multi-compartment enclosures can also provide good isolation between neighboring circuitry, as shown in Fig . 3.10(a). However, this packaging approach introduces additional losses in the system. The AMC of the gap waveguide technology can be used to package circuits and suppress the parallel plate cavity modes [107]. In [106] a bed of nails is used to improve the isolation performance among several high-gain amplifier chains. Moreover, packaging of a microstrip coupled-line bandpass filter [108] and SIW-GCPW bandpass filter [109], as well as a monolithic microwave integrated circuits (MMIC) power amplifier (PA) packaging solution in [110], are some of the recent works on using gap waveguide technology for passive and active packaging applications. Moreover, a spatial power splitter-combiner structure is presented in [111] to design of planar grid amplifiers packaged in gap waveguide technology.

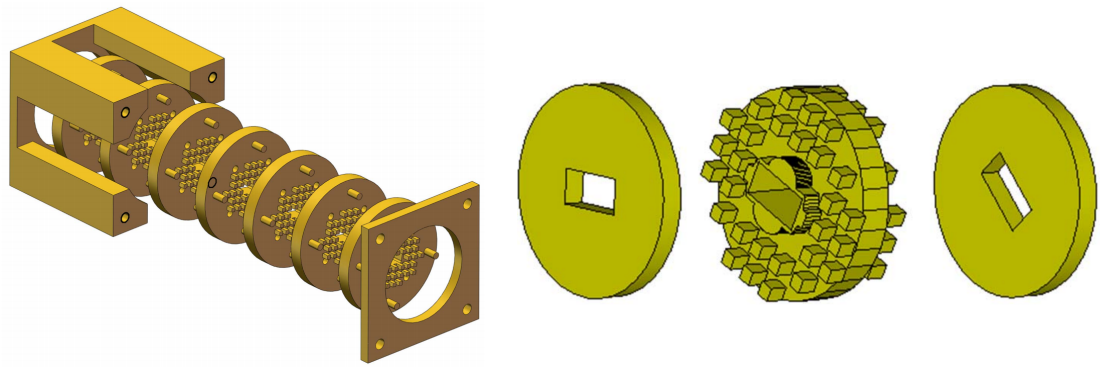

(a) (b)

Figure 3.11: Geometry gap waveguide twist. (a) 3-D exploded view of the 7-steps 90° twist [117]. (b) One-step 45° double-wing twist [118].

3.2.5 Contactless pin flange and twist

At high frequencies, hollow waveguides are widely used to maintain a low insertion loss. Therefore, standard waveguide flanges are used to connect and assemble different waveguide blocks, as well as for measurement purposes. A good and smooth connection between the flange surfaces without any gap is required to avoid potential leakage. A gap waveguide pin flange has been introduced in [112, 113] to remove the need for good joint contact in the mechanical assembly of waveguide structures. The pin flange provides a leakage-free contactless connection, which is advantageous at millimeter-wave frequencies. Furthermore, the realization of gap waveguide prototypes for frequencies above 100 GHz has been explored in [114–116] by fabricating pin flanges with micromachined technology in silicon and SU8.

This concept is further developed to design a rotatable waveguide twist to transform polarization between two waveguide ports. A Ka-band twist with 7 stacked layers that can provide 90° polarization rotation is presented in [117]. Moreover, single-step double-sided twist at E-band with a 45° twist is developed in [118] (Fig. 3.11).

3.3 Summary and Conclusions

In this chapter, brief basic theory and working principles of the gap waveguide technology has been given. The gap waveguide technology is a new type of guiding structure that can achieve low-loss performance, manufacturing flexibility, and cost effectiveness without the need for galvanic contact among the different building blocks of the waveguide structure. Therefore, gap waveguides can be mass-produced by applying some low cost fabrication techniques such as injection molding, die pressing, plastic hot embossing, or die-sink EDM. Gap waveguide technology has a strong potential and exhibits promising advantages for applications at the millimeter-wave frequency range. Several related works

on gap waveguides that show these advantages for different applications have been briefly presented. The metamaterial/metasurface background of gap waveguide technology is described in more detail in [60, 66].

Chapter 4

Gap Waveguide Passive Components Design for Millimeter-Wave Applications

One of the main goals of the conducted research in this thesis has been to design high efficiency low profile array antennas, as well as low loss passive components such as bandpass filters. Our second relevant goal is the realization of a compact and high performance gap waveguide module by integrating those passive components with the feed network of the array antenna.

In this chapter, a summary of developed gap waveguide passive components by the author, such as: transitions and interconnects, bandpass filters and diplexer, as well as array antennas; is introduced. The last section of this chapter deals with a description of different cost-effective manufacturing techniques that have been tested to fabricate some of the proposed gap waveguide antennas. The whole chapter is based on the content of Papers C, D, E, F, G, H, I, and J, where more detailed information about the different designs can be found.

4.1 Transition Design

Since the interface of most testing equipments at high frequency are based on standard hollow rectangular waveguides, low loss, simple and wideband transitions from gap waveguide transmission lines to conventional rectangular waveguide are needed. In this section, two low loss transition designs from groove gap waveguide to rectangular waveguide, and from groove gap waveguide to microstrip line, are presented. The first of these two transitions has been introduced in Paper I. This design consists of a simple and wideband way to interconnect groove gap waveguide to rectangular waveguide with easy assembly to cover the whole V-band (50-75 GHz). The key features of this transition are simplicity, easy assembly, low sensitivity to manufacturing and assembly errors, and wideband performance. Furthermore, the proposed design can be easily scaled to other frequency bands. The fabricated back-to-back prototype by using CNC milling in aluminum is shown in

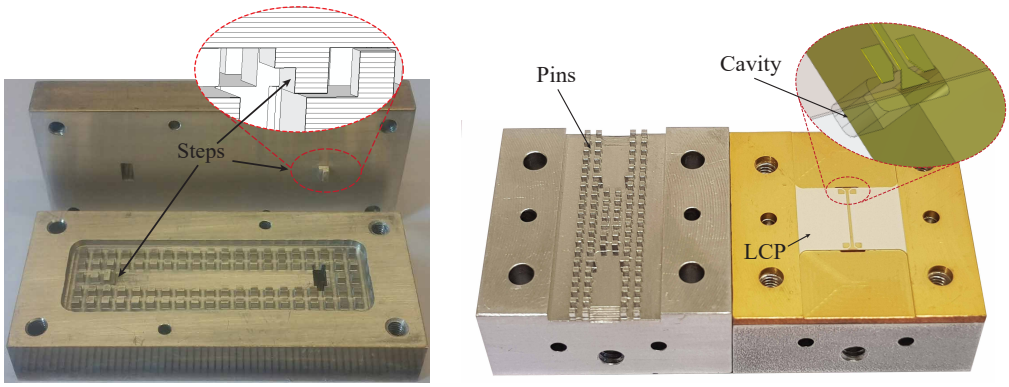

(a) (b)

Figure 4.1: Proposed gap waveguide transitions. (a) Fabricated back-to-back groove gap waveguide to rectangular waveguide right-angle transition [Paper I]. (b) Fabricated back-to-back groove gap waveguide to microstrip line transition [Paper K].

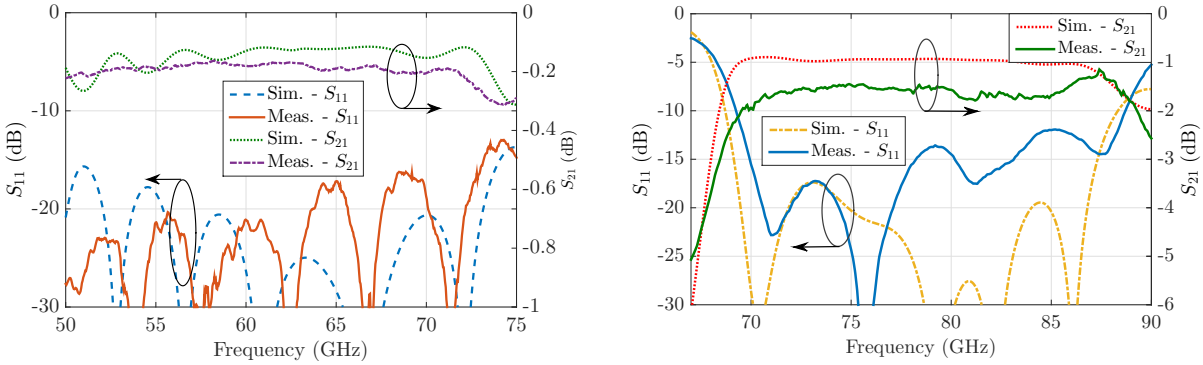

(a) (b)

Figure 4.2: Simulated and measured performance of the fabricated prototypes. (a) Groove gap waveguide to rectangular waveguide transition. (b) Groove gap waveguide to microstrip line transition.

Fig. 4.1(a). The groove gap waveguide line is formed in two separated metal plates, where a pin texture prevents any possible leakage. A simple step shaped metal piece at the end of the groove acts as a 90 ° E-plane bend to match the wave into the rectangular waveguide. In order to have a simple measurement setup and provide enough space for WR-15 waveguide flanges, the ports are located at different metal plates. Therefore, one step transition is placed on the pin texture and one on the top metal plate. Fig. 4.2(a) shows the measured S-parameters in comparison with the simulated results. The measurements for the back-to-back configuration show an insertion loss lower than 0.2 dB, and a reflection coefficient better than -16 dB from 50 to 75 GHz.

Fig. 4.1(b) shows a transition between a microstrip line to groove gap waveguide

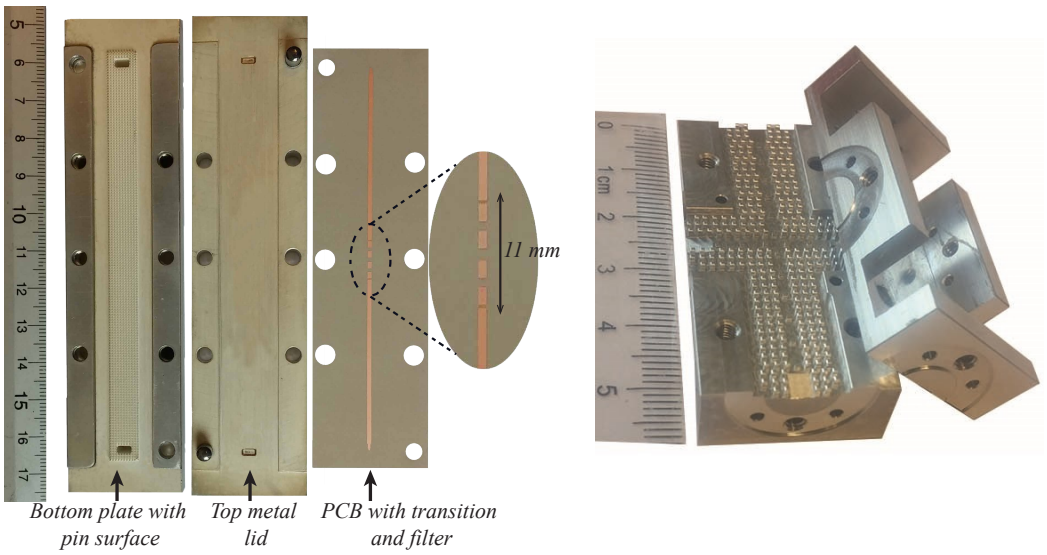

Figure 4.3: (a) A V-band end-coupled bandpass filter based on inverted-microstrip gap waveguide [Paper C]. (b) A 5^{th} order E-band hybrid diplexer-splitter based on groove gap waveguide [Paper K].

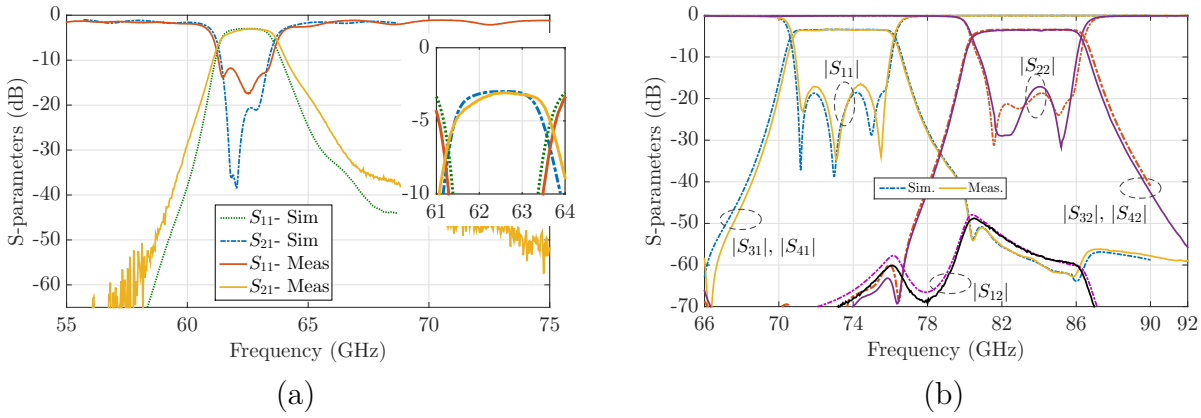

Figure 4.4: Simulated and measured performance of, (a) the fabricated inverted-microstrip gap waveguide filter, (b) the fabricated hybrid diplexer-splitter prototype.

([Paper K]). The proposed transition is formed in two distinct parts, where the energy from the microstrip line couples to the groove gap waveguide via a resonant cavity. The groove is created by a pin texture on the upper layer and a lid on the lower layer. An 8 mm long microstrip line is fabricated on 100 μm LCP substrate (ϵ_r=3.2) with 1 mm thick copper base. An E-plane probe is extended into the cavity and the quasi-TEM mode of the microstrip is matched to the TE_{10} mode of GGW by using the resonant characteristic of the cavity. The cavity has been made within the 1 mm thick copper

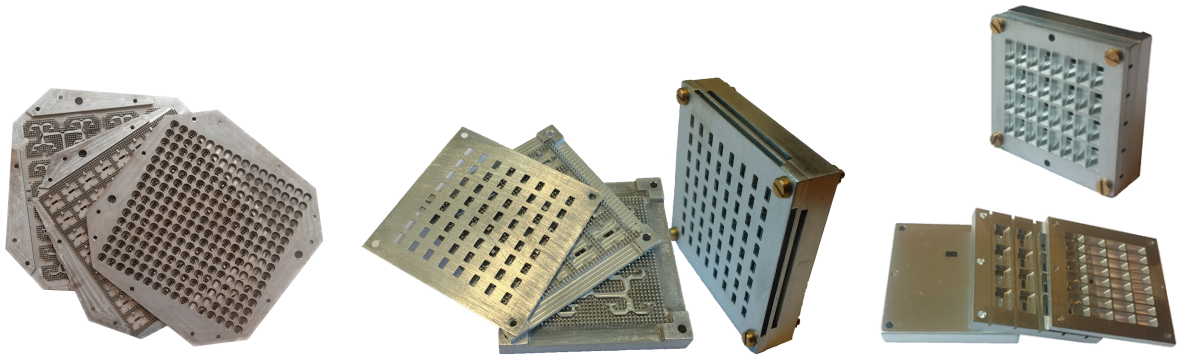

(a) (b) (c)

Figure 4.5: The proposed gap waveguide array antenna. (a) 16×16 slot array antenna at V-band [Paper E]. (b) 8×8 slot array antenna at V-band [Paper D]. (c) A Horn array antenna at E-band [Paper J].

plate. To simplify the fabrication, the cavities are realized by first making through holes with the required dimensions in the 1 mm copper plate, and afterwards the holes are closed from the backside with small metal pieces. The simulated and measured performance of the fabricated back-to-back transition is shown in Fig. 4.2(b). The measured reflection coefficient remains below -12 dB over the frequency band 69-87 GHz. A measured average insertion loss of 1.5 dB has been achieved over the frequency band 71-86 GHz. The measured results in [119] show that the insertion loss of a 50 Ω microstrip line on a 100 μm LCP substrate is around 0.11 dB/mm at 80 GHz. Therefore, by subtracting the loss of the 8 mm microstrip line of the fabricated back-to-back transition, the measured insertion loss of a single transition is estimated to be around 0.31 dB.

4.2 Bandpass Filter and Diplexer

Bandpass filters are essential passive components for most wireless communication systems. Low loss, inexpensive and suitable for mass-production are some of the required features of filters for millimeter-wave frequencies.

We have described the design of a 4^{th} order Chebyshev-type end-coupled bandpass filter in [Paper C] based on inverted microstrip gap waveguide that provides a 2 GHz bandwidth at 60 GHz center frequency. The fabricated prototype is embedded within a 10 cm inverted microstrip gap waveguide line that contains two back-to-back transitions to rectangular waveguide that were previously validated in [64], as shown in Fig. 4.3(a). The simulated and measured S-parameters of the prototype are presented in Fig. 4.4(a). The measurements exhibit an insertion loss of 3 dB in total, where the insertion loss of the filter itself is better than 1.6 dB (1.4 dB is the corresponding loss of the transitions and the extended line). Although microstrip bandpass filters have simple structures, their

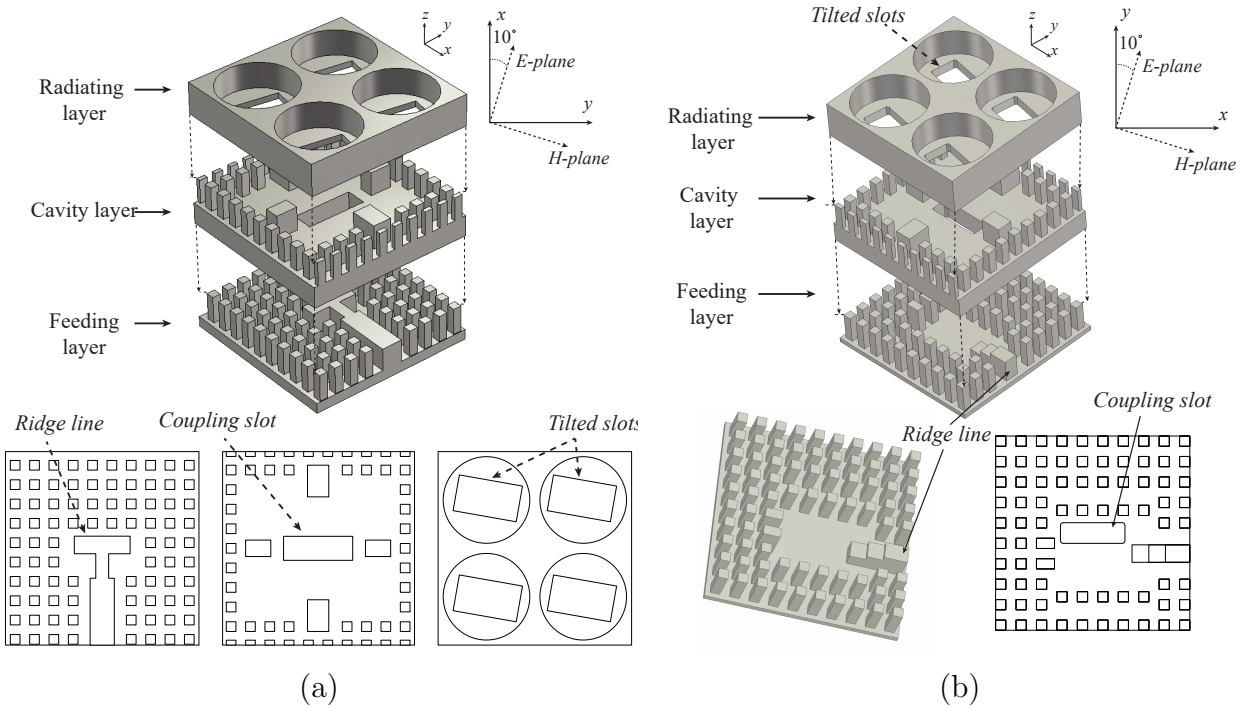

Figure 4.6: Multilayer gap waveguide 2 × 2 cavity-backed slot subarray with different excitation mechanism. (a) T-shaped ridged feeding. (b) Compact feeding with secondary cavity.

applications are limited to microwave frequencies due to high losses. A V-band third order bandpass filter realized in SIW technology is presented in [120]. The fabricated prototype shows an insertion loss of 3 dB at the center frequency of 62 GHz, mainly due to dielectric loss. On the other hand, the designed inverted microstrip gap waveguide in [Paper C] shows around half of that insertion loss of the corresponding SIW filter in [120].

Another gap waveguide filter example is the 5^{th} order hybrid diplexer-splitter which is shown in Fig. 4.3(b). This design consists of a novel architecture that allows for a direct integration with a feed-network of an array antenna ([Paper K]). In order to achieve a compact design, the output of the diplexer is directly connected to a power divider, so that the diplexer acts as a first stage of power division for corporate feeding of an array antenna. The measured and simulated performance of the fabricated prototype is presented in Fig. 4.4(b). The measured input reflection coefficients of the two channels are below -17 dB. The measured isolation between the two input ports ($|S_{12}|$), and the measured isolation between the two channels,($|S_{j1}|, |S_{j2}|$) are both smaller than 50 dB. Fig. 4.4(b) shows that the designed diplexer has a low loss performance. The measured transmission coefficients for both of the channels are better than -3.5 dB, which in an ideal lossless situation should be -3 dB. Therefore, the fabricated prototype shows a maximum 0.5 dB insertion loss.

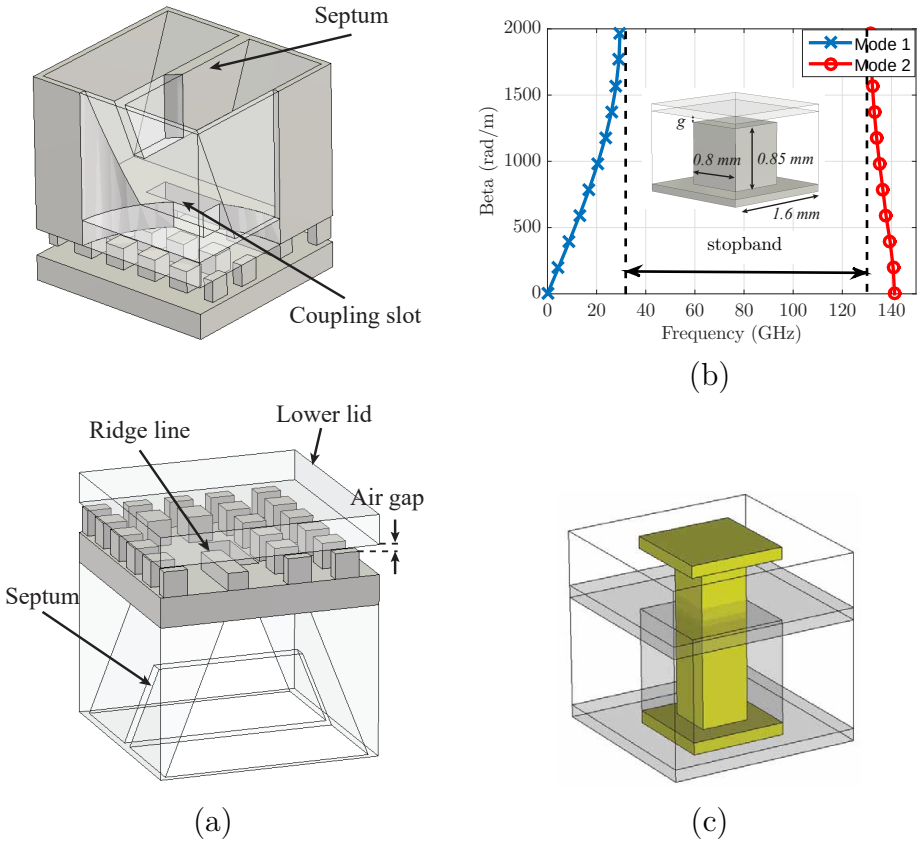

Figure 4.7: The proposed horn subarray with bigger pin texture [Paper J]. (a) Geometry of the subarray. (b) Dispersion diagram of the periodic pin unit cell with bigger size. (c) Comparison of the size and aspect ratio of two pin unit cells.

4.3 Gap Waveguide Array Antennas

We have designed several low-profile array antennas with high efficiency and wide impedance bandwidth based on gap waveguide technology, exhibiting flexible mechanical assembly and low loss. Fig. 4.5 shows some developed array antenna designs at V- and E-band. We have used a multi-layer configuration, where the galvanic and electrical contact among the layers is not required in gap waveguide technology. Several layers with different functionalities are vertically stacked up to form a compact and high performance array antenna.

Fig. 4.6 shows two cavity-backed slot subarrays with different feeding mechanisms, as radiating elements of the slot array antennas. Four slots with cylindrical cavities on the top of them are fed by an air-filled cavity. In Fig. 4.6(a) a T-shaped ridge is used to couple the quasi-TEM mode of the ridge gap waveguide feed network to the cavity via a coupling slot. With this type of feeding, there is only one pin row separation between the ridge lines near the T-shaped ridges in the final distribution feed-network of the designed array, as illustrated in Fig. 4.8. The latter is due to the need for a bend at the end of

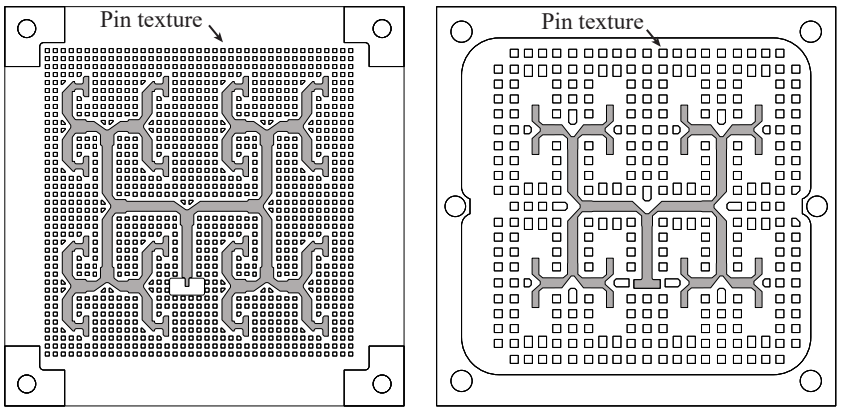

Figure 4.8: Different feeding network solutions. (a) Feed network by using T-shaped ridge [Paper D]. (b) Compact ridge gap waveguide feed network by using secondary cavities [Paper J].

each feeding branches to have an in-phase excitation of the elements of the array. Due to the limited space between the T-shaped section and the adjacent ridge line, the pins size and periodicity need to be small as well.

We have proposed a more compact feeding solution in [Paper F and J]. The quasi-TEM mode of the ridge line is first coupled to a secondary cavity and then to the subarray via a coupling slot, as shown in Fig. 4.6(a). With this new excitation, there are at least two pin rows between the ridge lines in the final feed network, and consequently adequate space to integrate for example a diplexer into the distributing feeding network, as described in detail in [Paper F].

Another advantage of the feeding via a secondary cavity is that we can use bigger pins with larger periodicity and still be able to accommodate the corporate feeding of array ([Paper J]). Fig. 4.7(a) shows a wideband horn subarray fed by ridge gap waveguide at E-band. The subarray dimensions in the E- and H-plane is larger than one wavelength, which causes grating lobes. The grating lobes and sidelobes in the H-plane have been suppressed by inserting a septum in the middle of the horn's aperture in the E-plane. The horn is fed by a ridge line from the backside.

Fig. 4.8 shows the ridge gap waveguide feed networks of a 8×8 slot array antenna at V-band ([Paper D]) and a horn array at E-band ([Paper J]), where the two different feeding mechanisms are illustrated, i.e. via T-shaped ridges and via secondary cavities. As can be seen, the new feeding mechanism via a secondary cavity allows to use bigger pins (with around twice of the size). Fig. 4.7(b) shows the dispersion diagram of the corresponding bigger pin unit cell, which can be compared to the dispersion diagram of the thinner pins that is presented in Fig. 3.4(a). The bigger pin unit cell has an aspect ratio of around one ($\frac{0.85}{0.8}$), which makes the fabrication much easier. A comparison of the size of the two pin unit cells is illustrated in Fig. 4.7(c) for an easier visualization.

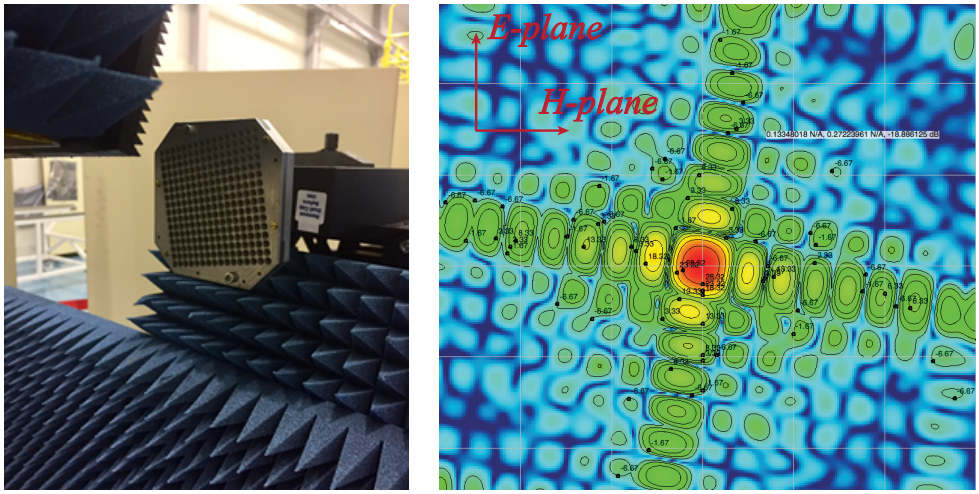

(a) (b)

Figure 4.9: (a) Near-field radiation patterns and gain measurement setup. (b) Measured 2-D far-field radiation pattern at 62 GHz.

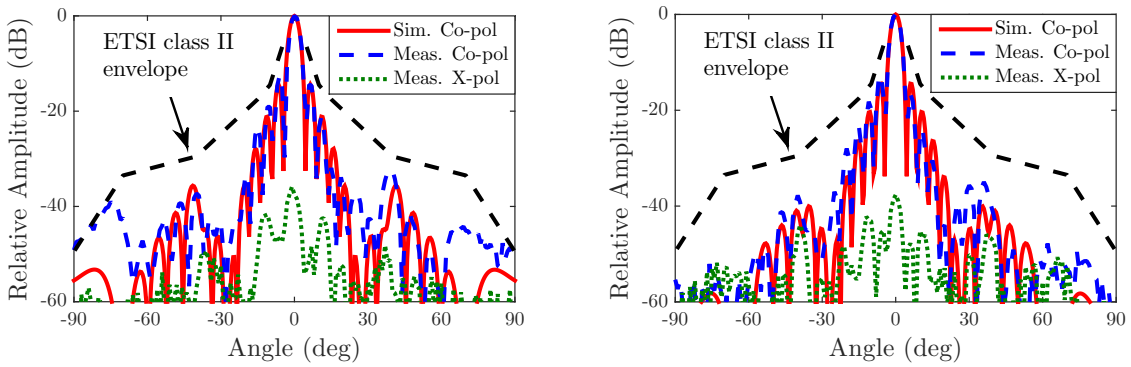

(a) (b)

Figure 4.10: Simulated and measured radiation patterns of the proposed array antenna at 62 GHz. (a) E-plane. (b) H-plane.

For backhaul wireless links high gain antennas with low far-sidelobe level in the horizontal principle plane are required, as specified by ETSI and FCC standards [121]. In the cavity-backed slot subarrays of Fig. 4.6, the slots are tilted by 10° in order to improve the far-field radiation characteristics of the antenna and satisfy the ETSI class II sidelobe requirement. In this way, the sidelobe levels of the antenna are reduced by separating the E- and H-planes of the antenna from the principal planes of the array. Fig. 4.9 shows the near-field measurement setup and the 2-D radiation pattern of the 16×16 slot array antenna proposed in [Paper E]. As can be seen, the high sidelobes are not in the E- and H-planes of the antenna, while the E- and H-planes are kept in the vertical and horizontal planes. The simulated and measured radiation patterns of the antenna in the E- and

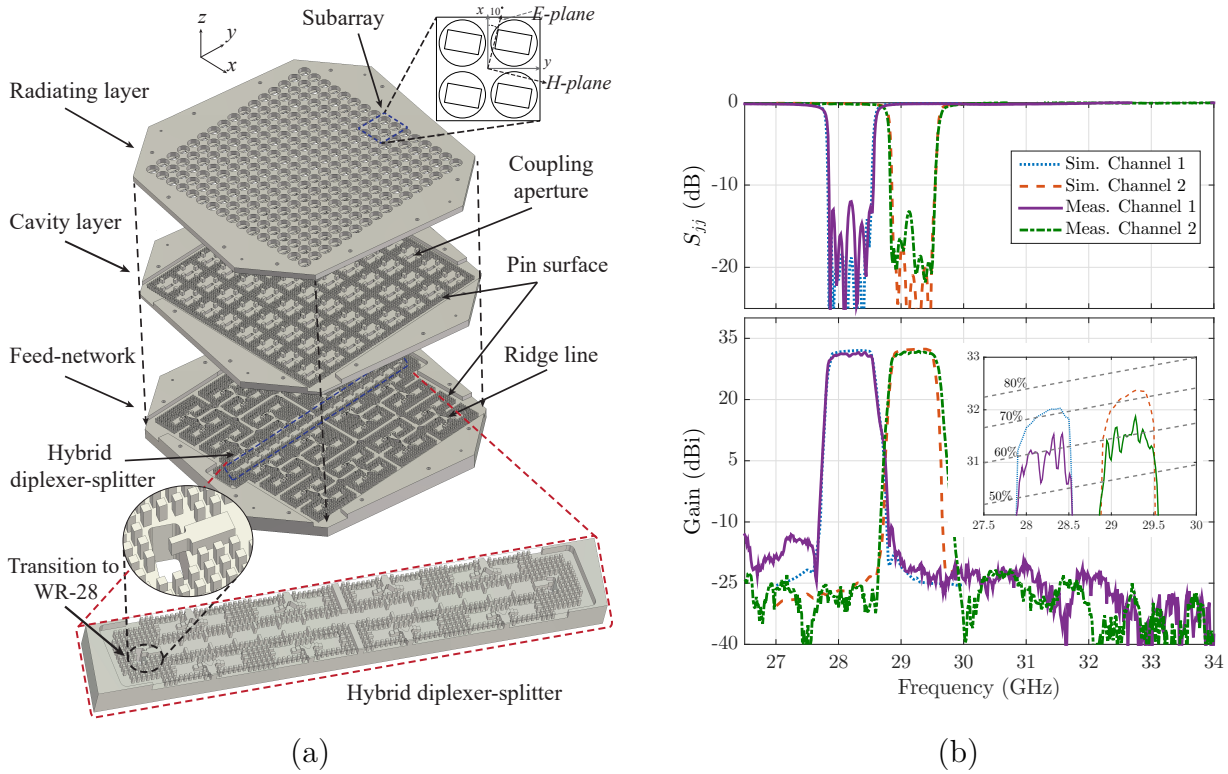

Figure 4.11: Compact integrated diplexer-antenna module at Ka-band [Paper F]. (a) Configuration of the proposed diplexer-antenna. (b) Simulated and measured reflection coefficients and gain.

H-planes at 62 GHz are presented in Fig. 4.10, where the ETSI class II mask is also illustrated. With the proposed approach a low far-sidelobe level has been achieved without reducing the aperture efficiency of the antenna that would happen by using, for example, amplitude tapering of the aperture power distribution of array.

4.4 Passive Component Integration

In this section we present two examples of how, by using gap waveguide technology, we can achieve a simple and compact passive component integration together with high gain array antennas in the same module.

4.4.1 Integrated antenna-diplexer module

Frequency-division duplexing (FDD) communication backhaul links are widely used to increase spectral efficiency and transmit and receive data simultaneously. A high gain antenna connected to a diplexer are key passive components of such systems, and by integrating them, significant reduction of the total size and cost of the system can be

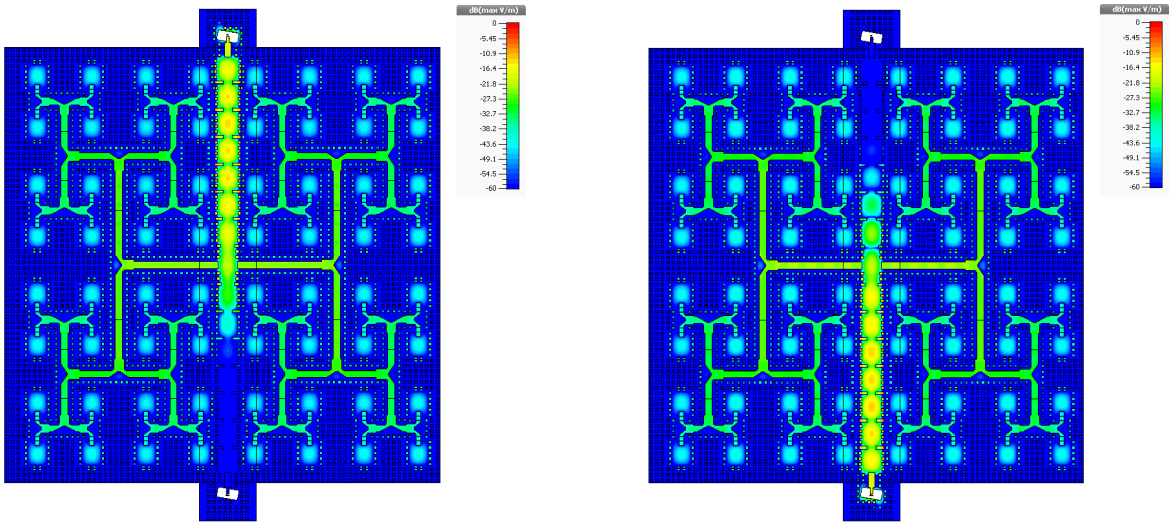

(a) (b)

Figure 4.12: Simulated E-field distribution within the feed-network of the integrated diplexer-antenna module at (a) 28.2 GHz, and (b) 29.2 GHz.

achieved. In [Paper F] we have presented the integration of a 7^{th} order diplexer with a corporate feed network of a high-gain gap waveguide 16×16 slot array antenna operating at Ka-band. The configuration of the integrated diplexer-antenna module is illustrated in Fig. 4.11(a). The designed module has two channels of 650 MHz bandwidths each with center frequencies 28.2 GHz and 29.2 GHz. The detailed design procedure of a new method for designing large-scale filters and diplexers based on the group delay responses of sub-circuits in combination with space mapping is also proposed in [Paper F].

The measured and simulated input reflection coefficients and gains of the designed integrated diplexer-antenna are presented in Fig. 4.11(b). The measured reflection coefficients of the two Tx/Rx ports are below -13 dB with very good agreement with simulated results. The filter response of the module is noticeable in the gain curves. The measured isolation of gain between the two channels is around 55 dB. The total measured antenna efficiency, considering the loss of the diplexer, is around 60%. The simulated time-averaged amplitudes of the E-field distribution within the feed-network of the integrated diplexer-antenna at the center frequencies of two Tx/Rx channels are illustrated in Fig. 4.12. As shown, despite the presence of a small gap between the layers and no perfect electrical contact, there is no leakage between the feeding ridge lines and also between the diplexer and adjacent ridge lines. The latter is due to the stopband of the pin texture, which prevents the propagation of the wave in unwanted directions.

4.4.2 Planar monopulse array antenna

Direction finding techniques are necessary for different millimeter-wave applications, such as finding the position of objects in radar systems, determining the line-of-sight direction

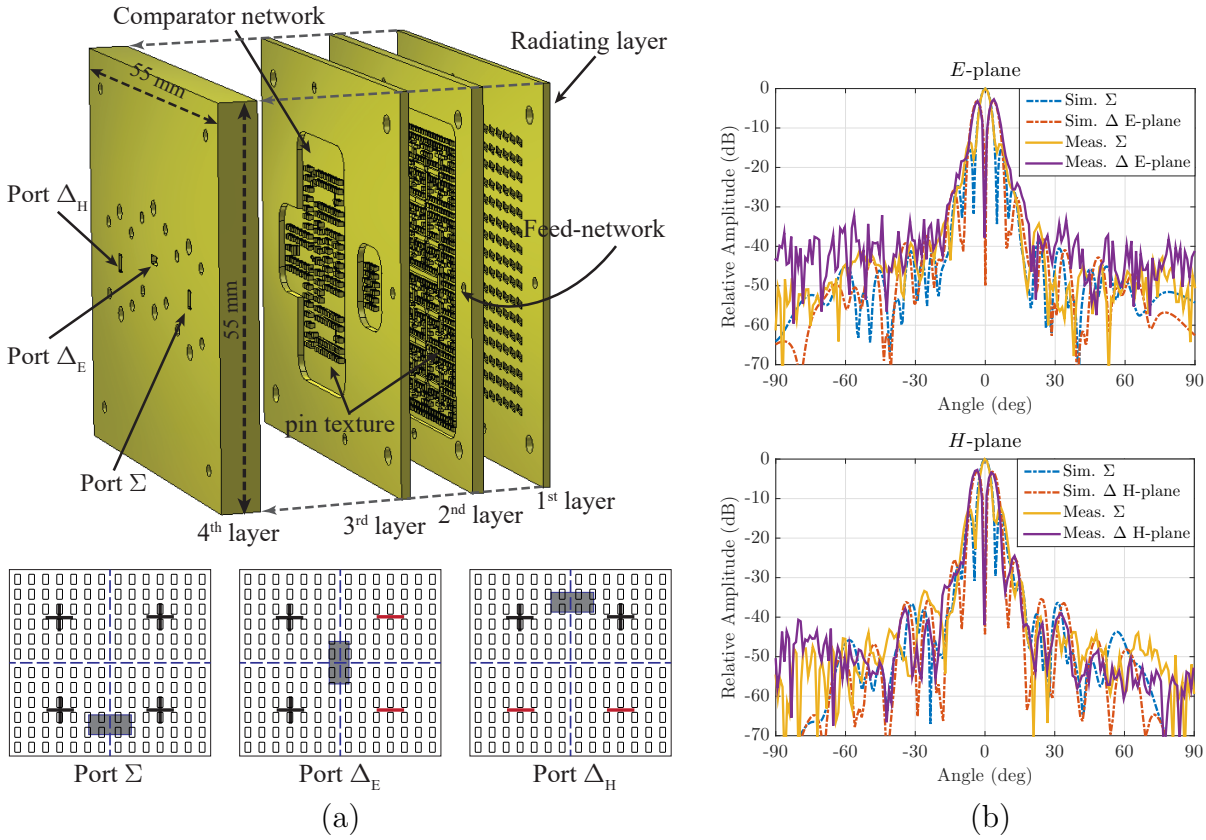

Figure 4.13: (a) Detailed description of the W-band monopulse array antenna and operating mechanism by exciting sum and difference ports. (b) Simulated and measured normalized sum and difference radiation pattern at E- and H-plane at 95 GHz.

in point-to-point wireless links, and detecting the location of unlicensed or undesired radiation sources in security applications. Our second proposed integrated module based on gap waveguide technology is a compact monopulse array antenna (see Fig. 4.13(a)), which is formed with four unconnected layers, and is aimed to be used in tracking applications at W-band (85–105 GHz) ([paper H]). We have designed a low-loss planar Magic-Tee, and afterwards a monopulse comparator network, consisting of two vertically stacked layers. The gap waveguide planar monopulse comparator network is integrated with a high-efficiency 16×16 corporate-fed slot array antenna. The measured results of the comparator network show that the amplitude and phase imbalance values remain less than 0.5 dB and 2°, respectively, at W-band. The fabricated monopulse array antenna shows a relative impedance bandwidths of 21% with input reflection coefficients better than -10 dB for the sum and difference ports. The simulated and measured radiation patterns of the monopulse antenna in the E-, and H-planes at 95 GHz are presented in Fig. 4.13(b). The simulated null in the difference pattern is around 50 dB below the maximum of the sum pattern over the band of interest. However, the measured null is around 40 dB below the maximum of the sum pattern, which could occur due to increased phase and amplitude errors in the comparator network or due to measurement accuracy.

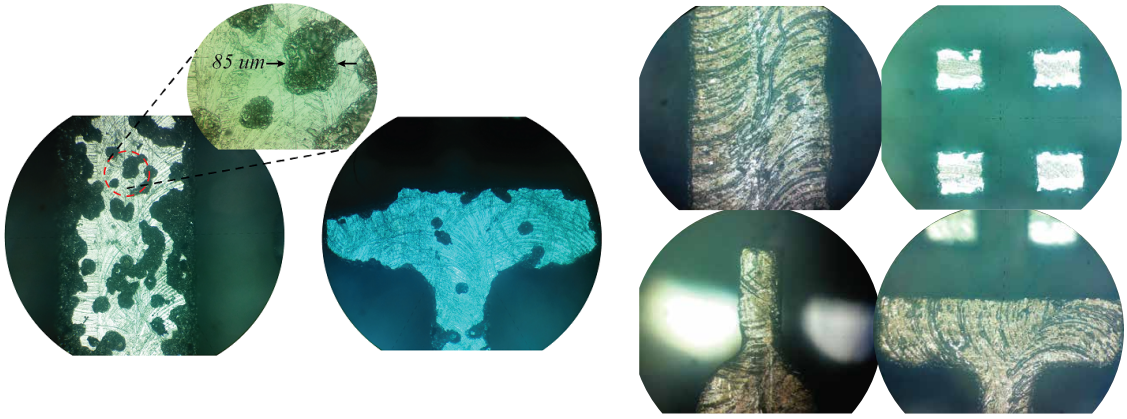

(a) (b)

Figure 4.14: Photograph of the manufactured feeding ridge and surface of two prototypes fabricated with die-sink EDM in, (a) aluminum , and (b) steel.

(a)

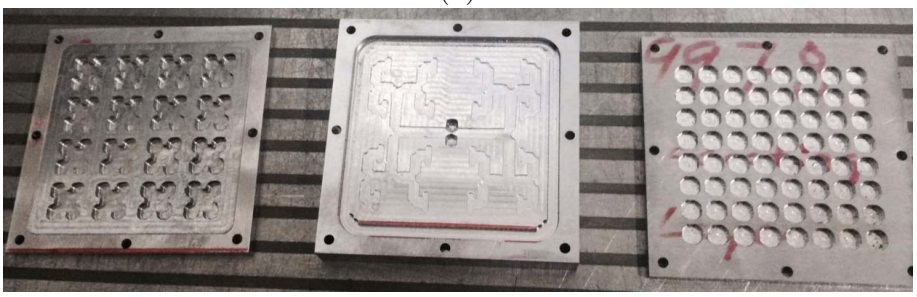

(b)

Figure 4.15: (a) Photograph of an 8×8 gap waveguide slot array antenna fabricated by die-sink EDM in steel. (b) Prepared metal pieces before applying EDM (from left to right: cavity layer, feeding layer, and slot layer).

4.5 Realization Methods and Fabrication Techniques

The main challenge of gap waveguide technology is to find a way to fabricate the textured structure (pin surface) with a cost-effective method. Due to the relatively complex pattern and physical dimensions of the textured structure, the fabrication of the modules presents a challenging task, especially at millimeter-wave frequencies. We have manufactured

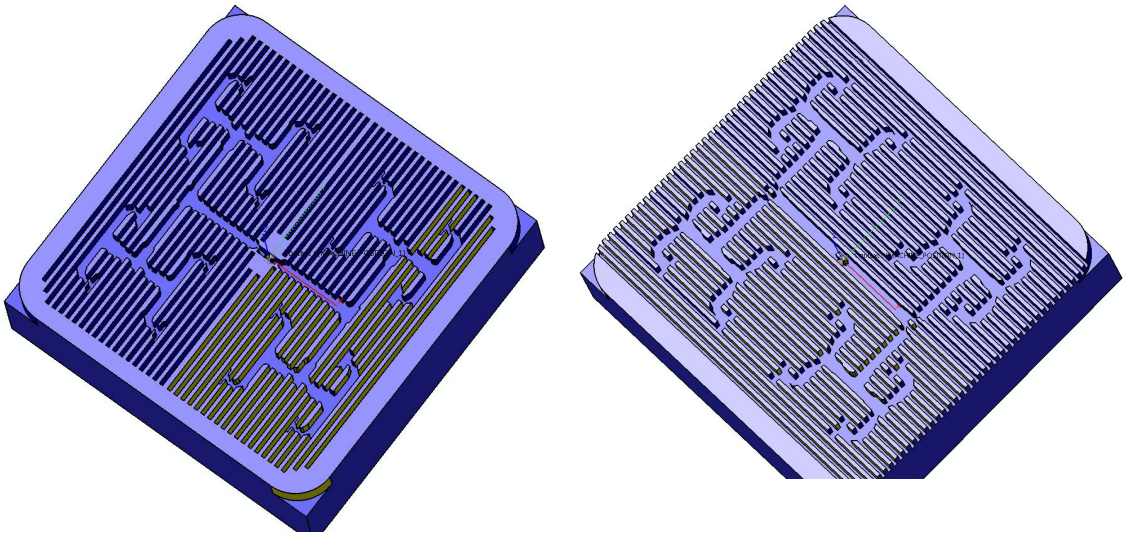

(a) (b)

Figure 4.16: Graphite electrodes that are used to form the distribution network. (a) Electrode with ridges in transverse direction. (b) Electrode with ridges in longitudinal direction.

several antennas by using CNC machining, such as the 8×8 slot array antenna with ridge gap waveguide corporate distribution network at V-band ([Paper D]) and the integrated diplexer-antenna at Ka-band ([Paper F]). Even though the CNC machining technique is a high accurate manufacturing method, it is is very time-consuming and not efficient to realize gap waveguide structures for mass-production. Therefore, we are continuously searching for more effective alternative manufacturing methods. In this section, we briefly present three alternative methods, i.e. die-sink EDM, 3-D direct metal printing, and micro-molding, that have been explored as part of the work of this thesis.

4.5.1 Die-sink EDM

In [Paper E], a fast modern planar 3-D method called die-sink Electric Discharge Machining (EDM) is used for the first time to manufacture a large planar high gain gap waveguide antenna at millimeter-wave frequencies. In EDM technique, a desired pattern is made by removing the material by applying high energy electrical discharges between two conductive materials (a workpiece and an electrode) that are separated by a dielectric liquid. The electrode consists of the negative of the desired pattern, and the high energy sparks makes this pattern to form a footprint in the surface of the workpiece. The electrode is usually made of graphite or copper alloys due to their high electrical and thermal conductivities, as well as high melting temperature. Thermal and electrical conductivities of the workpiece are the most important parameters that determine the manufacturability and the quality of the final product by using EDM process, since they determine how the

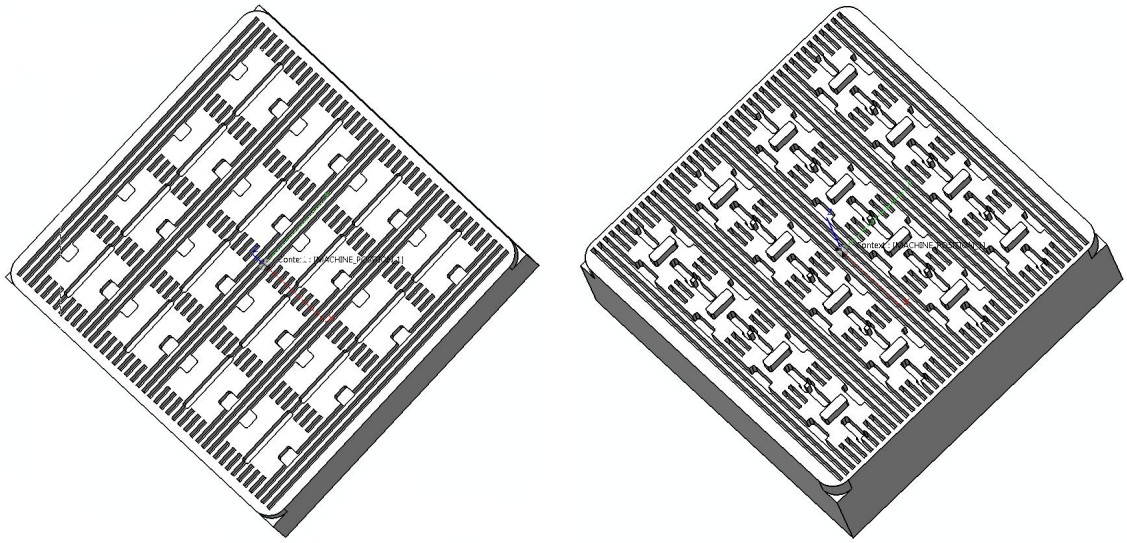

(a) (b)

Figure 4.17: Graphite electrodes used to form the cavity layer. (a) Electrode with ridges in transverse direction. (b) Electrode with ridges in longitudinal direction.

material heats up and vaporizes.

In [Paper E] aluminum is used to fabricate the antenna with EDM technique. The thermal conductivity of aluminum is 204 W/mK. That makes this material a good thermal conductor and difficult to efficiently heat up locally by sparks. Fig. 4.14(a) shows the surface roughness of the distribution network of the fabricated antenna in [Paper E], taken under microscope. During the manufacturing process some sparks hit the ridge surface and caused large surface roughness, since longer time was needed to remove the material from the workpiece. We have tried to make a similar antenna with EDM technique this time in steel ([Paper G]). Steel has lower thermal conductivity (42.6 W/mK) than aluminum, which makes it a better candidate material for EDM process. We have achieved a tolerance of around 15 μm for the fabricated prototype in steel, in contrast with the manufactured prototype in aluminum that showed 40-100 μm fabrication tolerances. Fig. 4.14(b) depicts a close look of the feed network of the fabricated antenna in steel. Despite of the marks on the surface of the ridge, which is due to the use of bigger milling tools and hardness of steel, the prototype has lower fabrication tolerances and better final conditions than the one in aluminum (Fig. 4.14(a)).

To explain the fabrication process with die-sink EDM, let's consider the multilayer corporate-fed 8×8 cavity-backed slot array antenna of Fig. 4.15(a), that are fabricated with EDM in steel. The antenna consists of three unconnected metal layers. In the first step, the workpieces are prepared by removing extra material with CNC milling. We used the EDM technique only to make the pin textures of the different layers. Several electrodes with different details of the resulting texture have been used to manufacture

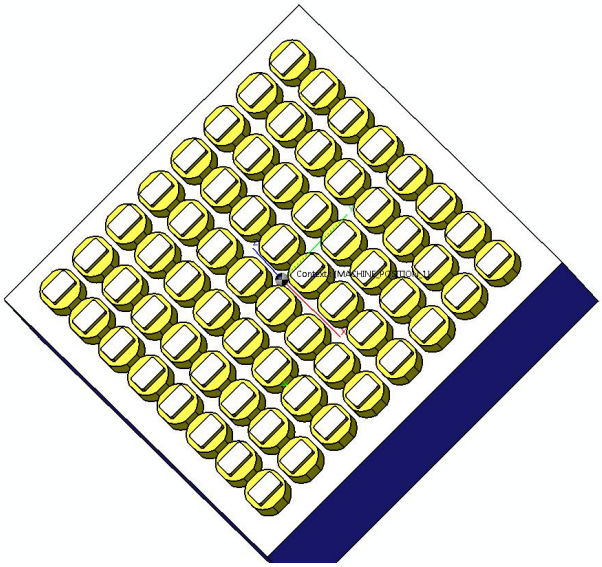

Figure 4.18: Graphite electrode used to form the radiating layer.

each layer. Fig.4.16 shows the two graphite electrodes that have been used to form the distribution network of the antenna. In order to create the pin texture, first an electrode containing small transversal ridges burns the metal surface, and afterwards, the procedure is completed by another electrode with ridges in longitudinal direction. Similar procedure is used to make the pins in the cavity layer. The other graphite electrodes that are used to form the cavity and radiation layers are illustrated in Fig.4.17 and Fig.4.18, respectively.

4.5.2 Direct Metal 3-D printing

3-D printing technology has been developed rapidly as an adaptive and alternative manufacturing technique for high frequency applications. This technology has advantages of low cost and rapid prototyping, even when fabricating complex structures. We have explored the use of this technology to fabricate gap waveguide structures more efficiently. A prototype consisting of a 4×4-element horn array antenna is manufactured by Direct Metal Laser Sintering (DMLS) 3-D printing technique. The fabricated prototype is shown in Fig.4.19(a). The simulated and measured results are presented in Fig.4.19(b). The proposed antenna has a relative bandwidth of 24% with input reflection coefficient better than -10 dB over the 69-88 GHz frequency band. The fabricated 3-D printed prototype shows around 2 dB lower gain than the same prototype made in aluminum with CNC milling. This is mainly due to the high surface roughness of the 3-D printed prototype.

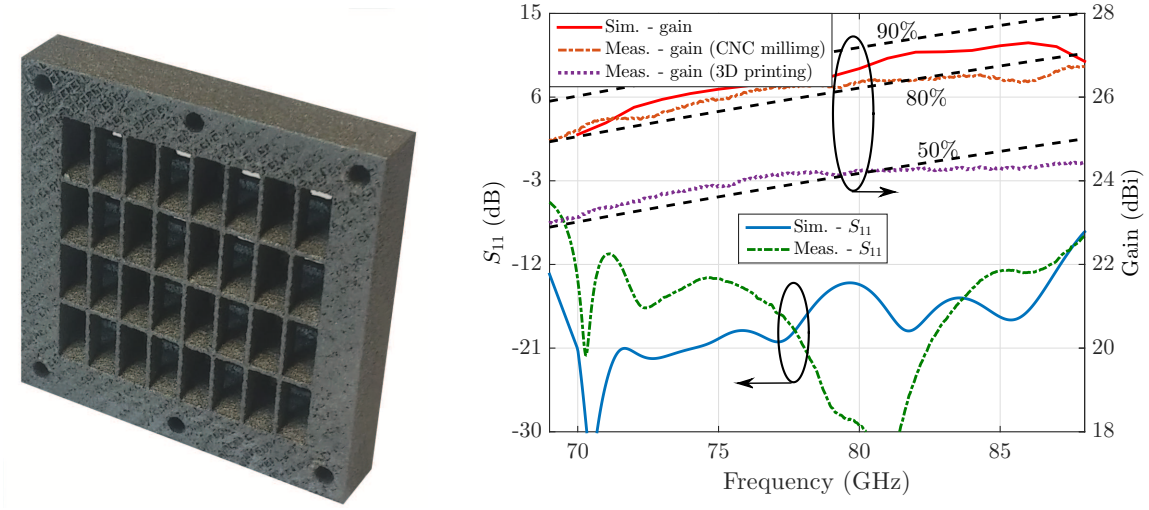

(a) (b)

Figure 4.19: (a)Photograph of the fabricated horn array antenna by 3-D metal printing [122]. (b) Simulated and measured performance of the 3-D printed prototype in comparison with the version fabricated by CNC milling.

4.5.3 Reaction Injection Micro-Molding (RIM)

The frequency range above 100 GHz has got a lot of attention over the last few years. The 145-GHz band is another interesting frequency band for point-to-point radio link systems. Traditional fabrication methods such as CNC milling become challenging and expensive for frequencies above 100 GHz due to the small features of waveguide structures. New fabrication techniques need to be used for effective manufacturing at those frequencies.

We have fabricated a slot array antenna at D-band by using a novel cold micro-molding technique. Fig.4.20 shows the fabricated prototype. Despite of the small dimensions of the pin texture in these frequencies, we have successfully managed to release the workpieces from the mold without losing any pin. However, more research and effort are still needed to mature the process and achieve a prototype with good performance. In the developed micro-molding process we have used an special polymer, so-called OSTEMER and micromachined mold which contains the negative of the desired pattern. The different steps of the RIM process are briefly summarized below :

- Make a master part using lithography in OSTEMER.
- Metalize the master part using physical vapor deposition (PVD) to get good release properties.
- Make silicon mold based on the master part.
- Fill the mold with OSTEMER in liquid state (very low viscosity).

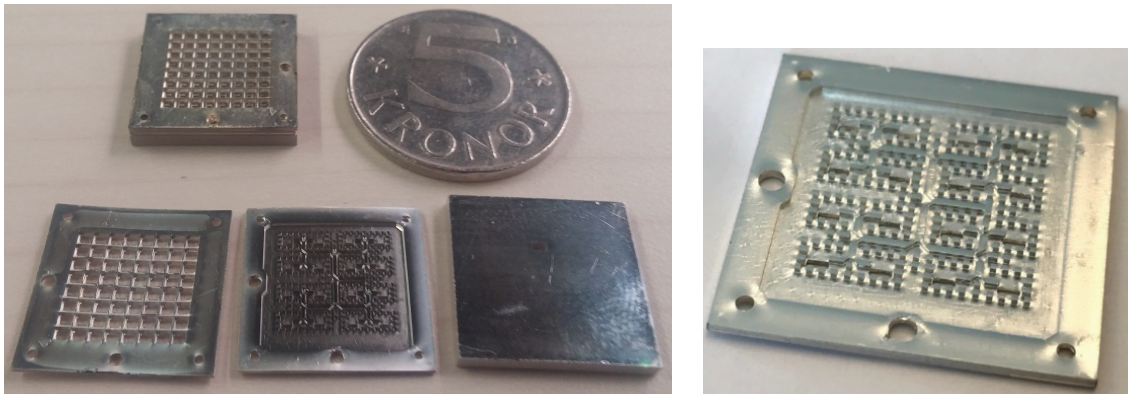

(a) (b)

Figure 4.20: Photograph of the fabricated slot array antenna at D-band by using micro-molding.

- UV expose to initiate the curing process.
- The part continues to fill during the UV curing process resulting in a close to perfect replication.
- Release the molded part which is in a "rubbery state".
- Fully cure the part using heat.
- Metalize molded part using PVD.

4.6 Summary and Conclusions

This chapter has briefly described the work done by the author on millimeter-wave gap waveguide passive components design such as low loss and wideband transitions, filters and diplexer, as well as the development of high gain and high efficiency array antennas based on gap waveguide technology. The integration of all these passive components in a compact and simple antenna system module showing assembly flexibility, has been demonstrated with an excellent agreement between simulations and experimental results. Furthermore, different cost-effective manufacturing techniques have been explored in order to find out a way to realize complete multi-layer gap waveguide array antenna modules in an efficient way, also taking into account the potential industrialization and mass-production of this technology.

Chapter 5

Multi-Gb/s Point-to-Point Radio Front-end Demonstrator

In wireless communication links it is important to send and receive data at the same time and maintain the data transmission in both directions. Frequency division duplex (FDD) and time division duplex (TDD) are the two widely used duplex schemes. The block diagram of a FDD wireless communication systems is shown in Fig. 5.1. In FDD systems, the transmitter and receiver operate simultaneously at different carrier frequencies to avoid interference. The Tx and Rx chains are connected to one antenna via a diplexer. At high frequencies, a FDD system usually consists of several bulky passive components, such as antennas and diplexers, which are separately assembled with high frequency circuitries containing transceivers, a local oscillator (LO), low-noise and high power amplifiers, and afterwards, the complete module is realized and packaged in bulky waveguide blocks. Our

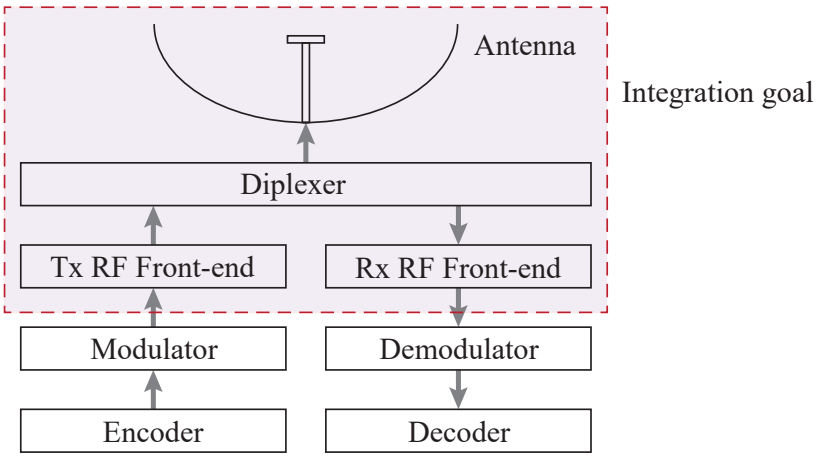

Figure 5.1: Block diagram of a wireless FDD communication system.

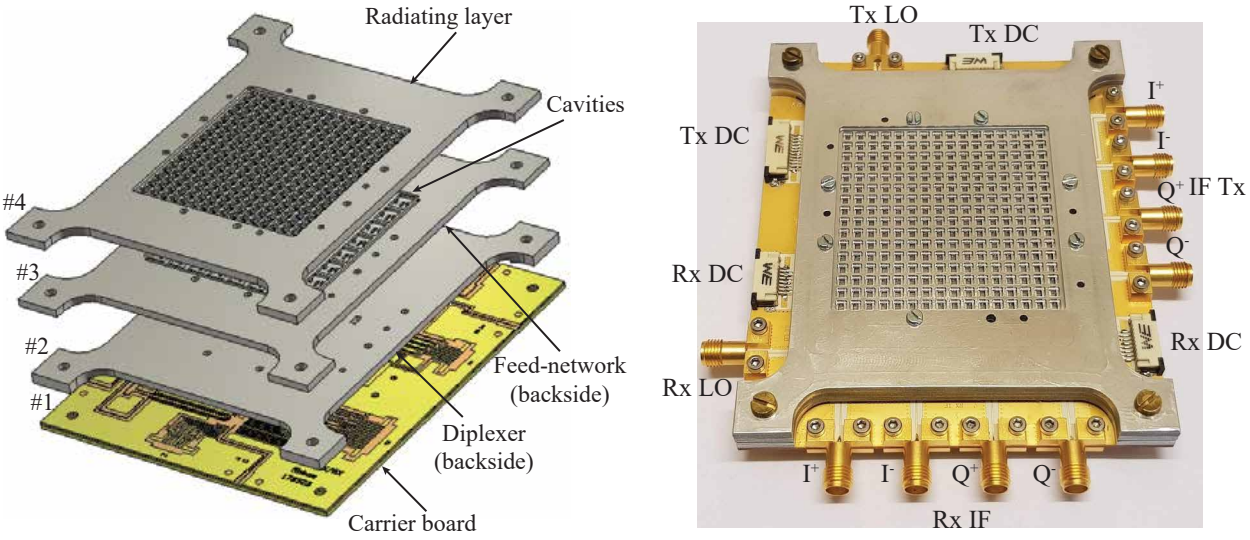

Figure 5.2: (a) Configuration of the proposed compact full duplex radio front-end. (b) Fabricated prototype [K].

ultimate goal is to achieve a compact integration of the Tx/Rx RF front-ends with the diplexer and a high gain antenna as it is illustrated in Fig. 5.1.

In this chapter, we present a summary of a developed high data rate integrated radio front-end module for point-to-point backhaul links operating at E-band. The design module consists of four vertically stacked unconnected layers based on gap waveguide technology. This chapter deals with the integration of active and passive components, based on the content of [Paper K], where a high gain array antenna, a diplexer, and a circuitry consisting of a transmitter (Tx) and a receiver (Rx) monolithic microwave integrated circuits (MMICs) on a carrier board are successfully integrated in one package with a novel architecture and a compact form. A more detailed description about the design can be found in [Paper K].

5.1 Integrated Full Duplex Radio Front-end Module

The configuration of the proposed integrated full duplex radio front-end module for multi-Gbit/s point-to-point wireless link applications is shown in Fig. 5.2. The module consists of a tightly integrated high gain array antenna, a 5^{th} order diplexer, and Tx and Rx chipsets on a carrier board in four distinct layers, where each layer has different functionality. The layers are vertically stacked up and integrated in a compact form. The proposed module has total dimensions of 110 mm×90 mm ×8.5 mm.

The bottom layer acts as a carrier printed circuit board (PCB) for two complete highly integrated GaAs transmitter and receiver MMICs. The Tx and Rx MMICs are placed

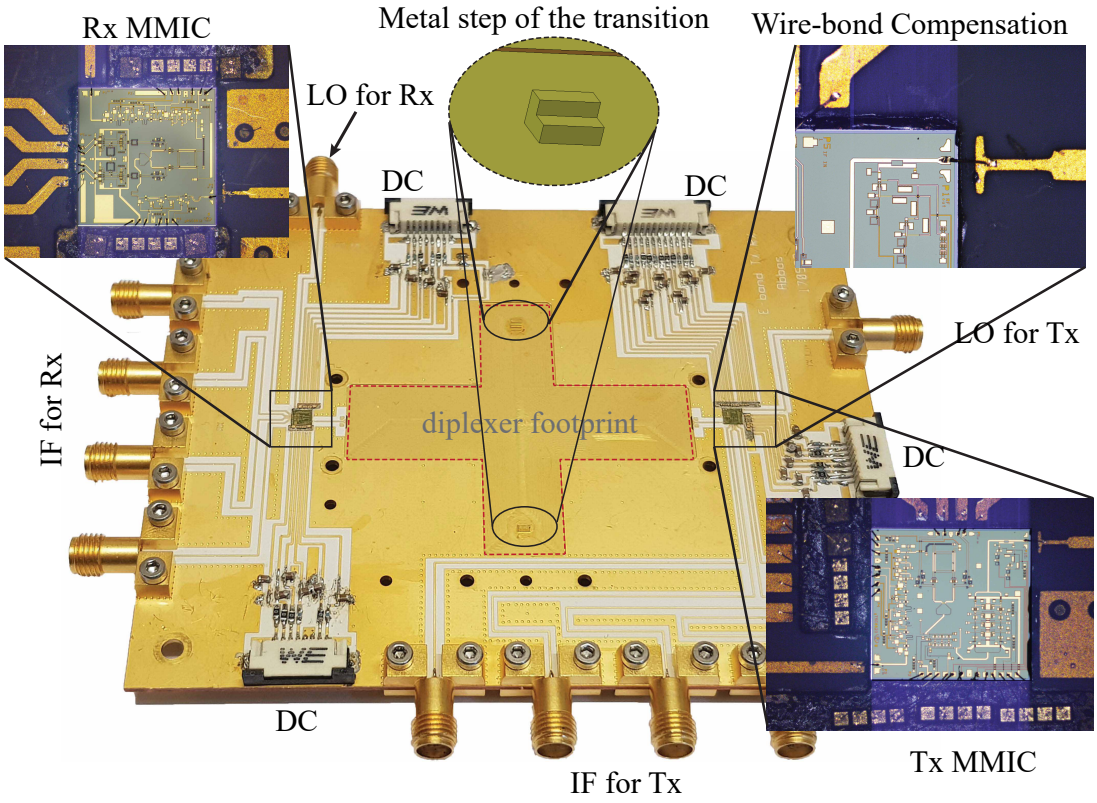

Figure 5.3: Carrier board consisting of Tx and Rx MMICs, wire-bond compensation, IF and LO coaxial ports, and microstrip to GGW transitions [K].

on the carrier board that consists of 100 μm Liquid Crystal Polymer (LCP) substrate on a 1 mm copper plate. Fig. 5.3 shows the designed PCB board with mounted Tx and Rx MMICs. The Tx and Rx dies are attached and wire bonded to the board. To minimize the effect of the wire-bond and reduce the loss, a matching section is used at the RF input/output of Rx/Tx MMICs to compensate the inductance of the wire-bond. Differential IF (0-12 GHz) inputs/outputs and LO inputs (11.8-14.3 GHz) are provided with coaxial interfaces. The LCP dielectric is removed around the footprint of the diplexer. A 5^{th} order hybrid diplexer-splitter is designed on the bottom side of layer 2 (see Fig. 5.2(a)) based on groove gap waveguide (GGW). The Tx and Rx MMICs are wire-bonded to microstrip lines on the PCB, and the RF signals are coupled to the diplexer via a transition. A distribution feed network is designed on the backside of layer 3. The outputs of the diplexer (on layer 2) are coupled to the next layer, i.e., the feed network, via a right-angle GGW to rectangular waveguide transition. Finally, the topside of layer 3 contains 8×8 cavities that uniformly feed the 16×16 slots on layer 4.

The performance of each building block of the designed module, i.e., the diplexer, the array antenna, the transitions, and the Tx/Rx circuitry, has initially been evaluated separately and then two integrated modules have been used to demonstrate a multi-gigabit

Table 5.1: Summary of the measured performance of the integrated radio front-end

Parameter	71-76 GHz	81-86 GHz
Diplexer insertion loss (dB)	0.5	0.5
Antennas+diplexer gain (dBi)	31	31.5
Microstrip to GGW transition loss (dB)	0.31	0.31
Transmitter gain (dB)	24	21
Transmitter P_{1dB} (dBm)	14	16
Receiver gain (dB)	20	24
Receiver noise figure (dB) *	5.5	5.5

* on-wafer measurements

data transmission. A summary of the measured performance of the fabricated prototypes is presented in Table 5.1.

5.2 Link budget analysis

Based on the characterized performance in Table 5.1, the link budget analysis can be done by calculating the received signal power given by (1) and the noise power given by (2) at the receiver input.

$$P_{sig} = P_{Tx} + 2 \times G_{Ant} - L_{FS} - L_{Rain} - L_{Atm} - L_M \tag{5.1}$$

$$P_{noise} = 10log_{10}(KTB) + NF_{Rx}\ (-75.9\ @\ B{=}1.8\ GHz) \tag{5.2}$$

where P_{Tx} is the transmitter output power, G_{Ant} is the Tx and Rx antenna gain, L_{FS} is the free space path loss given by (3), L_{Rain} is the loss due to rain (16.4 dB for 40 mm/h), L_{Atm} is the atmospheric attenuation (0.4 dB/km), L_M is margin (4 dB as suggested in [123] for the 71-86 GHz band), K is the Boltzmann's constant (1.38×10^{-23} W/(K.Hz)), T is the background temperature (290 K), B is the transmitted signal bandwidth, and NF_{Rx} is the receiver's noise figure.

$$L_{FS} = 20log_{10}(d_{[km]}) + 20log_{10}(f_{[GHz]}) + 92.45 \tag{5.3}$$

For a transmitting signal with 1.8 GHz bandwidth, a maximum hop-length (d) of around 500 m is expected for 16-QAM modulation with theoretical Signal-to-Noise Ratio (SNR) of 20.5 dB at a bit error rate (BER) of 10^{-6} [123]. We have considered 4 dB coding gain [123] and 16.4 dB loss due to rain in this calculation. The spectral efficiency can be improved by using higher modulation schemes. However, the hop-length needs to be reduced in order to achieve the required higher SNR. For a 64-QAM modulation, to obtain a BER of 10^{-6} an SNR of 26.5 dB is required [123]. This decreases the expected

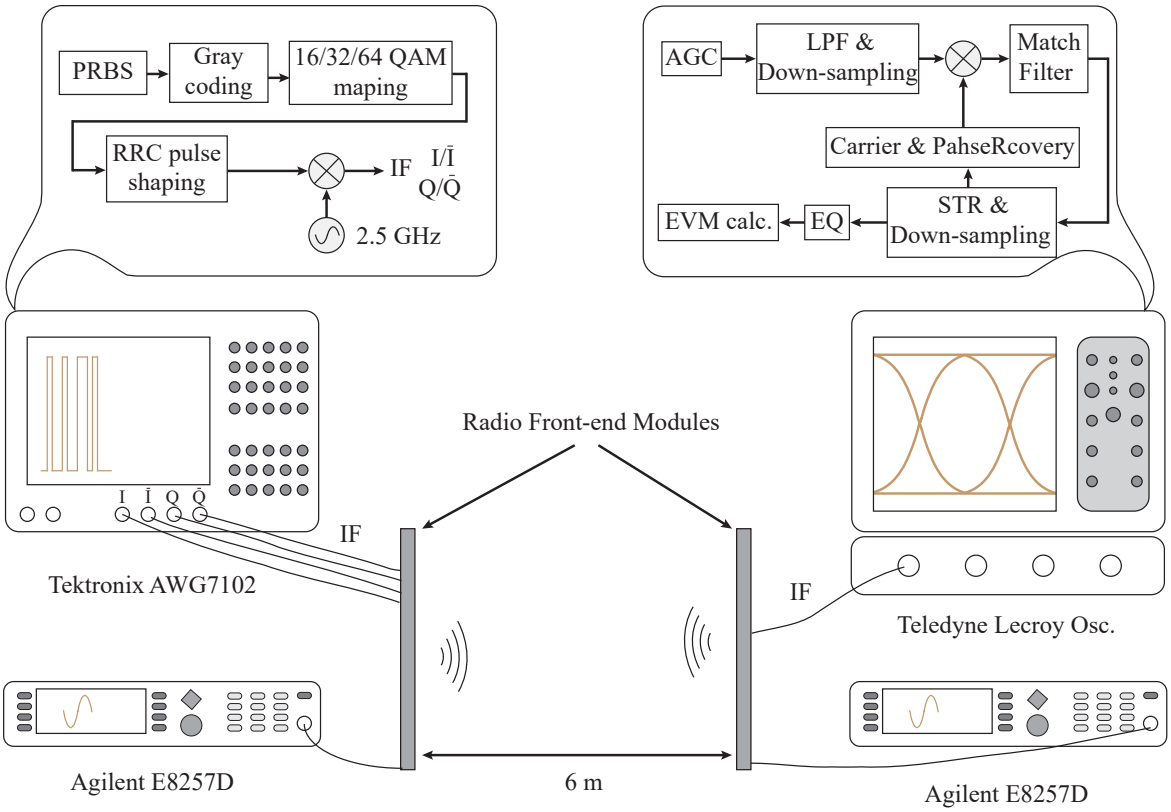

Figure 5.4: Sketch of the data transmission test setup by using an oscilloscope.

hop-length to 200 m by considering 7 dB back-off in P_{1dB} output power of the Tx to have the required linearity.

5.3 Wireless Link Demonstration

The designed module has the ability of full duplex wireless communication, i.e., to transmit in 71-76 GHz or 81-86 GHz bands, and receive in one of the lower or upper bands depending on which Rx MMIC is used in the carrier board. Real-time wireless data transmission has been performed by using two different setups. First, we have evaluated the link performance of the designed radio front-end modules by using an oscilloscope. However, in this setup, the maximum separation between the two radio units is limited. Therefore, we have demonstrated data transmission in longer distance by using two baseband modems. A summary of the achieved results by using the two mentioned setups are given in the next two subsections below.

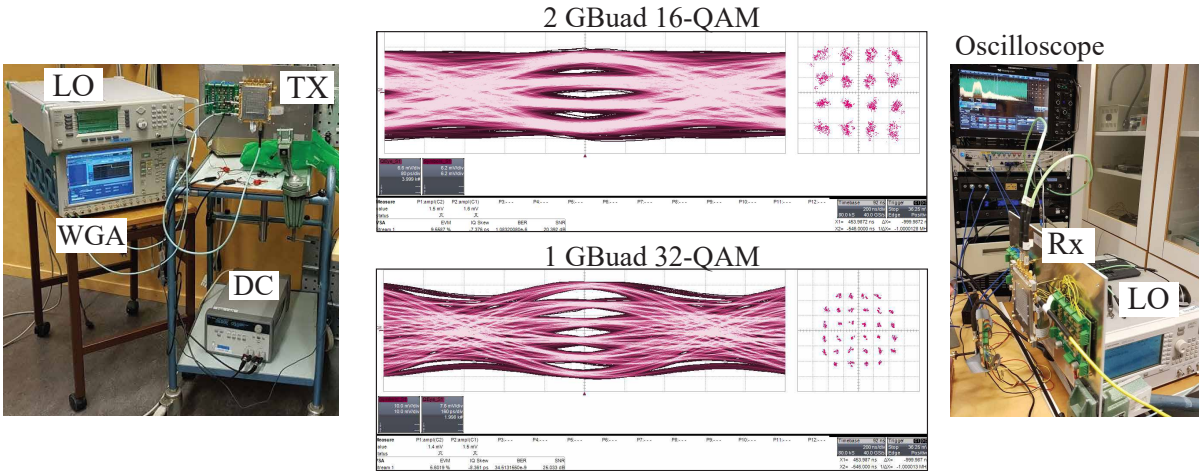

Figure 5.5: Photograph of the experiment setup of Fig. 5.4, and screen shots of 16 and 32-QAM received signal constellations.

Table 5.2: Summary of link performance using the experiment setup shown in Fig. 5.4

Center Freq. (GHz)	Modulation	Symbol/Data rate (GBd/s)/(Gbit/s)	Spectral eff. (bit/s/Hz)	EVM* (%)
72.1	16	1/4	2.96	5.3
	32	1/5	3.7	5.9
	64	1/6	4.44	4.76
73	16	2/8	2.96	9.5
74.6	16	1/4	2.96	5.25
	32	1/5	3.7	5.8
	64	1/6	4.44	4.8
82.1	16	1/4	2.96	5.1
	32	1/5	3.7	5.65
	64	1/6	4.44	4.7
83	16	2/8	2.96	9.3
84.6	16	1/4	2.96	5.25
	32	1/5	3.7	5.6
	64	1/6	4.44	4.73

* Error Vector Magnitude

5.3.1 Real-time data transmission by using oscilloscope

Fig. 5.4 illustrates the measurement setup used to transmit quadrature amplitude modulation (QAM) data by using an oscilloscope. The QAM modulated IQ signals at 2.5 GHz center IF frequency are produced by a Tektronix AWG7102 arbitrary waveform generator

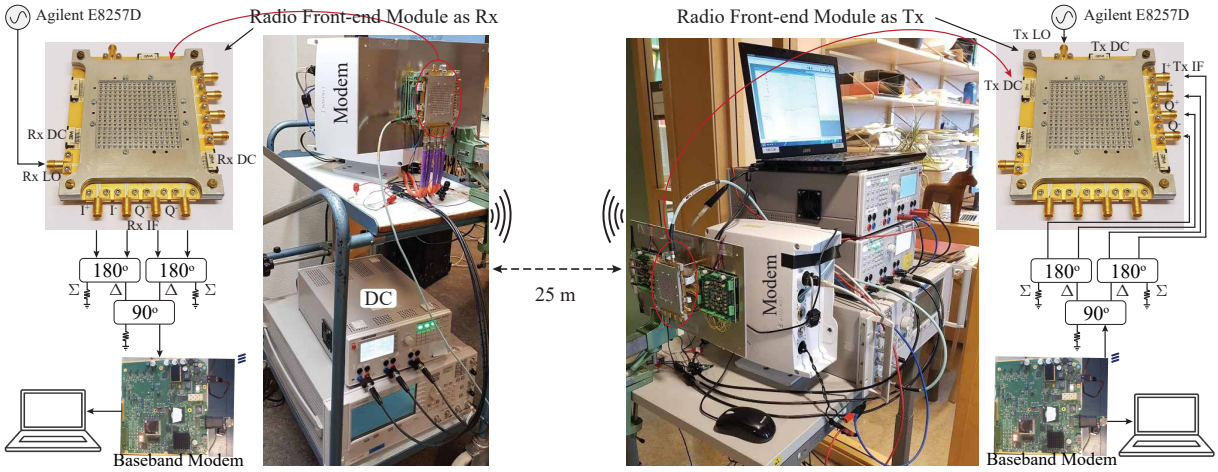

Figure 5.6: Real-time data transmission test setup by using baseband modems.

(AWG). A Pseudo-Random Binary Sequence (PRBS-9) pattern is mapped to gray-coded QAM modulated symbols. We have used root-raised cosine (RRC) filter for pulse shaping with a roll-off factor of 0.35. The AWG's outputs are connected to the Tx IF ports of the integrated radio front-end module, where it up-converts and sends the data at E-band. The LO frequency is provided by an Agilent E8257D signal generator. Another module receives and down-converts the signal to IF, where it is connected to a real-time Teledyne Lecroy oscilloscope with 100 GHz bandwidth. We have used the built-in Teledyne VSA software to demodulate and analyze the received data. A separate signal generator is used to provide LO for the RX module. The two modules are separated only 6 m due to the limited space in the lab measurements. The gain and output power of the Tx MMIC can be controlled by a Variable Gain Amplifier (VGA). Therefore, to avoid saturating the Rx at the other side of the link, we have decreased the Tx output power as well as slightly misaligned the two antennas. A summary of the achieved data rate and spectral efficiency for different modulation schemes is given in Table 5.2. A maximum data rate of 8 Gbit/s is achieved by using 16-QAM modulation with spectral efficiency 2.96 b/s/Hz.

5.3.2 Real-time data transmission by using modems

Fig. 5.6 illustrates the measurement setup of a real-time wireless data transmission by using baseband modems. QAM modulated IQ signals at 3.5 GHz center IF frequency are produced by a modem. The Tx IF ports of the radio front-end module are first combined by 180° couplers to achieve single ended ports for the I and the Q channels. Then the I/Q channels are connected with a 90° coupler to separate upper/lower sidebands (USB/LSB). The LO frequency is provided by an Agilent E8257D signal generator. The integrated radio front-end module up-converts and transmits the USB RF signals at center frequencies of 73.5 GHz and 83.5 GHz by LO at 11.67 GHz and 13.33 GHz, respectively. Another module receives and down-converts the signal to IF centered at 2 GHz. The Rx IF

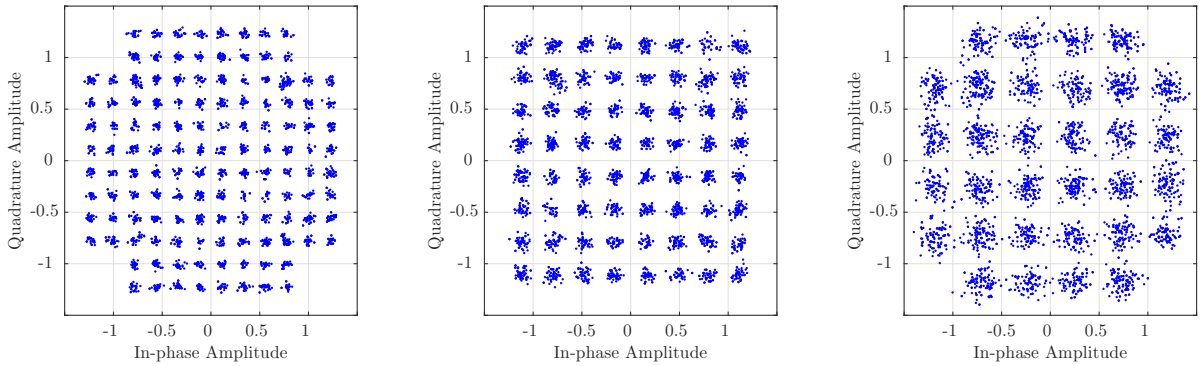

(a) (b) (c)

Figure 5.7: Constellation diagrams of the received signal using the experiment setup shown in Fig. 5.6. (a) 128-QAM with 4.66 Gbit/s at 73.5 GHz, (b) 64-QAM with 5.33 Gbit/s at 83.5 GHz, and (c) 32-QAM with 8 Gbit/s at 83.5 GHz.

Table 5.3: Summary of over-the-air data transmission test

Freq. (GHz)	Symb. rate (MBd/s)	Bandwidth (MHz)	Modulation	Data Rate (Gbit/s)	MSE* (dB)
73.5	666	750	64-QAM	3.99	-30.1
			128-QAM	4.66	-29.9
	888	1000	32-QAM	4.44	-25.9
			64-QAM	5.33	-25.7
	1599	1800	16-QAM	6.39	-22.7
			32-QAM	7.99	-22.5
83.5	666	750	64-QAM	3.99	-30
			128-QAM	4.66	-29.9
	888	1000	32-QAM	5.44	-25.9
			64-QAM	5.33	-25.8
	1599	1800	16-QAM	6.39	-22.6
			32-QAM	7.99	-22.4

* Mean Squared Error

ports are similarly combined with hybrid couplers and then connected to another modem. A separate signal generator is used for the RX module to provide LO at 11.92 GHz and 13.58 GHz for RF signals center frequencies of 73.5 GHz and 83.5 GHz, respectively. The two modules are separated by 25 m in indoor environment. Several modulation formats and symbol rates were tested at different frequencies.

A summarized measured link performance for different modulation schemes is pre-

sented in Table 5.3. A maximum data rate of 8 Gbit/s is achieved by using 32-QAM modulation with spectral efficiency of 4.44 b/s/Hz. Fig. 5.7 also presents the constellation diagrams for different modulations schemes.

5.4 Summary and Conclusions

In this chapter, we briefly presented the realization and experimental results of a compact integrated solution for multi-Gbit/s data transmission for point-to-point wireless link applications at E-band. A full-duplex FDD radio front-end module has been designed by integrating a high gain array antenna, a diplexer, together with RF circuitry consisting of Tx/Rx MMICs in one package. The proposed solution has a novel architecture consisting of four vertically stacked layers with a simple mechanical assembly. The realized gap waveguide based radio front-end provides the advantages of low loss, high efficiency, compact integration, as well as assembly flexibility, which makes it a suitable solution for small cell backhaul links.

Chapter 6

Multi-Layer Waveguide (MLW) Transmission Line

Transmission lines are the fundamental building blocks of any high frequency systems to guide, manipulate and transmit signals. They play an important role in passive and active components design and integration. In Chapter 1, we discussed the issues of the conventional guiding structures, such as metal-pipe hollow waveguides, and planar transmission lines (e.g., microstrip, SIW, and CPW) at high frequencies. The gap waveguide technology has been introduced in Chapter 3 as a low loss alternative with a flexible manufacturing and mechanical assembly. Several passive components and integrated modules have been designed and realized based on this technology, and presented in Chapter 4 and 5.

High frequency electronic components and systems provide advantages such as higher resolution, greater speed/bandwidth and smaller size. These are key enablers in many application areas including telecommunications, automotive radar, security imaging, etc. In this chapter we focus on the frequency range above 100 GHz. At those frequencies, the substrate based planar transmission line technologies have very high losses. On the other

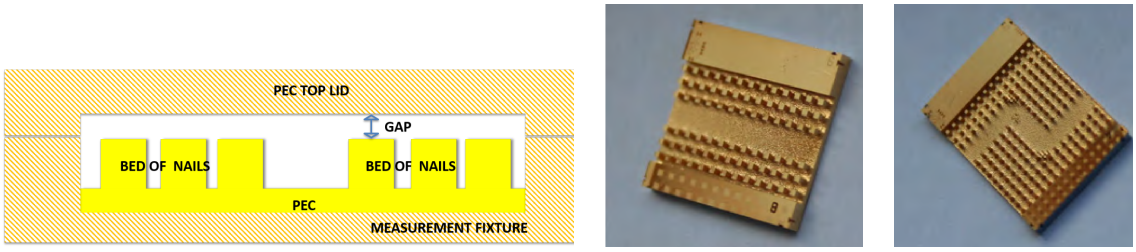

(a) (b) (c)

Figure 6.1: Micromachined groove gap waveguide line above 100 GHz in SOI [114, 124]. (a) Measurement fixture sketch. (b) Straight GGW line. (c) GGW line with double 90° bends.

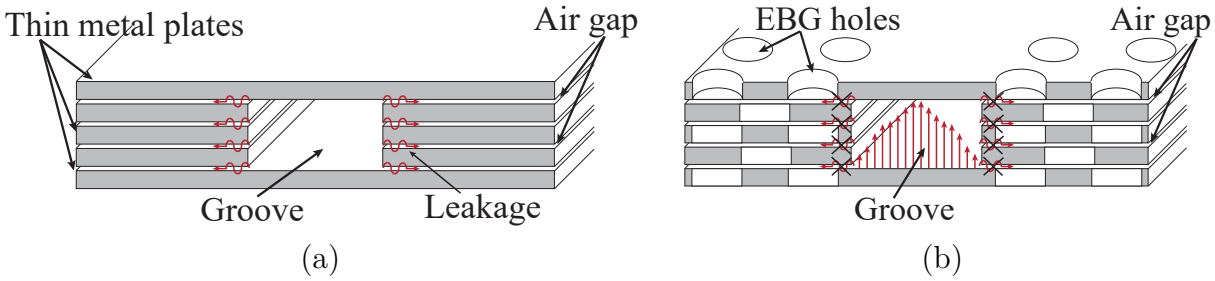

Figure 6.2: Configuration of the proposed MLW transmission line. (a) Cross-section view of the WR-6 waveguide which consists of 5 layers with small gaps between them. (b) Field-leakage suppression by using glide-symmetric holes.

hand, the metallic air-filled hollow waveguides constitute attractive low loss solutions, but their fabrication is challenging at frequencies beyond 100 GHz. Alternative fabrication approaches, such as adaptive manufacturing (3-D printing) [125–127], micromachining technology [128–130], and micro-molding [131] have been studied and developed recently to facilitate the fabrication process of waveguide structures. The 3-D printing technology has advantages of low cost and rapid prototyping, even for fabrication of complex structures. Micromachining is a high-precision elaborate manufacturing method to make high-performance waveguide devices.

The realization of gap waveguide structures is also not simple either for frequencies above 100 GHz. Fig. 6.1 shows the fabricated groove gap waveguide straight line and a line with two 90° bends at F-band (90-140 GHz) [114]. The pin textures containing the GGW lines are fabricated by Deep Reactive-Ion Etching (DRIE) on Silicon on Insulator (SOI) wafer. The fabricated prototypes are mounted on a gold plated brass support structure for the measurement setup. An insertion loss of 0.62 dB for the 12.8 mm long straight GGW line, and 0.42 dB for the 13.7 mm long GGW line with two 90° bends are reported at 110 GHz. Overall, the fabricated prototypes do not satisfy the low loss performance, as expected.

In this chapter, we present for the first time a novel way of constructing wave guiding structures by stacking several thin metal plates, suitable for millimeter-wave applications. The layers do not need to have electrical and galvanic contacts. This provides a low loss, robust design, simple mechanical assembly, and expectedly high manufacturability. This chapter is based on the content of [Paper L], where a more thorough explanation about the concept is presented. Our main goal is to introduce an innovative low-loss, low-cost, and mass-producible solution for applications above 100 GHz.

6.1 MLW Technology Configuration

Fig. 6.2 shows the configuration and arrangement of the proposed MLW transmission line. A rectangular waveguide is formed by vertically stacked unconnected thin metal

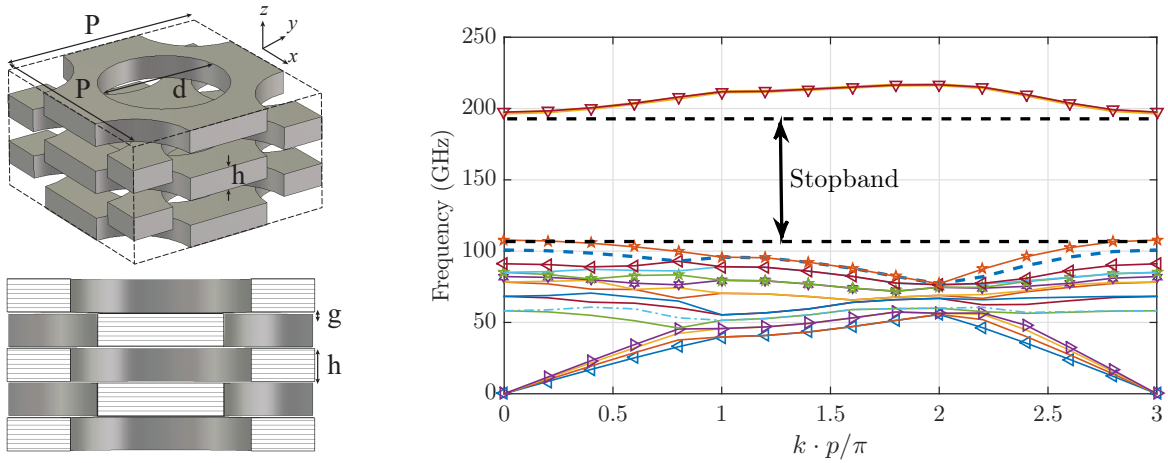

(a) (b)

Figure 6.3: (a) Configuration of the unit cell consisting of five metallic layers with circular holes. (b) Dispersion diagram for the infinite periodic unit cell. ($P = 1.86$ mm, $d = 1$ mm, $h = 0.2$ mm, and $g = 0.01$ mm).

plates. In Fig. 6.2(a), five layers are used to build up a rectangular shaped waveguide, by removing the channel in the middle layers. The height of the waveguide channel depends on the thickness and the number of the layers. Since the metal plates do not have electrical and galvanic contact, a strong field leakage occurs between the layers. In order to solve this problem we used an EBG structure to avoid any possible leakage. A periodic pattern of holes in a glide-symmetric arrangement is applied for this purpose, as shown in Fig. 6.2(b). The periodic holes provide stopband for a certain frequency band which suppresses the propagation of any wave in undesired directions. This introduces a huge mechanical assembly advantage and manufacturing flexibility. Each layer can be fabricated with its special pattern separately and we can simply assemble them together afterwards without the need of a complex and costly method.

Fig. 6.3(a) shows geometries of a periodic unit cell to provide a stopband that covers the desired operating frequency band. The unit cells consist of holes made in thin metal plates. The holes are allocated in a glide-symmetric configuration. A similar approach is introduced for the first time in [132,133] in order to construct metallic waveguides in split-blocks without having galvanic contact. The glide symmetry is a higher order symmetry than the simple periodic pin structure in gap waveguide technology. The holes of each layer have an offset of half of the period (P) with respect to the ones at the top and bottom layers. As shown in Fig. 6.3(a), there is a small gap (g) between the layers. The holes can have any arbitrary geometrical shape. The dispersion diagram of the unit cell for the given values are presented in Fig. 6.3(b). The unit cells provides a stopband which well covers the desired frequency band (100-200 GHz). Fig. 6.3(b) shows that, even though the unit cell consist of several unconnected layers, the structure does not support any modes

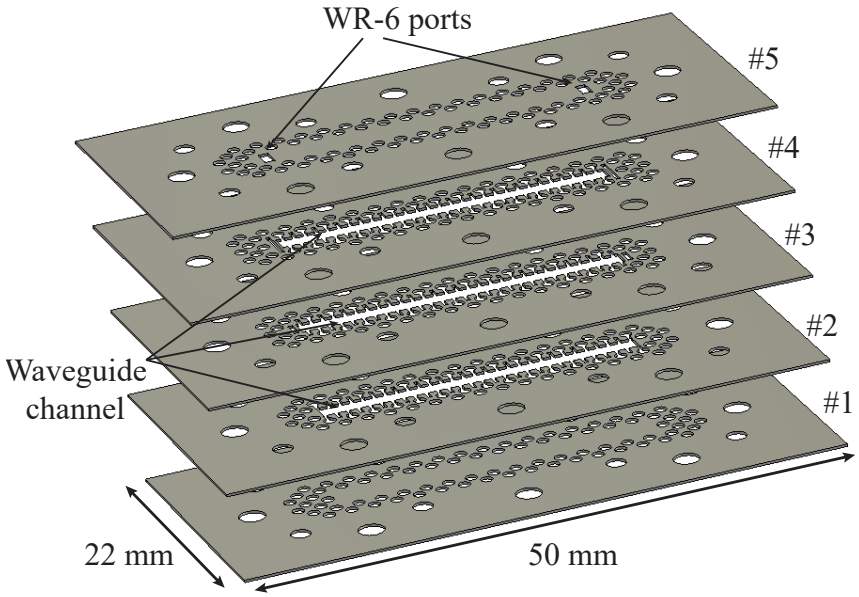

Figure 6.4: 3-D exploded view of the proposed multi-layer waveguide (MLW) transmission line configuration at D-band.

within the stopband. A comprehensive study on the effect of the unit cell parameters on the stopband performance for two unit cells with circular and diamond-shaped holes has been performed in [Paper K].

6.2 Straight MLW line with right-angle transitions at D-band

A straight air-filled waveguide line with the proposed architecture is designed in order to investigate the performance of the concept. The designed line has two standard WR-6 inputs at the top to have a simpler interface with the measurement equipment. The geometry of the straight MLW transmission line is illustrated in Fig. 6.4. The waveguide line consists of five 200 μm thick metal plates with a 10 μm gap between the layers. An elongated rectangular slot (as waveguide channel) with a width of 1.65 mm is removed from the middle layers. After stacking the layers, a rectangular waveguide line with dimensions 1.65 mm$\times$0.642 mm is formed. It is worthy to mention that the height of the designed waveguide is slightly smaller than the standard WR-6 waveguide (0.82 mm) at D-band. Therefore, we expect slightly higher loss than the standard waveguide.

Any discontinuity such as bends and T-junctions can cause severe leakage. Therefore, to investigate the potential use of this technology for the design of more complex waveguide structures, we have designed a double 90° bends waveguide line with a similar configuration (number of layers, gap size, and right-angle transitions) as the straight line

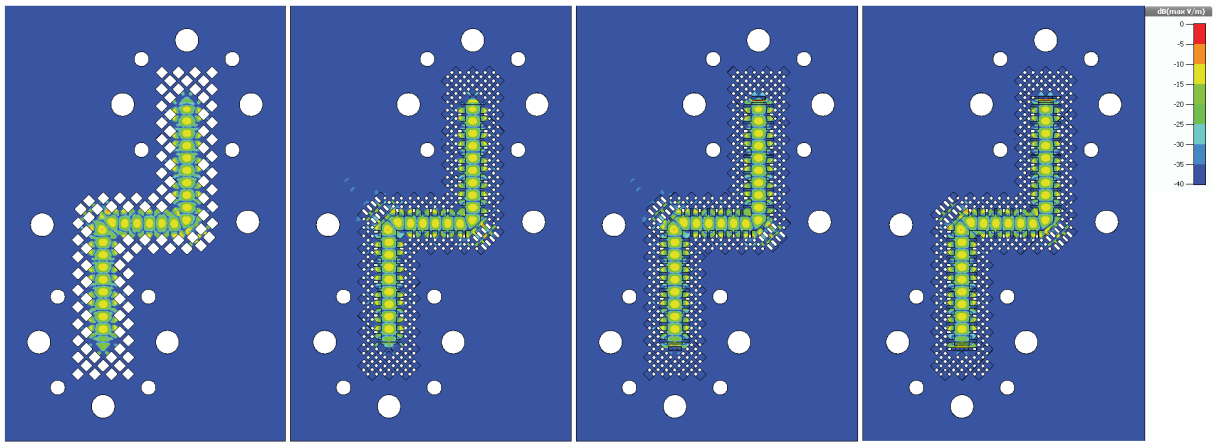

Figure 6.5: Simulated E-field distribution within the layers of a MLW line with double 90° bends at 140 GHz.

in Fig. 6.4. Fig. 6.5 shows the simulated amplitude of the E-field distribution within the different layers of the designed MLW line with double 90° bends at 140 GHz. As expected, there is no field leakage within the layers, even though there is a small gap between the layers and they do not have galvanic contacts. As mentioned before, the EBG glide-symmetric holes prevent the wave propagation and unwanted modes within the stopband.

6.3 First Demonstration at D-band

Fig. 6.6 shows the fabricated prototypes that have been made as a proof-of-concept of the proposed technology and for performance validation purpose. The special pattern of each layer is made on a 200 μm thick brass plate, by using metal chemical etching. The plates are silver plated in order to have lower conductive loss. The chemical etching provides a precise fabrication, which is scalable and suitable for mass production. Any arbitrary shape can be cut through thin metal plates with an aspect ratio of 1. The manufacturing tolerance is approximately $\pm$20 % of the metal thickness, which in our case becomes around $\pm$40 μm. Based on our experience, we have over-etching in most of the time, which makes the holes bigger than expected. Therefore, we have considered this effect and compensated the manufacturing tolerances in our design before fabrication. We decreased all the through holes dimensions 40 μm. By doing that, a maximum of 5 μm error in the final fabricated parts has been achieved. The layers are simply assembled and glued together by using non-conductive epoxy glue. The measured performance of the straight lines with circular and diamond-shaped holes is presented in Fig. 6.7. The measured reflection coefficient is below -18 dB over the frequency band 110-170 GHz, showing insertion loss values between 1.5-0.45 dB over the same frequency band.

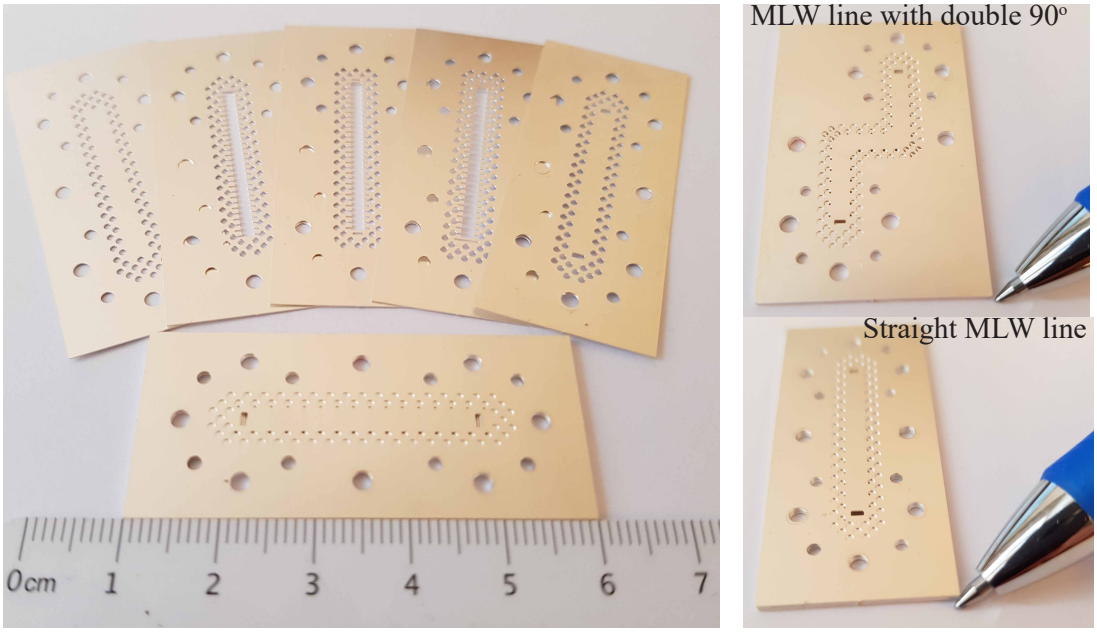

Figure 6.6: Photograph of the fabricated MLW lines by using chemical metal etching.

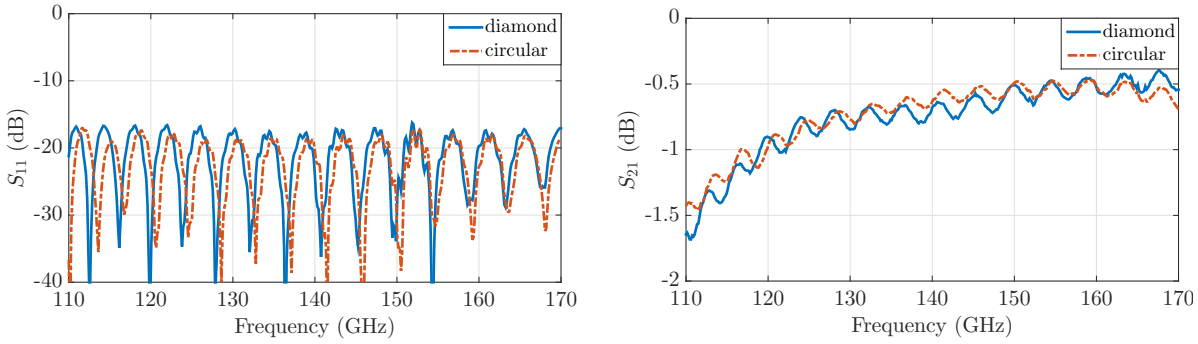

Figure 6.7: Measured performance of the fabricated straight MLW lines at D-band. (a) Reflection coefficient. (b) Transmission coefficient.

6.4 Discussion and Conclusions

We briefly described the configuration of a new air-filled transmission line technology with a novel architecture in this chapter. The results of a fabricated MLW transmission line using a simple manufacturing and assembly at D-band as a proof-of-consent is briefly presented. The possible field leakage due to the air gaps is prevented by using an EBG structure, consisting of glide-symmetric holes. The proposed technology could be an excellent candidate for designing compact and thin passive waveguide components and active components packaging, with a great potential for low-cost, light weight and mass-

Table 6.1: Comparison between state-of-the-art waveguide technologies

Ref.	Technology	Freq. (GHz)	Split-block	Loss (dB/mm)
Commercial	-	110-170	-	0.012
[135]	Microstrip	110-170	-	0.33
[136]	SIW	110-170	-	0.35
[137]	CNC (Al)	75-110	E-plane	0.005
[138]	3-D printing[1]	75-110	E-plane	0.011
[126]	3-D printing[2]	220-325	-	0.012
[127]	3-D printing[3]	110-170	-	0.019
[134]	Micromachining[4]	110-170	H-plane	0.016
[129]	Micromachining[5]	110-170	H-plane	0.03
[131]	Micro-molding	75-110	H-plane	0.03
[114]	GGW[6]	110	H-plane	0.048
[Paper K]	MLW	110-170	H-plane	0.02

[1] Stereolithography apparatus (SLA) with copper plating.
[2] Stereolithography apparatus (SLA) with copper plating.
[3] Selective laser melting (SLM) with Cu-155n powder.
[4] Deep reactive-ion etching (DRIE) in silicon with gold plating.
[5] Multilayer silver plated SU-8.
[6] Deep reactive-ion etching (DRIE) in SOI with gold plating.

producible at millimeter-wave frequencies.

TABLE 6.1 shows a comparison between the MLW technology and several published works on different technologies above 100 GHz. The commercial gold plated rectangular waveguide exhibits lower insertion loss than microstrip and SIW lines. The 3-D printed waveguides have comparable losses to the commercial one, after applying polishing techniques to maintain a low surface roughness. A very low insertion loss has been reported for the DRIE silicon micromachined waveguide in [134], by achieving very low surface roughness. The average measured insertion loss per unit length of the proposed MLW line is around 0.02 dB/mm at D-band. It should be remarked that the effect of the two right-angle transitions are also included in the reported insertion loss for MLW prototypes. Comparing with the dielectric based transmission lines, the MLW technology shows more than 10 times lower dissipative loss. Moreover, the fabricated prototypes show comparable low-loss performance than the hollow waveguide ones.

In addition, the proposed technology can be manufactured with very low cost techniques, by using mature fabrication methods such as metal laser-cutting and chemical etching. In Fig. 6.8 a comparison between hollow waveguide structure with different manufacturing methods, groove gap waveguide considering a low-cost fabrication method (molding), and MLW technology is presented. In this comparison we have considered

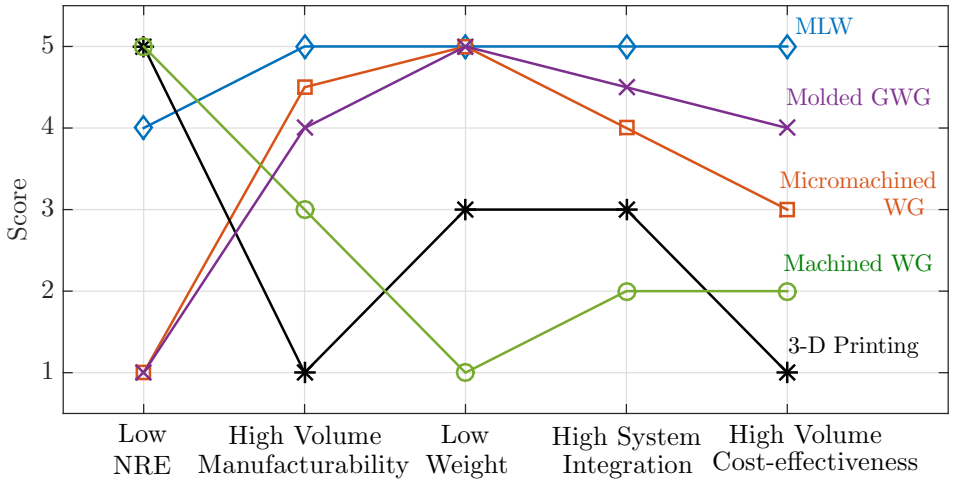

Figure 6.8: Comparison between different technologies.

different aspects, such as Non-Return Engineering (NRE) costs (cleanroom masks, initial tooling costs, etc.), high volume manufacturability, weight, ease of system integration, and cost-effectiveness.

3D printing technology can produce complicated structures, however its slow printing process reduces manufacturability. Micromachining technology offers low loss at the expense of high NRE, and thereby, high cost of electrically large waveguide components such as array antennas and integrated system. Moreover, system integration is not easy with this technology. It is difficult to interface micromachined devices with standard waveguide flanges or active components with power supply and wideband digital signal lines. This technology is more suitable for high volume production of small size RF MEMS devices, where thousands of samples can be realized on one wafer. Gap waveguide technology (GWG) uses a similar EBG concept, but the key difference is that in this technology a cost-effective realization of the pin texture in high volume is challenging. Low cost manufacturing techniques such as plastic injection molding and metal die casting have high NRE cost and require manufacturing precision which affects scalability. Metal machined hollow waveguide (WG) structures are often heavy and not suitable for low cost mass-production.

The MLW technology has excellent potential to act as an interconnect and integration platform for high frequency applications (100-300GHz). The proposed unique architecture opens up an opportunity to provide low-loss and cost-effective millimeter-wave waveguide components and system packaging.

Chapter 7

Contributions and Recommendations for Future Work

The gap waveguide technology, as a new waveguide structure to overcome the limitations of the traditional transmission lines, shows interesting properties such as low loss and flexible fabrication and assembly at high frequency bands. This thesis presents a collection of recent development of gap waveguide passive components, such as bandpass filters and planar array antennas, and a description of achievements in integration of passive and active components at millimeter-wave frequency bands. Moreover, the realization of gap waveguide structures is explored by using several different fabrication methods, such as die-sink EDM, direct metal 3-D printing, and micro-molding. An E-band radio frond-end demonstrator is presented to show the advantage of gap waveguide technology in packaging and complete system integration. Moreover, MLW technology is introduced as a promising novel transmission line that exhibits relevant features like low loss and cost-effectiveness, especially for beyond 100 GHz applications.

In the first part of the thesis, the reader is provided with an introduction and the background needed to understand the work described in the appended papers. In this section, a summary of the appended papers is given. Moreover, a brief description of the contribution by the author for each paper is provided .

Paper A: Simple Formula for Aperture Efficiency Reduction Due to Grating Lobes in Planar Phased Arrays, *(A. Vosoogh and P.-S. Kildal)*

In this paper, we make a generic study of grating lobes in a large slot array. A simple formula called "*grating efficiency*" is presented for aperture efficiency reduction due to the power lost in the grating lobes, see Chapter 10 in [50]. Array antennas with element spacing greater than one wavelength will produce grating lobes. Grating lobes are not a big problem in most new millimeter-wave applications, except for the fact that they reduce the aperture efficiency, and thereby the directivity. We numerically verify this

simple formula for a uniformly excited 32×32 element array of slots in an infinite ground plane.

My contribution- I performed the simulations, analyzed the data, and wrote the paper.

Paper B: Fundamental directivity limitations of dense array antennas: A numerical study using Hannan's embedded element efficiency, (P.-S. Kildal, A. Vosoogh, and S. Maci)

We show that the embedded element efficiency concept may be used to explain the so-called element-gain paradox in antenna arrays, i.e. that the array gain is always smaller than the sum of the element gains. However, the results presented here show that by using embedded element analysis, the realized gain of regular arrays becomes actually equal to the sum of the realized gains of the embedded elements. Thus, the embedded element efficiency dating back to Hannan in 1964 is more practical to use in design and numerical analysis than the more commonly used active element pattern approach. We also show that the embedded element efficiency can be approximated by a simple formula for element spacing smaller than half wavelength.

My contribution- I contributed in the simulation and data analysis.

Paper C: A V-band Inverted Microstrip Gap Waveguide End-coupled Bandpass Filter, *(A. Vosoogh, A. A. Brazález, and P.-S. Kildal)*

The main goal of this paper is to show that low cost end-coupled bandpass filters are feasible at millimeter-wave frequencies by using inverted microstrip gap waveguide technology. The inverted microstrip gap waveguide is advantageous for millimeter-wave applications because of its low loss, self-packaging characteristics, and cost-effectiveness. Since the wave propagates mainly in the air and surface waves do not exist, the width of the lines in gap waveguides become wider than typical microstrip and SIW. A fourth order Chebyshev-type end-coupled BPF is designed to provide a 2 GHz bandwidth at 60 GHz center frequency. The fabricated prototype is embedded within a 10 cm inverted microstrip gap waveguide that contains two back-to-back transitions to rectangular waveguide. The design of this transition can be found in [64]. Measurement results confirmed that the overall loss in inverted microstrip gap waveguide is lower than in conventional microstrip and SIW filters. Therefore, inverted microstrip gap waveguide has advantages of both easy PCB fabrication, and packaging characteristics of gap technologies. The fabricated prototype exhibits an insertion loss of 3 dB in the passband. However, the insertion loss of the filter itself is better than 1.6 dB after removing the loss contribution of the line and the back-to-back transitions. The measured results show that insertion loss of the inverted microstrip gap waveguide filter is around half of a corresponding SIW filter in [120]. The designed filter has a planar structure and acceptable loss, thus becoming suitable for integration with active and passive components.

My contribution- I contributed in the design of the bandpass filter, simulation, measurements, and writing the paper. A. A. Brazález designed the transition from rectangular waveguide to inverted microstrip waveguide.

Paper D: Corporate-Fed Planar 60 GHz Slot Array Made of Three Unconnected Metal Layers Using AMC pin surface for the Gap Waveguide, *(A. Vosoogh and P.-S. Kildal)*

In this paper, we propose a high efficiency and low profile corporate-fed 8×8-slot array antenna operating in the 60 GHz band. The antenna is built using three unconnected metal layers based on Artificial Magnetic Conductor (AMC) in gap waveguide technology. A 2×2 cavity-backed slot subarray is designed in a groove gap waveguide cavity. The cavity is fed through a coupling slot from a ridge gap waveguide corporate-feed network in the lower layer. The antenna shows better radiation pattern and higher aperture efficiency than the presented antenna in [88]. The fabricated antenna shows a relative bandwidth of 14% with input reflection coefficient better than -10 dB and an overall aperture efficiency larger than 65% (i.e., -2 dB) with about 25 dBi realized gain between 56.2 and 65.0 GHz. This paper presents for the first time such 8×8-slot planar array based on a fully corporate distribution network in ridge gap waveguide technology.

My contribution- I designed, simulated, performed the measurements, and wrote the paper.

Paper E: Wideband and High-Gain Corporate-Fed Gap Waveguide Slot Array Antenna with ETSI Class II Radiation Pattern in V-band, *(A. Vosoogh, P.-S. Kildal, and V. Vassilev)*

In this paper, we present a low profile multilayer corporate-fed 16×16 slot array antenna with high gain, high efficiency and wide impedance bandwidth for the 60 GHz band. The proposed antenna consists of three unconnected metal layers similar to presented array antenna in [Paper C]. A new wide bandwidth air-filled cavity-backed 2×2 slot subarray is designed to cover the whole unlicensed 60 GHz frequency band. A prototype consisting of 16×16 slots is manufactured by a fast modern planar 3-D machining method, i.e. die-sink Electric Discharge Machining (EDM). This is used for the first time to manufacture a large planar high gain antenna at millimeter-wave, as far as we know. The fabricated prototype has a relative impedance bandwidth of 17.6% with input reflection coefficient better than -10 dB. The E- and H-planes radiation patterns satisfy the ETSI class II co-polar sidelobe envelope, and the measured cross-polar level is more than -30 dB below the copolar level over the 56-75 GHz frequency band. The measured total aperture efficiency is better than 60% over the same band.

My contribution- I designed, simulated, performed the measurements, and wrote the paper.

Paper F: An Integrated Ka-band Diplexer-Antenna Array Module Based on Gap Waveguide Technology With Simple Mechanical Assembly and No Electrical Contact Requirements, *(A. Vosoogh, M. Sharifi Sorkherizi, A. Uz Zaman, J. Yang, and A. A. Kishk)*

This paper is our first attempt to design more complex modules by integrating passive components with the feed network of array antenna. We present the integration of a diplexer with a corporate feed network of a high gain slot array antenna at the Ka-band. The proposed integrated diplexer-antenna module consists of three distinct metal layers without the need of electrical contacts between the different layers. The designed module has two channels of 650 MHz bandwidths each with center frequencies 28.21 GHz and 29.21 GHz. The fabricated prototype provides good radiation and input impedance characteristics. The overall performance of the integrated diplexer-antenna module is quite promising, and this can open up new development of such integrated modules in the future.

My contribution- I designed the array antenna, contributed in integration, performed the measurements, and co-wrote the paper with M. Sharifi Sorkherizi. M. Sharifi Sorkherizi designed the diplexer.

Paper G: Zero-gap Waveguide: A Parallel Plate Waveguide With Flexible Mechanical Assembly for mm-Wave Antenna Applications, *(A. Vosoogh, A. Uz Zaman, V. Vassilev, and J. Yang)*

In this paper, a statistical analysis of a random contact of the pin texture and upper metal lid in a new type of gap technology guiding structure, so-called zero-gap, is presented in this paper. A new solution to overcome the problem of good electrical contact due to mechanical assembly with low losses is presented for millimeter-wave frequency applications. Our study shows that the key characteristic of gap waveguide structures is the height of the pins, which creates the parallel plate mode stop-band. This represents a manufacturing advantage especially for corporate feed network of array antennas.

My contribution- I designed, simulated, analyzed the data, performed the measurements, and wrote the paper.

Paper H: W-Band Low-Profile Monopulse Slot Array Antenna Based on Gap Waveguide Corporate-Feed Network, *(A. Vosoogh, A. Haddadi, A. Uz Zaman, J. Yang, H. Zirath, and A. A. Kishk)*

In this paper, we present a gap waveguide based compact monopulse array antenna, which is formed with four unconnected layers, for millimeter-wave tracking applications at W-band (85–105 GHz). A low-loss planar Magic-Tee is designed to be used in a monopulse comparator network consisting of two vertically stacked layers. The gap waveguide planar

monopulse comparator network is integrated with a high-efficiency 16×16 corporate-fed slot array antenna. The low-loss performance of the comparator network and the feed-network of the proposed array, together with the simple and easy manufacturing and mechanical assembly, makes it an excellent candidate for W-band compact direction-finding systems.

My contribution- I contributed in the design, simulation, measurements, and co-writing the paper with A. Haddadi.

Paper I: Simple And Broadband Transition Between Rectangular Waveguide And Groove Gap Waveguide For mm-Wave Applications, *(A. Vosoogh, A. Uz Zaman, and J. Yang)*

We present a vertical wideband transition between a standard WR-15 rectangular waveguide and groove gap waveguide in this paper. The designed transition is compact and has a simple geometry with a very good input matching and low loss over a wide frequency band, which are demanding for future millimeter-wave applications. This transition can be used as an interface between gap waveguide components, such as filters, diplexers, and planar array antennas to any device with standard waveguide flanges. The measured performance for the back-to-back configuration of this transition is presented.

My contribution- I designed, evaluated the performance of the transition by measurements, and wrote the paper.

Paper J: Wideband Horn Array Antenna With Gap Waveguide Corporate-Feed Network at E-Band, *(A. Vosoogh, A. Haddadi, A. Uz Zaman, and J. Yang)*

In this paper, we present a low-profile wideband horn array antenna with ridge gap waveguide corporate feed network at E-band. The radiating performance of the antenna is improved by introducing a septum in the E-plane of the horn unit cell. The measured results of the fabricated prototypes consisting of a 4×4-element horn array are presented and compared with the full wave simulations.

My contribution- I designed, performed the simulations, measured, and co-writing the paper with A. Haddadi.

Paper K: Compact Integrated Full Duplex Gap Waveguide Based Radio Front-end For Multi-Gbit/s Point-to-Point Backhaul Links at E-band, *(A. Vosoogh, M. Sharifi Sorkherizi, V. Vassilev, A. Uz Zaman, J. Yang, Z. S. He, A. A. Kishk, and H. Zirath)*

In this paper, we present the design of a high data rate radio front-end module for point-to-point backhaul links operating at E-band. The design module consists of four vertically stacked unconnected layers without any galvanic and electrical contact requirements

among the building blocks, by using gap waveguide technology. A high gain array antenna, a diplexer, and a circuitry consisting of a transmitter (Tx) and a receiver (Rx) monolithic microwave integrated circuits (MMICs) on a carrier board are successfully integrated in one package with a novel architecture and a compact form. The performance of each building block of the designed module is initially evaluated separately, and afterwards, two integrated modules are used to demonstrate a multi-gigabit data transmission. The proposed radio front-end provides the advantages of low loss, high efficiency, compact integration, and a simple mechanical assembly, which makes it a promising solution for the deployment of small cell backhaul links. The proposed integrated module shows the flexibility and great potential that gap waveguide technology can offer in system integration and packaging of modules with high complexity.

My contribution- I designed the array antenna, transitions and packaging, performed and contributed in the measurements and data transmission experiment, and wrote the paper. M. Sharifi Sorkherizi designed the hybrid diplexer-splitter, and V. Vassilev and Z. S. He helped with the carrier board design and data transmission setup and experiment.

Paper L: Novel Air-Filled Waveguide Transmission Line Based on Multi-Layer Stacked Thin Metal Plates, *(A. Vosoogh, H. Zirath, and Z. S. He)*

This article presents a novel way of constructing wave guiding structures by stacking several thin metal plates for millimeter-wave applications. The metallic layers do not require any electrical contacts among them. An air-filled multi-layer waveguide (MLW) transmission line is successfully designed, manufactured, and experimentally validated at D-band. Five vertically stacked thin metal layers are used to build up an air-filled rectangular waveguide line. The layers are simply assembled by allowing a small air gap among them, without the need of using advanced manufacturing methods such as adhesive bonding techniques. The possible field leakage due to the air gaps is prevented by using an electromagnetic band gap (EBG) structure, consisting of glide-symmetric holes. The proposed concept could be an excellent candidate for designing compact and thin passive waveguide components and active components packaging, with a great potential for low-cost, light weight and mass-producible at millimeter-wave frequencies.

My contribution- I designed and simulated the MLW lines, assembled, performed the measurements, and wrote the paper.

7.1 Suggestions for Future Work

After the work performed in this thesis, it is relevant to remark that there still exist many hardware challenges that need to be addressed at millimeter-wave frequencies, and it needs to be mentioned the possible research directions for future work. In this thesis, we have presented the recent developmental on gap waveguide technology and we have

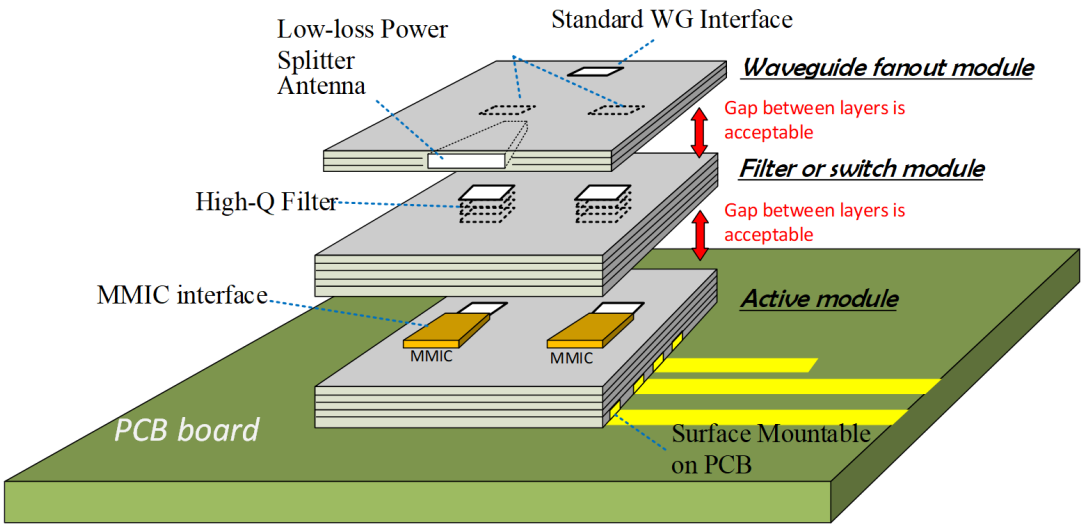

Figure 7.1: Illustration of MLW platform concept.

introduced the so-called MLW technology for high frequency applications. In this section, we give some recommendations for possible research directions for these two technologies.

Gap waveguide technology:

- Investigation for more cost-effective manufacturing techniques to simplify the fabrication of gap waveguide components and investigate ways to mass-produce them, especially for frequency bands beyond 100 GHz.
- Designing of more complex planar passive components with high performance, such as dual polarized array antennas, steerable and switchable beam array antennas by using passive beamforming networks, e.g., butler matrix and Rotman lens.
- System level integration and packaging.

MLW technology:

Since MLW is a novel technology, there are many interesting research opportunities to explore the potential of this technology in different applications. Fig. 7.1 shows our vision for an integration and interconnected platform based on MLW technology. Passive components such as antennas and bandpass filters can be integrated with the active parts in the same package to form a compact surface-mount device (SMD) solderable device. The proposed technology functions as a millimeter-wave system platform by providing a low loss interconnect and package solution. Several thin metal layers are stacked to constitute different functional modules. Galvanic connection between the layers/modules is not required, since we use an EBG structure to eliminate any possible leakage. This concept is believed to offer key advantages, such as fast assembly, high placement tolerance,

high system reconfigurability, and low cost, making it extremely attractive for industrial adoption.

References

[1] "Spectrum issues on wireless backhaul-radio spectrum policy group," [online] Available: *http://rspg-spectrum.eu/wp-content/uploads/2013/05/RSPG15-607-Final_Report-Wireless_backhaul.pdf*, June 2015.

[2] D. Lockie and D. Peck, "High-data-rate millimeter-wave radios," *IEEE Microwave Magazine*, vol. 10, no. 5, 2009.

[3] "Microwave backhaul evolution-reaching beyond-100 GHz," [online] Available: *https://www.ericsson.com/en/ericsson-technology-review/archive/2017/microwave-backhaul-evolution-reaching-beyond-100ghz*, 2017.

[4] S. Landstrom, A. Furuskär, K. Johansson, L. Falconetti, and F. Kronestedt, "Heterogeneous networks–increasing cellular capacity," *Ericsson review*, vol. 1, pp. 4–9, 2011.

[5] "Evolving LTE to fit the 5G future," [online] Available: *https://www.ericsson.com/en/ericsson-technology-review/archive/2017/evolving-lte-to-fit-the-5g-future*, 2017.

[6] J. Hasch, E. Topak, R. Schnabel, T. Zwick, R. Weigel, and C. Waldschmidt, "Millimeter-wave technology for automotive radar sensors in the 77 GHz frequency band," *IEEE Transactions on Microwave Theory and Techniques*, vol. 60, no. 3, pp. 845–860, 2012.

[7] X. Yang, L. Liu, N. H. Vaidya, and F. Zhao, "A vehicle-to-vehicle communication protocol for cooperative collision warning," in *Proceedings of The First Annual International Conference on Mobile and Ubiquitous Systems: Networking and Services (MOBIQUITOUS 2004)*. Boston, Massachusetts, USA, 2004, pp. 114–123.

[8] L. Yujiri, "Passive millimeter wave imaging," in *Proceedings of the 2006 IEEE MTT-S International Microwave Symposium Digest*. San Francisco, CA, USA, 2006, pp. 98–101.

References

[9] Y. H. Choung, "V-band crosslink antenna," in *Proceedings of the 2005 IEEE Antennas and Propagation Society International Symposium.* Long Beach, CA, USA, 2005, pp. 387–390.

[10] P. Smulders, "Exploiting the 60 GHz band for local wireless multimedia access: prospects and future directions," *IEEE communications magazine*, vol. 40, no. 1, pp. 140–147, 2002.

[11] C. J. Hansen, "WiGiG: Multi-gigabit wireless communications in the 60 GHz band," *IEEE Wireless Communications*, vol. 18, no. 6, pp. 6–7, 2011.

[12] K.-C. Huang and Z. Wang, *Millimeter wave communication systems.* John Wiley and Sons, 2011, vol. 29.

[13] E. Alfonso and P.-S. Kildal, "Parabolic cylindrical reflector antenna at 60 GHz with line feed in gap waveguide technology," in *Proceedings of the 7th European Conference on Antennas and Propagation (EuCAP).* Gothenburg, 2013, pp. 1–4.

[14] J. Hansryd, Y. Li, J. Chen, and P. Ligander, "Long term path attenuation measurement of the 71–76 GHz band in a 70/80 GHz microwave link," in *Proceedings of the 4th European Conference on Antennas and Propagation (EuCAP).* Barcelona, 2010.

[15] "Specific attenuation model for rain for use in prediction methods," ITU-R Recommendations, ITU-R P.8383-3, Geneva, Switzerland, 2005.

[16] K. Nishikawa, S. Sugitani, K. Inoue, T. Ishii, K. Kamogawa, B. Piernas, and K. Araki, "Low-loss passive components on BCB-based 3D MMIC technology," in *Proceedings of the 2001 IEEE MTT-S International Microwave Symposium Digest*, vol. 3. Phoenix, AZ, USA, 2001, pp. 1881–1884.

[17] G. Six, G. Prigent, E. Rius, G. Dambrine, and H. Happy, "Fabrication and characterization of low-loss TFMS on silicon substrate up to 220 GHz," *IEEE Transactions on Microwave Theory and Techniques*, vol. 53, no. 1, pp. 301–305, 2005.

[18] A. L. V. López, S. K. Bhattacharya, C. A. D. Morcillo, J. Papapolymerou, and D. Choudhury, "Novel low loss thin film materials for wireless 60 GHz application," in *Proceedings of the 60th Electronic Components and Technology Conference (ECTC)*, 2010, pp. 1990–1995.

[19] K. Wu, D. Deslandes, and Y. Cassivi, "The substrate integrated circuits-a new concept for high-frequency electronics and optoelectronics," in *Proceedings of the 6th International Conference on Telecommunications in Modern Satellite, Cable and Broadcasting Service (TELSIKS 2003).* Yugoslavia, 2003.

[20] D. Deslandes and K. Wu, "Accurate modeling, wave mechanisms, and design considerations of a substrate integrated waveguide," *IEEE Transactions on Microwave Theory and Techniques*, vol. 54, no. 6, pp. 2516–2526, 2006.

[21] M. Bozzi, M. Pasian, L. Perregrini, and K. Wu, "On the losses in substrate integrated waveguides," in *Proceedings of the 2007 European Microwave Conference (EuMC)*, 2007.

[22] F. Xu and K. Wu, "Guided-wave and leakage characteristics of substrate integrated waveguide," *IEEE Transactions on Microwave Theory and Techniques*, vol. 53, no. 1, pp. 66–73, 2005.

[23] J. Yu, V. A. Khlebnikov, and M.-H. Ka, "Wideband grating-lobe suppression by rotation of the phased array stations in the SKA low-frequency sparse aperture array," *IEEE Transactions on Antennas and Propagation*, vol. 63, no. 9, pp. 3939–3946, 2015.

[24] W. Jian *et al.*, "Research on grating lobe reduction in limited-scan phased array antenna," in *Cross Strait Quad-Regional Radio Science and Wireless Technology Conference (CSQRWC)*. China, 2013, pp. 230–233.

[25] K. C. Kerby and J. T. Bernhard, "Sidelobe level and wideband behavior of arrays of random subarrays," *IEEE transactions on antennas and propagation*, vol. 54, no. 8, pp. 2253–2262, 2006.

[26] M. G. Bray, D. H. Werner, D. W. Boeringer, and D. W. Machuga, "Optimization of thinned aperiodic linear phased arrays using genetic algorithms to reduce grating lobes during scanning," *IEEE Transactions on antennas and propagation*, vol. 50, no. 12, pp. 1732–1742, 2002.

[27] Z. Ding, W. Gao, J. Liu, T. Zeng, and T. Long, "A novel range grating lobe suppression method based on the stepped-frequency SAR image," *IEEE Geoscience and Remote Sensing Letters*, vol. 12, no. 3, pp. 606–610, 2015.

[28] N. Levanon and E. Mozeson, "Nullifying ACF grating lobes in stepped-frequency train of LFM pulses," *IEEE Transactions on Aerospace and Electronic Systems*, vol. 39, no. 2, pp. 694–703, 2003.

[29] A. Borji, D. Busuioc, and S. Safavi-Naeini, "Efficient, low-cost integrated waveguide-fed planar antenna array for Ku-band applications," *IEEE Antennas and Wireless Propagation Letters*, vol. 8, pp. 336–339, 2009.

[30] Y. J. Cheng, Y. X. Guo, and Z. G. Liu, "W-Band large-scale high-gain planar integrated antenna array," *IEEE Transactions on Antennas and Propagation*, vol. 62, no. 6, pp. 3370–3373, Jun. 2014.

[31] J. Wu, Y. J. Cheng, and Y. Fan, "A wideband high-gain high-efficiency hybrid integrated plate array antenna for V-band inter-satellite links," *IEEE Transactions on Antennas and Propagation*, vol. 63, no. 4, pp. 1225–1233, Apr. 2015.

[32] E. Levine, G. Malamud, S. Shtrikman, and D. Treves, "A study of microstrip array antennas with the feed network," *IEEE Transactions on Antennas and Propagation*, vol. 37, no. 4, pp. 426–434, 1989.

[33] B. Cao, H. Wang, Y. Huang, and J. Zheng, "High-gain L-probe excited substrate integrated cavity antenna array with LTCC-based gap waveguide feeding network for W-band application," *IEEE Transactions on Antennas and Propagation*, vol. 63, no. 12, pp. 5465–5474, 2015.

[34] B. Cao, H. Wang, and Y. Huang, "W-band high-gain TE-mode slot antenna array with gap waveguide feeding network," *IEEE Antennas and Wireless Propagation Letters*, vol. 15, pp. 988–991, 2016.

[35] D. K. Cheng *et al.*, *Field and wave electromagnetics*. Pearson Education India, 1989.

[36] T. Sehm, A. Lehto, and A. V. Raisanen, "A high-gain 58-GHz box-horn array antenna with suppressed grating lobes," *IEEE Transactions on Antennas and Propagation*, vol. 47, no. 7, pp. 1125–1130, 1999.

[37] M. Zhang, J. Hirokawa, and M. Ando, "An E-band partially corporate feed uniform slot array with laminated quasi double-layer waveguide and virtual PMC terminations," *IEEE Transactions on Antennas and Propagation*, vol. 59, no. 5, pp. 1521–1527, 2011.

[38] S. S. Oh, J.-W. Lee, M.-S. Song, and Y.-S. Kim, "Two-layer slotted-waveguide antenna array with broad reflection/gain bandwidth at millimetre-wave frequencies," *IEE Proceedings - Microwaves, Antennas and Propagation*, vol. 151, no. 5, pp. 393–398, 2004.

[39] S. Park, Y. Tsunemitsu, J. Hirokawa, and M. Ando, "Center feed single layer slotted waveguide array," *IEEE transactions on antennas and propagation*, vol. 54, no. 5, pp. 1474–1480, 2006.

[40] S. Fujii, Y. Tsunemitsu, G. Yoshida, N. Goto, M. Zhang, J. Hirokawa, and M. Ando, "A wideband single-layer slotted waveguide array with an embedded partially corporate feed," in *Proceedings of the 2008 International Symposium on Antennas and Propagation (ISAP)*, 2008.

[41] B. Lee, K. Jung, and S.-H. Yang, "High-efficiency planar slot-array antenna with a single waveguide-fed cavity-backed subarray," *Microwave and optical technology letters*, vol. 43, no. 3, pp. 228–231, 2004.

[42] Y. Kimura, T. Hirano, J. Hirokawa, and M. Ando, "Alternating-phase fed single-layer slotted waveguide arrays with chokes dispensing with narrow wall contacts," *IEE Proceedings - Microwaves, Antennas and Propagation*, vol. 148, no. 5, pp. 295–301, Oct. 2001.

[43] H. Kirino and K. Ogawa, "A 76 GHz multi-layered phased array antenna using a non-metal contact metamaterial waveguide," *IEEE Transactions on Antennas and Propagation*, vol. 60, no. 2, pp. 840–853, 2012.

[44] Y. Miura, J. Hirokawa, M. Ando, Y. Shibuya, and G. Yoshida, "Double-layer full-corporate-feed hollow-waveguide slot array antenna in the 60-GHz band," *IEEE Transactions on Antennas and Propagation*, vol. 59, no. 8, pp. 2844–2851, Aug. 2011.

[45] J. Hirokawa and M. Ando, "Efficiency of 76-GHz post-wall waveguide-fed parallel-plate slot arrays," *IEEE Transactions on Antennas and Propagation*, vol. 48, no. 11, pp. 1742–1745, 2000.

[46] Y. Kimura, A. Akiyama, J. Hirokawa, M. Ando, N. Goto *et al.*, "Alternating phase-fed waveguide slot arrays with a single-layer multiple-way power divider," *IEE Proceedings - Microwaves, Antennas and Propagation*, vol. 144, no. 6, pp. 425–430, Dec. 1997.

[47] L. Wang, Y.-X. Guo, and W.-X. Sheng, "Wideband high-gain 60-GHz LTCC L-probe patch antenna array with a soft surface," *IEEE Transactions on Antennas and Propagation*, vol. 61, no. 4, pp. 1802–1809, 2013.

[48] W. Yang, H. Wang, W. Che, Y. Huang, and J. Wang, "High-gain and low-loss millimeter-wave LTCC antenna array using artificial magnetic conductor structure," *IEEE Transactions on Antennas and Propagation*, vol. 63, no. 1, pp. 390–395, Jan. 2015.

[49] J. Xu, Z. N. Chen, X. Qing, and W. Hong, "Bandwidth enhancement for a 60 GHz substrate integrated waveguide fed cavity array antenna on LTCC," *IEEE transactions on antennas and propagation*, vol. 59, no. 3, pp. 826–832, Mar. 2011.

[50] P.-S. Kildal, *Foundations of Antenna Engineering: A Unified Approach for Line-of-sight and Multipath*, 2015, [online] Available: *https://www.kildal.se*.

[51] P. W. Hannan, "The element-gain paradox for a phased-array antenna," *IEEE Transactions on Antennas and Propagation*, vol. 12, no. 7, pp. 423–433, 1964.

[52] R. C. Hansen, *Microwave scanning antennas: array systems.* Academic Press, 1966, vol. 3.

[53] D. Pozar, "The active element pattern," *IEEE Transactions on Antennas and Propagation*, vol. 42, no. 8, pp. 1176–1178, 1998.

[54] P.-S. Kildal and K. Rosengren, "Correlation and capacity of MIMO systems and mutual coupling, radiation efficiency, and diversity gain of their antennas: simulations and measurements in a reverberation chamber," *IEEE Communications Magazine*, vol. 42, no. 12, pp. 104–112, 2004.

[55] W. K. Kahn, "Element efficiency: a unifying concept for array antennas," *IEEE Antennas and Propagation Magazine*, vol. 49, no. 4, pp. 48–56, 2007.

[56] P.-S. Kildal, E. Alfonso, A. Valero-Nogueira, and E. Rajo-Iglesias, "Local metamaterial-based waveguides in gaps between parallel metal plates," *IEEE Antennas and Wireless Propagation Letters*, vol. 8, pp. 84–87, 2009.

[57] P.-S. Kildal, "Artificially soft and hard surfaces in electromagnetics," *IEEE Transactions on Antennas and Propagation*, vol. 38, no. 10, pp. 1537–1544, 1990.

[58] D. Sievenpiper, L. Zhang, R. F. Broas, N. G. Alexopolous, and E. Yablonovitch, "High-impedance electromagnetic surfaces with a forbidden frequency band," *IEEE Transactions on Microwave Theory and techniques*, vol. 47, no. 11, pp. 2059–2074, 1999.

[59] E. Rajo-Iglesias and P.-S. Kildal, "Numerical studies of bandwidth of parallel-plate cut-off realised by a bed of nails, corrugations and mushroom-type electromagnetic bandgap for use in gap waveguides," *IET Microwaves, Antennas and Propagation*, vol. 5, no. 3, pp. 282–289, 2011.

[60] A. U. Zaman and P.-S. Kildal, "Gap waveguides for mmWave antenna systems and electronic packaging," chapter in *Handbook of Antenna Technologies*, Springer 2016.

[61] P.-S. Kildal, A. U. Zaman, E. Rajo-Iglesias, E. Alfonso, and A. Valero-Nogueira, "Design and experimental verification of ridge gap waveguide in bed of nails for parallel-plate mode suppression," *IET Microwaves, Antennas and Propagation*, vol. 5, no. 3, pp. 262–270, Feb. 2011.

[62] E. Rajo-Iglesias and P.-S. Kildal, "Groove gap waveguide: A rectangular waveguide between contactless metal plates enabled by parallel-plate cut-off," in *Proceedings of the 4th European Conference on Antennas and Propagation (EuCAP)*. Barcelona, 2010, pp. 1–4.

[63] H. Raza, J. Yang, P.-S. Kildal, and E. A. Alós, "Microstrip-ridge gap waveguide–study of losses, bends, and transition to WR-15," *IEEE Transactions on Microwave Theory and Techniques*, vol. 62, no. 9, pp. 1943–1952, 2014.

[64] A. A. Brazález, E. Rajo-Iglesias, J. L. Vazquez-Roy, A. Vosoogh, and P.-S. Kildal, "Design and validation of microstrip gap waveguides and their transitions to rectangular waveguide, for millimeter-wave applications," *IEEE Transactions on Microwave Theory and Techniques*, vol. 63, no. 12, pp. 4035–4050, 2015.

[65] H. Raza, J. Yang, P.-S. Kildal, and E. Alfonso, "Resemblance between gap waveguides and hollow waveguides," *IET Microwaves, Antennas and Propagation*, vol. 7, no. 15, pp. 1221–1227, 2013.

[66] P. Kildal, "Metasurfing for industrial applications since 1988," in *Slide presentation published in the Forum at web based FERMAT Journal edited by R. Mittra*, 2015.

[67] A. A. Brazález, J. Flygare, J. Yang, V. Vassilev, M. Baquero-Escudero, and P.-S. Kildal, "Design of F-band transition from microstrip to ridge gap waveguide including Monte Carlo assembly tolerance analysis," *IEEE Transactions on Microwave Theory and Techniques*, vol. 64, no. 4, pp. 1245–1254, 2016.

[68] M. Sharifi Sorkherizi, "Microwave filters based on new design concepts in several technologies with emphasis on the printed ridge gap waveguide technology," Ph.D. dissertation, Concordia University, 2016.

[69] F. Fan, J. Yang, and P.-S. Kildal, "Half-height pins-a new pin form in gap waveguide for easy manufacturing," in *Proceedings of the 10th European Conference on Antennas and Propagation (EuCAP)*. Davos, 2016, pp. 1–4.

[70] F. Fan, J. Yang, V. Vassilev, and A. U. Zaman, "Bandwidth investigation on half-height pin in ridge gap waveguide," *IEEE Transactions on Microwave Theory and Techniques*, vol. 66, no. 1, pp. 100–108, 2018.

[71] M. S. Sorkherizi, A. Dadgarpour, and A. A. Kishk, "Planar high-efficiency antenna array using new printed ridge gap waveguide technology," *IEEE Transactions on Antennas and Propagation*, vol. 65, no. 7, pp. 3772–3776, 2017.

[72] D. Zarifi, A. Farahbakhsh, A. U. Zaman, and P.-S. Kildal, "Design and fabrication of a high-gain 60-GHz corrugated slot antenna array with ridge gap waveguide distribution layer," *IEEE Transactions on Antennas and Propagation*, vol. 64, no. 7, pp. 2905–2913, 2016.

[73] J. Liu, A. Vosoogh, A. U. Zaman, and J. Yang, "Design and fabrication of a high-gain 60-GHz cavity-backed slot antenna array fed by inverted microstrip gap waveguide," *IEEE Transactions on Antennas and Propagation*, vol. 65, no. 4, pp. 2117–2122, 2017.

[74] A. J. Sáez, A. Valero-Nogueira, J. I. Herranz, and B. Bernardo, "Single-layer cavity-backed slot array fed by groove gap waveguide," *IEEE Antennas and Wireless Propagation Letters*, vol. 15, pp. 1402–1405, 2016.

[75] A. U. Zaman, E. Rajo-Iglesias, E. Alfonso, and P.-S. Kildal, "Design of transition from coaxial line to ridge gap waveguide," in *Proceedings of the IEEE International Symposium on Antennas and Propagation (APSURSI)*, 2009, pp. 1–4.

[76] A. A. Brazález, A. U. Zaman, and P.-S. Kildal, "Design of a coplanar waveguide-to-ridge gap waveguide transition via capacitive coupling," in *Proceedings of the 6th European Conference on Antennas and Propagation (EuCAP)*. Prague, 2012, pp. 3524–3528.

[77] A. Aljarosha, A. U. Zaman, and R. Maaskant, "A wideband contactless and bondwire-free MMIC to waveguide transition," *IEEE Microwave and Wireless Components Letters*, vol. 27, no. 5, pp. 437–439, 2017.

[78] A. U. Zaman, T. Vukusic, M. Alexanderson, and P.-S. Kildal, "Design of a simple transition from microstrip to ridge gap waveguide suited for MMIC and antenna integration," *IEEE Antennas and Wireless Propagation Letters*, vol. 12, pp. 1558–1561, 2013.

[79] U. Nandi, A. U. Zaman, A. Vosoogh, and J. Yang, "Novel millimeter wave transition from microstrip line to groove gap waveguide for MMIC packaging and antenna integration," *IEEE Microwave and Wireless Components Letters*, vol. 27, no. 8, pp. 691–693, 2017.

[80] A. U. Zaman, V. Vassilev, H. Zirath, and N. Rorsman, "Novel low-loss millimeter-wave transition from waveguide-to-microstrip line suitable for MMIC integration and packaging," *IEEE Microwave and Wireless Components Letters*, vol. 27, no. 12, pp. 1098–1100, 2017.

[81] A. Vosoogh, A. Uz Zaman, and J. Yang, "Simple and broadband transition between rectangular waveguide and groove gap waveguide for mm-Wave applications," in *Proceedings of the IEEE International Symposium on Antennas and Propagation (APSURSI)*, 2018.

[82] A. U. Zaman and P.-S. Kildal, "Wide-band slot antenna arrays with single-layer corporate-feed network in ridge gap waveguide technology," *IEEE Transactions on Antennas and Propagation*, vol. 62, no. 6, pp. 2992–3001, Jun 2014.

[83] P. Taghikhani, J. Yang, and A. Vosoogh, "High gain V-band planar array antenna using half-height pin gap waveguide," in *Proceedings of the 11th European Conference on Antennas and Propagation (EuCAP)*. Paris, 2017, pp. 2758–2761.

[84] M. Ferrando-Rocher, A. Zaman, J. Yang, and A. Valero-Nogueira, "A dual-polarized slotted-waveguide antenna based on gap waveguide technology," in *Proceedings of the 11th European Conference on Antennas and Propagation (EuCAP)*. Paris, 2017, pp. 3726–3727.

[85] D. Zarifi, A. Farahbakhsh, and A. U. Zaman, "A gap waveguide-fed wideband patch antenna array for 60-GHz applications," *IEEE Transactions on Antennas and Propagation*, vol. 65, no. 9, pp. 4875–4879, 2017.

[86] A. Farahbakhsh, D. Zarifi, and A. U. Zaman, "A mmWave wideband slot array antenna based on ridge gap waveguide with 30% bandwidth," *IEEE Transactions on Antennas and Propagation*, vol. 66, no. 2, pp. 1008–1013, 2018.

[87] M. Ferrando-Rocher, J. I. Herranz, A. Valero-Nogueira, and B. Bernardo, "Performance assessment of gap waveguide array antennas: CNC milling vs. 3D printing," *IEEE Antennas and Wireless Propagation Letters*, 2018.

[88] S. A. Razavi, P.-S. Kildal, L. Xiang, E. Alfonso Alos, and H. Chen, "2 × 2-slot element for 60-GHz planar array antenna realized on two doubled-sided pcbs using SIW cavity and EBG-type soft surface fed by microstrip-ridge gap waveguide," *IEEE Transactions on Antennas and Propagation*, vol. 62, no. 9, pp. 4564–4573, Sep. 2014.

[89] E. Pucci, E. Rajo-Iglesias, J.-L. Vazquez-Roy, and P.-S. Kildal, "Planar dual-mode horn array with corporate-feed network in inverted microstrip gap waveguide," *IEEE Transactions on Antennas and Propagation*, vol. 62, no. 7, pp. 3534–3542, 2014.

[90] H. Attia, M. S. Sorkherizi, and A. A. Kishk, "60 GHz slot antenna array based on ridge gap waveguide technology enhanced with dielectric superstrate," in *Proceedings of the 9th European Conference on Antennas and Propagation (EuCAP)*. Lisbon, 2015, pp. 1–4.

[91] M. Rezaee, A. U. Zaman, and P.-S. Kildal, "A groove gap waveguide iris filter for V-band application," in *Proceedings of the 23rd Iranian Conference on Electrical Engineering (ICEE)*, 2015, pp. 462–465.

[92] M. S. Sorkherizi and A. A. Kishk, "Self-packaged, low-loss, planar bandpass filters for millimeter-wave application based on printed gap waveguide technology," *IEEE Transactions on Components, Packaging and Manufacturing Technology*, vol. 7, no. 9, pp. 1419–1431, 2017.

[93] B. Ahmadi and A. Banai, "Direct coupled resonator filters realized by gap waveguide technology," *IEEE Transactions on Microwave Theory and Techniques*, vol. 63, no. 10, pp. 3445–3452, 2015.

[94] E. Pucci, A. U. Zaman, E. Rajo-Iglesias, P.-S. Kildal, and A. Kishk, "Study of Q-factors of ridge and groove gap waveguide resonators," *IET Microwaves, Antennas and Propagation*, vol. 7, no. 11, pp. 900–908, 2013.

[95] A. U. Zaman, P.-S. Kildal, A. A. Kishk *et al.*, "Narrow-band microwave filter using high-Q groove gap waveguide resonators with manufacturing flexibility and no

sidewalls," *IEEE Transactions on Components, Packaging and Manufacturing Technology*, vol. 2, no. 11, pp. 1882–1889, 2012.

[96] A. del Olmo-Olmeda, M. Baquero-Escudero, V. E. Boria-Esbert, A. Valero-Nogueira, and A. J. Berenguer-Verdu, "A novel band-pass filter topology for millimeter-wave applications based on the groove gap waveguide," in *Proceedings of the IEEE MTT-S International Microwave Symposium Digest*, 2013, pp. 1–4.

[97] E. A. Alós, A. U. Zaman, and P.-S. Kildal, "Ka-band gap waveguide coupled-resonator filter for radio link diplexer application," *IEEE Transactions on Components, Packaging and Manufacturing Technology*, vol. 3, no. 5, pp. 870–879, 2013.

[98] A. Berenguer, M. Baquero-Escudero, D. Sanchez-Escuderos, B. Bernardo-Clemente, and V. E. Boria-Esbert, "Low insertion loss 61 GHz narrow-band filter implemented with groove gap waveguides," in *Proceedings of the 44th European Microwave Conference (EuMC)*, 2014, pp. 191–194.

[99] D. Sun and J. Xu, "A novel iris waveguide bandpass filter using air gapped waveguide technology," *IEEE Microwave and Wireless Components Letters*, vol. 26, no. 7, pp. 475–477, 2016.

[100] B. Al-Juboori, Y. Huang, D. Klugmann, M. Hussein, and J. Zhou, "Millimeter wave cross-coupled bandpass filter based on groove gap waveguide technology," in *Proceedings of the 10th UK-Europe-China Workshop on Millimetre Waves and Terahertz Technologies (UCMMT)*, 2017, pp. 1–4.

[101] M. Rezaee and A. U. Zaman, "Realisation of carved and iris groove gap waveguide filter and E-plane diplexer for V-band radio link application," *IET Microwaves, Antennas and Propagation*, vol. 11, no. 15, pp. 2109–2115, 2017.

[102] M. S. Sorkherizi, A. Khaleghi, and P.-S. Kildal, "Direct-coupled cavity filter in ridge gap waveguide," *IEEE Transactions on Components, Packaging and Manufacturing Technology*, vol. 4, no. 3, pp. 490–495, Mar. 2014.

[103] M. S. Sorkherizi and A. A. Kishk, "Completely tuned coupled cavity filters in defected bed of nails cavity," *IEEE Transactions on Components, Packaging and Manufacturing Technology*, 2016.

[104] A. Vosoogh, A. A. Brazález, and P.-S. Kildal, "A V-band inverted microstrip gap waveguide end-coupled bandpass filter," *IEEE Microwave and Wireless Components Letters*, vol. 26, no. 4, pp. 261–263, Apr. 2016.

[105] M. S. Sorkherizi and A. A. Kishk, "Fully printed gap waveguide with facilitated design properties," *IEEE Microwave and Wireless Components Letters*, vol. 26, no. 9, pp. 657–659, 2016.

[106] A. U. Zaman, M. Alexanderson, T. Vukusic, and P.-S. Kildal, "Gap waveguide PMC packaging for improved isolation of circuit components in high-frequency microwave modules," *IEEE Transactions on Components, Packaging and Manufacturing Technology*, vol. 4, no. 1, pp. 16–25, 2014.

[107] E. Rajo-Iglesias, A. U. Zaman, and P.-S. Kildal, "Parallel plate cavity mode suppression in microstrip circuit packages using a lid of nails," *IEEE Microwave and Wireless Components Letters*, vol. 20, no. 1, pp. 31–33, 2010.

[108] A. A. Brazález, A. U. Zaman, and P.-S. Kildal, "Improved microstrip filters using PMC packaging by lid of nails," *IEEE Transactions on Components, Packaging and Manufacturing Technology*, vol. 2, no. 7, pp. 1075–1084, 2012.

[109] J. Zhang, X. Zhang, D. Shen, and K. Wu, "Gap waveguide PMC packaging for a SIW-GCPW-based filter," *IEEE Microwave and Wireless Components Letters*, vol. 26, no. 3, pp. 159–161, 2016.

[110] B. Ahmadi and A. Banai, "Substrateless amplifier module realized by ridge gap waveguide technology for millimeter-wave applications," *IEEE Transactions on Microwave Theory and Techniques*, vol. 64, no. 11, pp. 3623–3630, 2016.

[111] R. Maaskant, W. A. Shah, A. U. Zaman, M. Ivashina, and P.-S. Kildal, "Spatial power combining and splitting in gap waveguide technology," *IEEE Microwave and Wireless Components Letters*, vol. 26, no. 7, pp. 472–474, 2016.

[112] E. Pucci and P.-S. Kildal, "Contactless non-leaking waveguide flange realized by bed of nails for millimeter wave applications," in *Proceedings of the 6th European Conference on Antennas and Propagation (EuCAP)*. Prague, 2012, pp. 3533–3536.

[113] E. Alfonso, S. Carlred, S. Carlsson, and L.-I. Sjöqvist, "Contactless flange adapters for mm-wave measurements," in *Proceedings of the 11th European Conference on Antennas and Propagation (EuCAP)*. Paris, 2017, pp. 1690–1693.

[114] S. Rahiminejad, H. Raza, A. U. Zaman, S. Haasl, P. Enoksson, and P.-S. Kildal, "Micromachined gap waveguides for 100 GHz applications," in *Proceedings of the 7th European Conference on Antennas and Propagation (EuCAP)*. Gothenburg, 2013.

[115] S. Rahiminejad, E. Pucci, S. Haasl, and P. Enoksson, "Micromachined contactless pin-flange adapter for robust high-frequency measurements," *Journal of Micromechanics and Microengineering*, vol. 24, no. 8, p. 084004, 2014.

[116] S. Rahiminejad, E. Pucci, V. Vassilev, P.-S. Kildal, S. Haasl, and P. Enoksson, "Polymer gap adapter for contactless, robust, and fast measurements at 220–325 GHz," *Journal of Microelectromechanical Systems*, vol. 25, no. 1, pp. 160–169, 2016.

References

[117] D. Sun and J. Xu, "Real time rotatable waveguide twist using contactless stacked air-gapped waveguides," *IEEE Microwave and Wireless Components Letters*, vol. 27, no. 3, pp. 215–217, 2017.

[118] J. Yang, "E-band one-step 45° double-wing gap waveguide twist for waveguide WR12," in *Proceedings of the 2017 International Symposium on Antennas and Propagation (ISAP)*. Phuket, 2017, pp. 1–2.

[119] D. C. Thompson, O. Tantot, H. Jallageas, G. E. Ponchak, M. M. Tentzeris, and J. Papapolymerou, "Characterization of liquid crystal polymer (LCP) material and transmission lines on LCP substrates from 30 to 110 GHz," *IEEE Transactions on Microwave Theory and Techniques*, vol. 52, no. 4, pp. 1343–1352, 2004.

[120] S. T. Choi, K. S. Yang, K. Tokuda, and Y. H. Kim, "A V-band planar narrow bandpass filter using a new type integrated waveguide transition," *IEEE microwave and wireless components letters*, vol. 14, no. 12, pp. 545–547, 2004.

[121] "Fixed Radio Systems- Characteristics and requirements for point-to-point equipment and antennas," Tech. Rep. ETSI EN 302 217-4-2 (V1. 5.1), [online] Available: *http://www.etsi.org/WebSite/homepage.aspx*, 2010.

[122] A. Vosoogh, P.-S. Kildal, V. Vassilev, A. U. Zaman, and S. Carlsson, "E-band 3-D metal printed wideband planar horn array antenna," in *Proceedings of the 2016 International Symposium on Antennas and Propagation (ISAP)*. Okinawa, Japan, 2016.

[123] *Fixed Radio Systems; Parameters affecting the Signal-to-Noise Ratio (SNR) and the Receiver Signal Level (RSL) threshold in point-to-point receivers; Theory and practice*, document ETSI TR 103 053 V1.1.1, 2014.

[124] S. Rahiminejad, *Microsystem technology for microwave applications at frequencies above 100 GHz*, PhD Thesis, Department of Microtechnology and Nanoscience, Chalmers University of Technology, 2016.

[125] B. Zhang, Y.-X. Guo, H. Zirath, and Y. P. Zhang, "Investigation on 3-D-printing technologies for millimeter-wave and terahertz applications," *Proceedings of the IEEE*, vol. 105, no. 4, pp. 723–736, 2017.

[126] A. von Bieren, E. De Rijk, J.-P. Ansermet, and A. Macor, "Monolithic metal-coated plastic components for mm-wave applications," in *Proceedings of the 39th International Conference on Infrared, Millimeter, and Terahertz waves (IRMMW-THz)*, 2014, pp. 1–2.

[127] B. Zhang and H. Zirath, "Metallic 3-D printed rectangular waveguides for millimeter-wave applications," *IEEE Transactions on Components, Packaging and Manufacturing Technology*, vol. 6, no. 5, pp. 796–804, 2016.

[128] X. Zhao, J. Bao, G. Shan, Y. Du, Y. Zheng, Y. Wen, and C. H. Shek, "D-band micromachined silicon rectangular waveguide filter," *IEEE Microwave and Wireless Components Letters*, vol. 22, no. 5, pp. 230–232, 2012.

[129] D. Glynn, T. He, J. Powell, Y. Tian, X. Shang, and M. J. Lancaster, "Submillimetre rectangular waveguides based on SU-8 photoresist micromachining technology," in *Proceedings of the 2016 46th European Microwave Conference (EuMC)*, 2016, pp. 1346–1349.

[130] B. Beuerle, J. Campion, U. Shah, and J. Oberhammer, "A very low loss 220–325 GHz silicon micromachined waveguide technology," *IEEE Transactions on Terahertz Science and Technology*, vol. 8, no. 2, pp. 248–250, 2018.

[131] F. Sammoura, Y.-C. Su, Y. Cai, C.-Y. Chi, B. Elamaran, L. Lin, and J.-C. Chiao, "Plastic 95-GHz rectangular waveguides by micro molding technologies," *Sensors and Actuators A: Physical*, vol. 127, no. 2, pp. 270–275, 2006.

[132] M. Ebrahimpouri, O. Quevedo-Teruel, and E. Rajo-Iglesias, "Design guidelines for gap waveguide technology based on glide-symmetric holey structures," *IEEE Microwave and Wireless Components Letters*, vol. 27, no. 6, pp. 542–544, 2017.

[133] M. Ebrahimpouri, E. Rajo-Iglesias, Z. Sipus, and O. Quevedo-Teruel, "Cost-effective gap waveguide technology based on glide-symmetric holey EBG structures," *IEEE Transactions on Microwave Theory and Techniques*, vol. 66, no. 2, pp. 927–934, 2018.

[134] J. Campion, O. Glubokov, A. Gomez, A. Krivovitca, U. Shah, L. Bolander, Y. Li, and J. Oberhammer, "An ultra low-loss silicon-micromachined waveguide filter for D-band telecommunication applications," in *Proceedings of the 2018 IEEE/MTT-S International Microwave Symposium*, 2018, pp. 583–586.

[135] W. T. Khan, A. Ç. Ulusoy, and J. Papapolymerou, "D-band characterization of coplanar wave guide and microstrip transmission lines on liquid crystal polymer," in *Proceedings of the 63rd Electronic Components and Technology Conference (ECTC)*. London, 2013, pp. 2304–2309.

[136] S. Li, M. Yi, S. Pavlidis, H. Yu, M. Swaminathan, and J. Papapolymerou, "Investigation of surface roughness effects for D-band SIW transmission lines on LCP substrate," in *Proceedings of the 2017 IEEE Radio and Wireless Symposium (RWS)*, 2017, pp. 121–124.

[137] I. Stil, A. Fontana, B. Lefranc, A. Navarrini, P. Serres, and K. Schuster, "Loss of WR10 waveguide across 70–116 GHz," in *Proceedings of the 22nd International Symposium on Space Terahertz Technology*, 2012, pp. 1–3.

[138] M. D'Auria, W. J. Otter, J. Hazell, B. T. Gillatt, C. Long-Collins, N. M. Ridler, and S. Lucyszyn, "3-D printed metal-pipe rectangular waveguides," *IEEE Transactions on Components, Packaging and Manufacturing Technology*, vol. 5, no. 9, pp. 1339–1349, 2015.

Part II

Included Papers